UNIVERSITY OF CALIFORNIA
RIVERSIDE

Zinc Bromine Flow Battery for PV-battery Microgrid: Analysis, Modeling, Control, and Field Demonstration

A Dissertation submitted in partial satisfaction
of the requirements for the degree of

Doctor of Philosophy

in

Electrical Engineering

by

Hao Xin

June 2021

Dissertation Committee:

Dr. Alfredo A. Martinez-Morales, Co-Chairperson
Dr. Matthew Barth, Co-Chairperson
Dr. Hamed Mohsenian-Rad
Dr. Hamidreza Nazaripouya

The Dissertation of Hao Xin is approved:

_____

_____

_____

Committee Co-Chairperson

_____

Committee Co-Chairperson

University of California, Riverside

To my wife You Zhou, and all of our family for all the support.

ABSTRACT OF THE DISSERTATION

Zinc Bromine Flow Battery for PV-battery Microgrid: Analysis, Modeling, Control, and Field Demonstration

by

Hao Xin

Doctor of Philosophy, Graduate Program in Electrical Engineering
University of California, Riverside, June 2021
Dr. Alfredo A. Martinez-Morales and Dr. Matthew Barth, Co-Chairpersons

The rapid deployment of renewable energy has been driven by cost reductions, public policy for reducing greenhouse gases and societal strides towards sustainability. However, the intermittent nature of renewable energy systems imposes challenges in its design and operation due to operational constraints, system limitations, and in some cases conflicting objectives. Energy storage systems have become an essential part in supporting the further penetration, reliability and resiliency of renewable energy. In this dissertation, a novel Zinc Bromine Flow Battery (ZBFB) energy storage system is researched and demonstrated as a controllable distributed energy resource. Analysis, optimal design, modeling and control algorithms are used to optimize performance and demonstrate practical use case applications.

Although ZBFB systems are a promising energy storage technology, specific operational constrains based on their unique design and inherent characteristics raise new practical challenges. Specifically, the main operating constrains of ZBFB described in this dissertation are with regards to two main aspects: 1) the requirement for constant

charging power during charging period, and 2) the need for a refresh mode (cleaning cycle) that is required to prevent energy capacity loss over multiple charge/discharge cycles.

The main motivations in this dissertation are to optimize control, improve system performance, maximize benefits and perform field-demonstrations in practical use case applications, while accounting for constraints specific to ZBFBs. The work includes aspects of modelling of the ZBFB refresh mode, emission reduction control algorithms, techno-economic analysis and control algorithms for specific use cases. Chapter 1 introduces the main motivations and problem statement of this dissertation. Chapter 2 describes the research background of this dissertation and conducts a literature review on several related topics; including ZBFB technologies, battery system control algorithms, methods and modeling of the ZBFB refresh mode, and emission reduction control strategy of PV-battery hybrid systems. Chapter 3 introduces the control algorithm for a large-scale ZBFB system coupled with two biogas combined heat & power generators to prevent minimum import violations, minimize the operational power buffer, and maximize the amount of on-site renewable generation. Chapter 4 introduces a techno-economic analysis between ZBFB and Li-ion battery in a microgrid topology for a load shifting application is carried out. Chapter 5 describes a novel model for ZBFB systems based on their specific physical and operational characteristics. A control algorithm for reducing both emissions and energy costs based on the developed ZBFB model is presented. Chapter 6, conclusions of this dissertation.

TABLE OF CONTENTS

LIST OF TABLES

LIST OF FIGURES

1. INTRODUCTION

1.1 Motivation

With increasing global population and industrialization of societies worldwide, the growing electricity demand has been met through an increased consumption of fossil fuels. According to the International Energy Agency (IEA) data from 1990 to 2018, the world overall energy use grew by 60.6% while the world population increased 44.2% [1]. Thus, the average energy use per person increased 11.5% from 1990 to 2018. Fossil energy resources played an import role in meeting electric energy demand, accounting for 84.3% of total electricity generation. However, a number of negative consequences related to the excessive use of fossil fuels have become more evident. The global rising temperatures due to increased greenhouse gas emissions (GHG) has been a trigger for catastrophic climate events around the world. For instance, the devastating wildfire in California [2], the rapidly disappearing Arctic ice caps [3] and accelerated sea level rise [4] are just a few examples. Global climate change, energy shortage and increasing GHG emissions have raised awareness and put emphasis on the need to reduce fossil fuel energy use. Thus, the challenge at hand is to meet increasing global energy demand while reducing the use of fossil fuel resources.

To address the aforementioned issues, numerous technology solutions aim at finding a pathway that enables electricity systems to meet two important goals, affordability of electric energy and reduction in air pollution. One prominent example are Distributed Renewable Energy Systems (DRES), commonly paired with an energy storage system. DRES refers to a variety of renewable energy generation systems, which generate and deliver electricity at or near the location where it is used. The end-user has the flexibility to adjust the system size based on site specific requirements. Although

renewable energy generation has various advantages from an environmental and sustainable point of view, the intermittent, fluctuating, and uncontrollable nature of renewable energy creates several challenges for incorporating renewable energy directly into the existing electric grid or support the daily energy demand on its own.

Fortunately, energy storage systems (ESS) with the appropriate control algorithms can offset the inherent constraints and challenges of renewable energy resources [5]. ESSs have become an essential part of renewable power generation and utilization. Among the various types of ESS technologies, flow battery has become an attractive option for DRES. In particular, the Zinc Bromine Flow Battery (ZBFB), as a member of the flow batteries family has several advantages including long lifetime, independent scaling of energy and power characteristics, use of relatively inexpensive and abundant raw materials, very deep depth of discharge levels without significantly impacting total cycle life, and safety features such as the ability of completely stopping battery operation by simply shutting down the pumps [5]. Although ZBFB is identified as a promising electrochemical energy storage technology, the unique features and physical operational constrains of ZBFB create new challenges for practical applications and widespread use. Since the ZBFB technology has not yet been deployed on a large scale, currently, there is limited research on the particular features and practical requirements on ZBFB in real applications.

By appropriately controlling the ZBFB as the energy storage component in DRES applications, several benefits can be verified or tested: 1) evaluate feasibility of ZBFB utilized in real applications within specific design and operational constrains; 2) test and compare the technological and economic performance of ZBFB compared to most commonly used energy storage system; 3) present a model that performs

simulations to deepen the understanding of the operation of ZBFB, its performance, and benefits achieved through the proposed applications; and 4) identify control algorithm for reducing GHG emissions by utilizing the above mentioned battery model.

1.2 Problem statement and contribution of the dissertation research

It is well recognized that ZBFBs have a great potential to serve as the energy storage system in DRES, due to a long lifespan and high depth of discharge without damaging battery performance. However, there is only a limited number of research reports focused on the specific characteristics inherent to ZBFB. As a result, the existing understanding and modelling of ZBFB systems are not complete or accurate, since they do not take into consideration some operating constrains arising from the principle of operation of ZBFB.

In this dissertation, two main constrains of ZBFBs in use cases are presented and discussed. First, a ZBFB is utilized as an ESS to implement and demonstrate new support functions, taking into consideration size optimization, control algorithm, revenue-maximization, and emission reduction, while considering the "constant charging power" limit constraint. Second, the need for a "refresh mode" is researched by developing a model to simulate the refresh process of ZBFB with an equivalent counting cycle algorithm. This model allows to simulate ZBFB operation, by focusing on the operating principles of ZBFB by using a mixed integer linear programming (MILP) approach.

The specific contributions of the dissertation can be summarized as:

- Develop a novel model to incorporate the "refresh mode" and "constant charging power" operational constraints of ZBFB.
- Develop a control algorithm for two conflicting objectives, minimizing DRES

energy cost, while reducing system GHG emission with ZBFB “refresh mode”.

- Develop a cooperative control of multiple ZBFB systems with “constant charging power” operational constrains to prevent minimum import violation.
- Develop a techno-economic analysis model for the optimal solar PV and ZBFB energy system size considering “constant charging power”.

1.3 Organization of the dissertation research

The dissertation is organized as follows: Chapter 2 describes the research background of this dissertation and conducts a literature review on several related topics, including information about solar energy, the general architecture and basic chemical reactions involved in the ZBFB, the specific operational constraints of ZBFB in real applications, and the principles behind those constraints. Chapter 3 introduces the control algorithm for a large-scale ZBFB system coupled with two biogas combined heat & power generators to prevent minimum import violations, minimize the operational power buffer, and maximize the amount of on-site renewable generation. Chapter 4 carries out a techno-economic analysis between ZBFB and Li-ion battery in a microgrid topology for a load shifting application. Chapter 5 describes a novel model for ZBFB systems based on their specific physical and operational characteristics. A control algorithm for reducing both emissions and energy costs based on the developed ZBFB model is presented. ZBFB actual data is utilized to develop an operational model and perform simulations to further advance the understanding of ZBFB system, their performance and benefits achieved through the proposed use case applications. Chapter 6, concludes this dissertation.

2. RESEARCH BACKGROUND AND LITERATURE REVIEW

Distributed generation is defined as "*electric power generation within distribution networks or on the customer's side of the network*" [6]. DRES is one type of distributed generation, which mainly utilizes renewable energy generation as the electric power source. DRES could not only reduce the influence of fluctuation of available renewable energy [7], but also could upend traditional transmission and distribution (T&D) installation, reduce conduction loss, all the while increasing the reliability and resiliency against unforeseen blackouts caused by natural disasters, provide arbitrage, and facilitate voltage/frequency correction on the customer side of the meter [8]. DRES are commonly utilized in residential and commercial applications. The renewable energy technology and energy storage system are the main components of DRES. The detailed information of features and characteristics of main components deployed in this study are discussed in this chapter.

2.1 Renewable energy resources

Driven by the adverse impacts by fossil fuels on the environment and climate, renewable energy resources have become the main alternative energy source of interest. Renewable energy resources are increasingly being utilized in the energy market for meeting energy needs and environmental sustainability goals. According to the Department of Energy (DOE), in 2018, renewable energy made up 20.5% of total installed electricity generating capacity and 17.6% of total annual generated electricity in the United States, as shown in Figure 2-1. In the past 25 years, natural gas, renewable energy and hydro have accounted for over 94% of U.S. capacity additions. The new installations of renewable energy generation capacity consist of wind and solar harnessing technologies, whose combined capacity reached 19.5GW in 2018 [9].

Figure 2-1 indicates hydro power, wind and solar power are the three dominant energy sources in renewable energy sector.

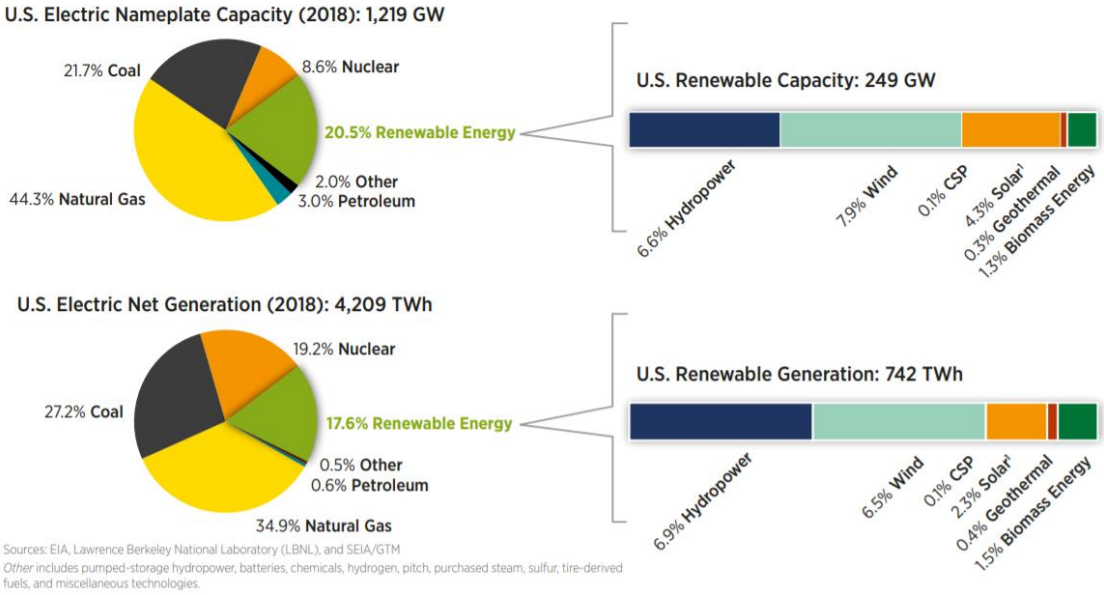

Figure 2-1. U.S. Electric Nameplate Capacity and Electric Net Generation (2018) [6]

In practical applications, the three main renewable energy generating technologies possess various advantages and some drawbacks.

Hydropower is a reliable and significant renewable power source, while its optimal utilization is challenged by geographical locations, capital investment and potential environmental impacts [10][11][12][13].

Wind energy is one of the least expensive energy sources, which makes it competitive with some conventional energy generation [14], however, it raises some concerns in terms of potential destruction to flying and gliding animals [15], and life cycle GHG emission [16]. The wind energy harnessing technology has an inherent peculiarity - larger turbines can capture higher wind power compared to the small turbine, making them much more efficient [17]. Due to this characteristic, the small-

scale wind energy generation system usually come with efficiency limitations, making them less cost competitive, which constraints vast deployment of small-scale wind generation systems [18].

Solar energy is harnessed by two main technologies: concentrating solar power (CSP) and photovoltaic (PV) solar [19]. Nowadays, CSP which utilizes solar thermal energy, are at the beginning of their commercial stage [20]. One of the merits of solar PV is its modular nature. Solar PV can be installed in urban homes to provide several kW output with a few modules or millions of panels can be used in MW utility-scale PV plant to support regional demand [21]. Solar PV technology is paving the way for various scale and dynamic energy applications.

Due to its geographical location, natural climate, financial incentives and the mature industrial capacity, California has became the leading state in the U.S. in the deployment of solar energy. Based on a report from the DOE [22], the cumulative solar capacity and annual solar capacity additions in California in 2018, reached 22,498 MW_{dc} and 2,913 MW_{dc}, respectively.

Beyond the reasons mentioned above, rising electricity prices coupled with the decreasing solar PV system prices, have driven the proliferation of solar energy use among residential and commercial customers [23]. Based on an EIA report, the electricity retail price has increased around 54% in last decade. While the PV module price has dropped 79% [24]. The renewable energy generating systems discussed in this dissertation belong to the PV technology type.

Many studies provide PV solar panel generation model, which is based on the Global Horizontal Irradiance (GHI) and other environmental variables including outdoor temperature [25][26]. Here a general photovoltaic generation model based on

maximum power point tracking is used. The solar panel system output power is given by Eq. 2-1

$$P_{pv} = C_{pv} F_{pv} \left(\frac{I_t}{I_{t,stc}}\right) \left[1 + \alpha_c \left(T_C - T_{C,STC}\right)\right] \quad (2\text{-}1)$$

where C_{pv} denotes PV rated power capacity (kW), F_{pv} is the de-rating factor, I_t is the solar radiation incident on the PV array in (kW/m^2), $I_{t,stc}$ represents the solar incident radiation at standard test conditions (STC) (1 kW/m^2), α_c is the temperature coefficient of power (%/°C), T_C is the PV array temperature (°C), $T_{C,STC}$ represents the PV panel temperature under standard test conditions (25 °C). The PV array temperature can be calculated by Eq. 2-2

$$T_c = T_a + \left[\frac{T_{c,NOCT} - T_{a,NOCT}}{I_{t,NOCT}}\right] I_t \quad (2\text{-}2)$$

T_c and T_a denote the panel temperature and ambient temperature, respectively. $I_{t,NOCT}$ indicates solar irradiation at nominal operating cell temperature (NOCT), which is taken to be 0.8 kW/m^2, $T_{c,NOCT}$ denotes the nominal operational cell temperature, which is generally 45°C to 47°C [27], $T_{a,NOCT}$ denotes the atmospheric temperature at NOCT condition, which is chosen as 20°C in this study. The weather data and irradiation information are obtained from the National Solar Radiation Database (NSRDB) [28].

The System Advisor Model (SAM) is a free software model developed by the National Renewable Energy Laboratory (NREL) for predicting the performance of various renewable energy systems and providing analysis of financial feasibility, which is used to evaluate financial and technical performance over a project's life for renewable energy deployment projects [29]. SAM utilizes hourly weather files in typical meteorological year (TM2, TM3) or NSRDB weather data to predict annual

performance of the solar system. The hourly solar energy prediction has been employed in this study.

2.2 ZBFB electrochemical process

The ZBFB shares many of the overall advantages of flow batteries. ZBFB also has its own advantages as well: 1) one of the longest cycle life battery among all batteries types (e.g. >10,000 cycles); 2) 100% depth of discharge (DOD); 3) Higher theoretical energy density (440Wh/kg); and, 4) a relative low cost of primary materials [30].

The ZBFB is a modular system comprised of a cell stack containing functional electrodes attached to the two current collectors (separated via membranes), electrolyte storage tanks, delivery pumps and pipes. The ZBFB relies on the electrolyte circulation system to deliver electrochemically active species to electrode surfaces in order to achieve charge transfer and cause electrical current to flow. The main electrolyte used in ZBFB is zinc bromide ($ZnBr_2$) dissolved to form an aqueous solution, with the same formulation being used in circulatory loops servicing both the cathode and anode during operation [31]. A simple ZBFB unit cell is illustrated in Figure 2-2, with multiple cell stacks combined in series to form a battery.

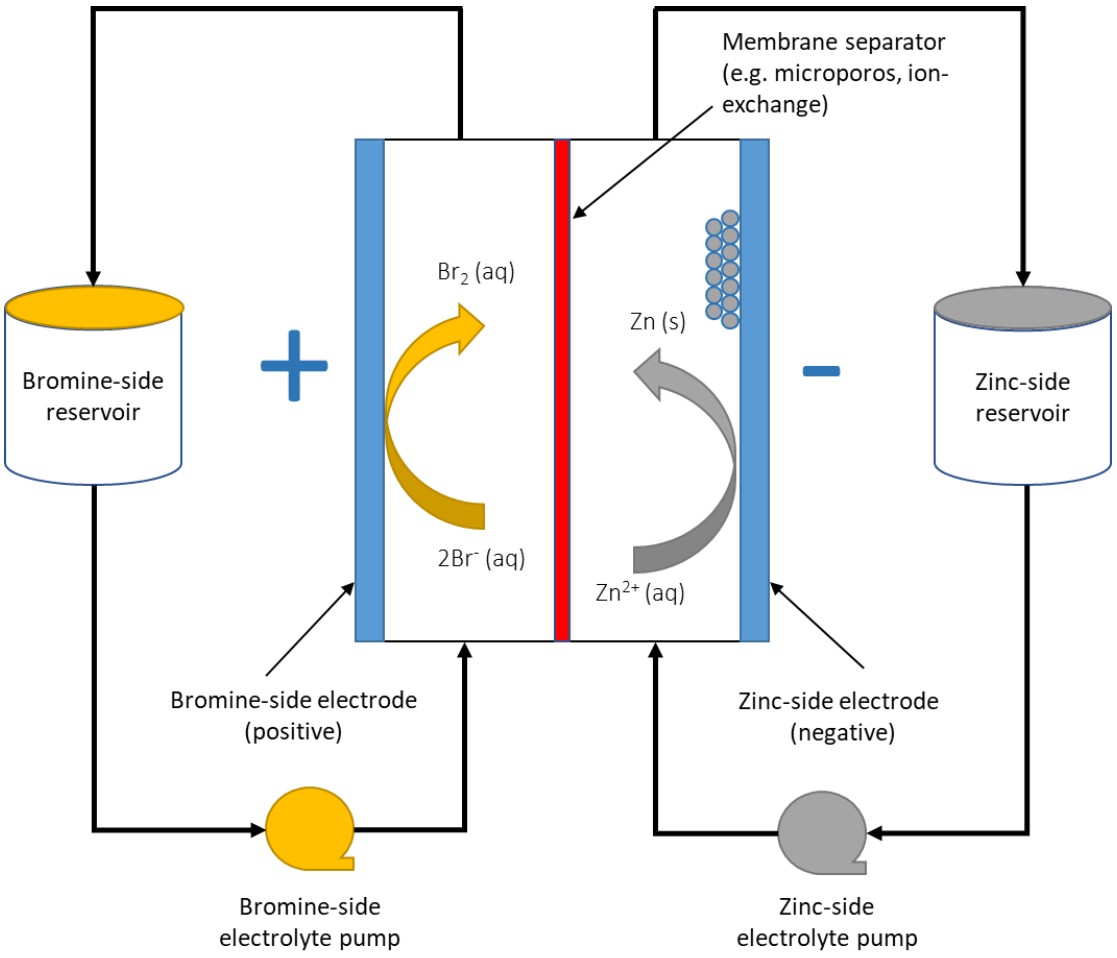

Figure 2-2. A basic ZBFB unit cell during charging process [31]

As shown in Figure 2-2, the zinc half-cell of the ZBFB behaves very similarly to an electroplating system. During the charging process, cationic zinc is removed from the aqueous solution to be deposited onto the negative electrode, as shown by Eq. 2-3:

$$Zn^{2+} + 2e^{-} \rightarrow Zn,\ E0 = -0.76\ V\ vs\ SHE \quad (2\text{-}3)$$

Meanwhile, bromide anions are converted to bromine, as shown by Eq. 2-4:

$$2Br^{-} \rightarrow Br_2 + 2e^{-},\ E0 = 1.08\ V\ vs\ SHE \quad (2\text{-}4)$$

And the overall battery electrochemical reaction is shown by Eq. 2-5:

$$Zn^{2+} + 2Br^{-} \rightarrow Zn + Br_2,\ E0 = 1.84\ V\ vs\ SHE \quad (2\text{-}5)$$

where SHE means standard hydrogen electrode and E0 is the reduction potential. During discharging process, zinc and bromide are generated at the respective electrodes [32].

In this dissertation, an innovative ZBFB system has been researched and evaluated. The new ZBFB utilizes an activated solid titanium electrode as the Zn plating surface, which allows for the use of a single flow loop of electrolyte as opposed to dual flow loops. This novel design also eliminates the need for an ion exchange membrane. This innovative design employs three main improvements [33]: 1) simplify the general zinc bromine flow battery structure with only one electrolyte tank, as shown in Figure 2-3, 2) improve the operating time of ZBFB without membrane exchange operation by using a solid titanium electrode, 3) provide higher energy density (3.1 kWh/ft^2) compared with traditional design (1.7 kWh/ft^2). Metallic electrodes are deployed in ZBFB due to their lower internal resistance, but it also results in higher costs and some degradation, such as corrosion or dissolution, which is detrimental to the long-term performance and operation of the flow battery [34]. Even though the novel ZBFB has very unique structure and comparatively higher energy density, the dendrite formation which is the main reason for the specific operational constraints of flow batteries, also applies to this ZBFB.

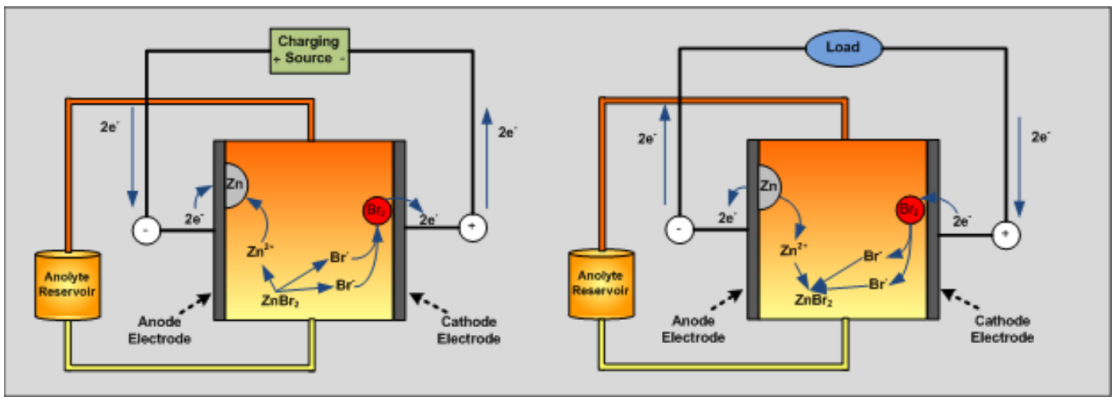

Figure 2-3. Schematic of a Zinc Bromine Flow Battery System [33]

2.3 ZBFB operational constrains

In this study, there are two notable constraints of ZBFB, which present new challenges compared with the well-known battery systems. The two operational constraints are: 1) constant charging power during charging period and 2) refresh operation after discharge cycle. The first constraint, restricts the battery to charging with constant power until the target state of charge (SOC) is reached. The second one is a unique process requirement for the ZBFB, forcing the battery to remain offline until the refresh process is completed. It is worth noting that both constraints are very unique requirements compared to other commonly used battery systems, like Li-ion battery or lead-acid battery systems.

The ZBFB stores and releases electricity though a reversible electrochemical reaction. The main electrolyte used in ZBFB is zinc bromide dissolved in an aqueous solution to form an electrolyte, with the same formulation being used in circulatory loops servicing both the cathode and anode during operation [31]. During charging process, zinc is deposited at the negative electrode, and bromine is produced at the positive electrode. The charging process stores chemical energy in separate locations, inside the battery block as zinc metal and outside the battery block in the electrolyte

tank [30]. During discharge, zinc metal oxidizes reforming the zinc ion and bromine is reduced to bromide ion, then the bromine is subsequently complexed with the organic poly-bromide in solution [35]. To improve the performance and cycle life of these batteries, this review paper provides fundamental information on zinc electrodeposition and summarizes recent developments in the relevant flow battery chemistries, along with recent applications. The future challenges and opportunities for this technology are discussed [36].

2.3.1 Dendrite formation

As mentioned above, the zinc is deposited at the negative electrode during the charging process. During this process dendrite formation of zinc is formed due to non-uniform distribution of active reacting species and charge density. The non-uniform conditions play a leading role in the formation of dendrites [37].

Dendrite formation does not only decrease the battery efficiency, but also damages the membrane and can reduce the distance between electrodes causing channel blockage and short-circuiting. Several research studies state that dendrite formation of Zn has become one of the biggest obstacles hindering its further commercialization [38] [39] [40]. Dendrite formation does not only impede the further utilization of ZBFB, but it is also common in other battery technologies, like the commonly used Li-ion batteries [41] [42] [43] [44].

Some research efforts have focused on improving the uniformity of zinc deposition and de-plating in ZBFBs during the charging and discharging phases, respectively [31]. Generally, the zinc dendrite formation includes an initiation and a growth stage. The over potential is the dominant factor for the initiation stage, while the initiation time and the deposition morphology of further growth are largely related

to the localized current density [45]. Published research study [46] reviewed the fundamental stages of dendrite formation in electrochemical reactions and their role in this process. Another study [47] confirmed the growth of zinc dendrite precursors in $ZnBr_2$ solutions and concluded that the propagation rate of the precursors was constant within the limits of the diffusion layer boundary. The report [48] studied the mechanism of dendrite growth and defined the critical current density and over-potential for dendrite tip growth, and divided the formation process into an initiation phase and growth phase. Another study [45] analyzed the initiation time of dendrites and concluded the initiation of zinc dendrites have relationship with over-potential, electrolyte concentration, and temperature. Other scientific reports have explored the dendrite formation from different perspectives such as the electrolyte, electrode, and battery properties. One research study [49] found the dendrite height is related to zinc loading, current density and electrolyte flow rate. Another research study [39] claimed the Br/Br^- redox reaction was coupled with the zinc deposition reaction, the uneven redox reaction on the positive electrode was accompanied by non-uniform zinc deposition and zinc dendrite formation, which degraded battery stability. The dominant strategies for preventing dendritic growth include reducing the concentration gradient of ions, eliminating the non-uniform localized current density, and changing the nuclear potential of zinc ions. Improving the electrolyte and electrode performance as well as managing the physical properties of the battery would be of great importance to the above-mentioned strategies [45].

Furthermore the researchers outline the distinctive operational requirements based on their unique updated ZBFB design. Other published research works [50] [51] concluded that the ZBFB battery needed to be charged with constant current density.

Another research report [52] required battery to be charged at constant current. Another study [53] employed the charging mechanism with constant electrolyte flow rate on positive and negative sides. However, one published study [54] claimed the battery should be charged at constant voltage. In this study, actual operation of the battery requires that the constant charging power is adopted.

2.3.2 Stripping operation

The nature of the dendrite formulation requires that the ZBFB should be completely discharged to prevent further dendrite growth and maintain the health of the batteries. The operating mode that requires that the ZBFB be periodically stripped to properly clean and maintain battery system is referred to as *refresh mode* (also *stripping mode* or *self-cleaning mode*). This is handled automatically by the Battery Manage System (BMS). However, this requires that the ZBFB is periodically taken offline [33]. In the current technology development state, the stripping operation maybe one effective method to release or eliminate the influence of dendrite formation.

Refresh operation is desirable to remove the deposited (plated) solid Zinc from electrode. This operation is repetitively forced by the BMS and to be initiated it needs a battery to be fully discharged [55]. During this process, the ZBFB is in an idle state, therefore it cannot respond to any requests from an outside controller. During refresh cycle, the battery system is disconnected from the output terminals, but the external energy source has to be connected to supply the circulation pumps and BMS controller. When using ZBFB as energy storage system, there are two big drawbacks. The first one, the ZBFB refresh mode must be scheduled or be carefully controlled to prevent conflicts arising from energy demand from the battery while operating in refresh mode. Although it is trivial and convenient for test batteries in the laboratory, stripping cycle

maybe be difficult to perform on every battery operating cycle in real applications. For instance, if ZBFB system needs to do a load-shifting during the workdays, this battery should operate at least five cycles without stripping cycle, because this battery must be required to provide energy to meet the local DRES load, whenever the system needs it [56]. The second disadvantage is the requirement of external energy to support system operation, which suggests ZBFB comes at higher capital investment cost and lower round-trip efficiency [57]. Refresh mode ensures that zinc is deposited on a fresh surface in the subsequent cycle, which is helpful to generate uniform and smooth electroplating on the electrodes' surface. However, the first new cycle efficiency would be slightly lower, due to the base coat of zinc being re-plated [30]. There are some research have been shown implement of refresh mode is very significant and general process in zinc bromine flow battery operating no matter in both laboratory experiment and practical applications [49] [56].

A published study [58] revealed the current efficiency (or coulombic efficiency) stays about 90% for each electrode after about 15 cycles without the need for electrode stripping. Yet another research study [59] claimed the standard zinc/bromine battery operating conditions consist of charging and discharging, followed by complete stripping of any zinc remaining on the anode. The refresh mode was important for the reproducibility of the battery operating cycles. The report [60] indicated that Zinc Bromine battery deploying one more period to strip the stacks of all zinc after SOC has reached 0%. Therefore, the battery system has the ability to operate to 100% depth of discharge on a daily basis, utilizing its full rated capacity.

There are several methods to implement the refresh mode in practical applications and simulations. First and most trivial is implementing refresh cycle after

every battery charge-discharge cycle. Some reports [33] [61] require that the batteries be completely discharged to prevent dendrite growth and maintain the health of the batteries. This requires that the batteries be periodically stripped to properly clean and maintain them. However, this requires that energy storage system periodically stay offline. The author [62] stated the stripping cycle is repetitively forced every 120 hours. One report [49] indicated the battery efficiency would decline after a number of cycles. Within a set of no-strip cycles, this efficiency loss is exhibited as decreasing capacity. A different report [63] indicated stripping procedure should be performed once every four or five full charge-discharge cycles. The author of another study [30] suggested ZBFB strip cycle should be performed after five operating cycles.

Considering the time battery is not available during stripping cycle, the question about how long should stripping cycle take is an important one to ask. One study [62] reported one complete maintenance cycle takes from 2 h up to as many as 20 h depending on the means of discharge. Another report [49] claimed this process needed more than 500 minutes. However, battery discharge would stop when reaching cut-off voltage, and since the battery should be fully discharged, the output voltage of the battery should be finally 0V. In order to further discharging battery energy to make battery voltage drop from cut-off voltage to 0V, one designed strip resistor should be connected with battery terminal. By doing so, the battery can fully discharge until it reaches 0V, while the stripping cycle time can be controlled [64].

One researcher claims that if the next generation of ZBBs is to have significantly better operating efficiencies, there is an imperative that electroplating and de-plating processes at the zinc-side electrode be fully understood and subsequently optimized to make significant improvement in electro-chemistry field [65].

2.4 Emission performance of DRES

There is no doubt that renewable energy generation holds the key in reducing the environmental impact of fossil fuels, and decreasing reliance on traditional energy sources [66]. While at the same time, energy storage systems have been touted as a promising solution for the intermittent nature of renewable resources, and therefore a valuable contribution towards broader utilization of renewable energy and distributed energy resource systems. For a hybrid system, end-users are not only focused on economic benefits of the system, but also its de-carbonization potential. Many studies have proposed renewable portfolio standards, requirement of GHG emission reduction. For example, Self-Generation Incentive Program (SGIP) provides incentive for GHG emission reduction, which requires qualifying prospective projects to achieve 5 kg CO2/kWh without significantly impacting energy bill saving [67]. Unfortunately, while renewable energy generation combined with storage system is effective in meeting electricity power demand and energy, it remains unclear how effective a hybrid system can be in reducing GHG emissions, under current market structure and grid-connected system.

There are two main operation mechanisms of energy storage that can cause increased emissions for grid-connected hybrid system [68]. The first is caused by the market electricity retail price incentives, which encourage users to charge the system during off-peak hours and discharge during peak afternoon or evening periods. In general, the marginal electricity generation during off-peak times is often produced by coal fired plants and the marginal generation during peak periods is produced by natural gas plants, which means that storage is effectively displacing cleaner natural gas-generated electricity with coal fired generated electricity. Using an average GHG

emissions factor for grid energy, when assessing the impacts of energy storage system, would ignore the difference of GHG emission rates associated with the grid energy used for charging and discharging at different times. Second, all storage technologies experience energy losses due to their internal resistance, defined by their round-trip efficiency. This inefficiency means that storage effectively loses some of the energy that it stores, requiring the system to store extra electrical energy, and consequently generate more GHG emissions related to these losses. These two characteristics of energy storage operation remain true, whether the storage system is operated with a revenue-maximizing goal in mind or operated with load-shifting or demand response goal in mind. But researchers have not yet agreed on which one of them plays the primary role in the emission process [69] [70].

Prior research has focused on the economic benefits of storage systems, which emphasize revenue-maximization or cost of energy minimization, without concern for the GHG emissions effect. As the result, the utilization of energy storage could increase the hybrid system's overall CO_2 emission level [71]. The study examines the social benefits provided by energy storage systems on the Texas electricity market with quite limited renewable penetration. Under current storage technologies' limitations, utilizing battery would increase daily CO_2 emissions [72]. The study simulates the emissions impacts of wind generation paired with energy storage, within a market-based electric power system. Another research study indicates that storage can have a negative impact on GHG emissions [73]. One research study tested the role of residential energy storage system in GHG emissions. The grid-connected residential energy storage system operated under either optimizing economic benefit mode or GHG emission reduction mode. Residential energy storage system mostly increases

GHG emissions when users seek to minimize their electricity cost. However, when the system was operated in minimizing GHG emissions mode, the system could reduce average emissions by 2.2−6.4% [74]. This study provides optimized schedules of plug-in electric vehicle charging, for either standard or vehicle-to-grid use, which were compared with charging schedules to characterize the potential for GHG emission reductions across charging characteristics, regional driving, and marginal energy generation trends. It determined that optimized charging could reduce CO_2 emissions [75]. Utility-scale energy storage provides operational flexibility for managing electricity demand, integrating renewable energy, and improving system reliability. However, it has been established that revenue-maximizing utility-scale energy storage tends to increase system GHG emissions in the current US electricity grid [76]. One study found that the impacts of adding energy storage are highly case-dependent. In electric distribution systems with high renewable generation penetration levels and significant renewable curtailment, adding energy storage reduces GHG emissions; in other systems, the impacts on emissions could be positive, neutral, or negative [77].

Furthermore, ignoring of the environmental impact of hybrid system consisting of renewable energy generation and storage system is incompatible with the original purpose of renewable energy resources. A research article [78] proposed a control scheme, which deploys energy storage to perform load-shifting in a medium scale microgrid network. Simulation results prove that the proposed control scheme can improve annual profits from 4.3% to 24% of the annual cost without storage. Meanwhile, this control strategy can yield positive impacts on GHG emissions. The research paper establishes a bi-level optimization model for optimizing dispatch of thermal units and the demand side's reaction while considering energy-saving and

emission-reduction potentials on generation and demand sides [79]. One methodology is presented to implement electric thermal storage (ETS) with hydro-electric and wind resources to meet load growth in isolated grid networks. ETS when properly controlled and dynamically responsive on the smart grid, is found to be effective in reducing diesel consumption, and thus GHG emissions [80]. At the current electricity market state and the pursuit towards maximizing economic benefits, the hybrid microgrid system comprised of energy storage is more likely to increase GHG emission. However, when taking GHG emissions into consideration during microgrid control, one has to consider the microgrid system design problem.

3. REAL-TIME CONTROL OF FLOW BATTERY FOR PREVENTING MINIMUM IMPORT VIOLATION

3.1 Introduction and background

Due to increase of electricity retail prices and environmental impact of fossil fuels, renewable energy sources are becoming more popular among end user. However, incorporating renewable power sources into the existing electricity grid is challenging, due to the variable and uncontrolled nature of many renewable sources. With continual renewable energy deployment growth, the utility companies and grid operators employ various regulation methods aimed to maintain the main power grid resilience and stability. California Rule 21 is one such example of regulatory guidelines. According to Rule 21 non-export agreement requirements [81], self-generating utility customer should import a minimum of 5% of nominal total generation capacity power from the grid. Whenever this requirement is not satisfied, the utility company considers the event a minimum import violation. The consequences of such import violations are decoupling the connection between customer and the on-site renewable generation from the utility grid. The use of electrical energy storage (EES) could be one solution to this issue, by absorbing energy during import violation.

The Victor Valley Wastewater Reclamation Authority (VVWRA) located in Victorville, California, provides wastewater treatment for an area populated by nearly 400,000 residents. Wastewater treatment is an energy intensive process. VVWRA has an average power demand of more than 1 MW and its annual electric energy consumption exceeds 9,000 MWh. In accordance with VVWRA's vision for environmental preservation, sustainable energy future, affordable and predictable energy costs, the authority deployed two onsite 800 kW biogas Combined Heating and

Power (CHP) generators [82]. The CHP generators utilize biogas that is produced as a by-product of the wastewater treatment process to generate energy and offset the majority of their electrical energy needs. To accommodate future facility expansion and related forecasted increase in energy consumption the onsite power generation capacity is more than the average load demand of the entire facility. Therefore, VVWRA receives power from two sources: 1) onsite biogas CHP generators, and 2) Southern California Edison (SCE) utility company. Based on the definition of minimum import violation discussed in the previous section, for VVWRA, the minimum import violation is triggered when imported power from SCE drops below 80 kW for more than 2 seconds. The consequences of a violation are an automatic decoupling of the onsite CHP generators and a portion of the facility's wastewater treatment equipment from the grid. This results in a temporary power loss to critical equipment, followed by increased grid power import, demand peak, and flaring of unused biogas, as well as the discarding of water that was in the process of being ultraviolet (UV) treated.

In order to effective preventing the import violation, one energy storage system has been decided to implement to increase load or absorbed renewable energy to solve this issue. The ZBFB, one member of RFBs, has become more appealing and promising candidate due to its high energy density, high cell voltage and use of abundant and low-cost materials [83] [84]. One of the great benefits of the ZBFB as a potential future low-cost EES is the low cost of electrolyte. Both bromine and zinc are common chemical materials, already manufactured at industrial scale [85] [86]. In this study, an innovative flow battery is utilized as the battery energy system to prevent the minimum import violations. Unlike conventional flow batteries that use two low loops (two tanks, two pumps) interacting across a set of membranes, this new type flow battery uses activated

solid titanium electrodes, and a system design with a single flow loop without membranes [87]. The aforementioned improvements greatly reduce both system and operating costs, enabling longer system life and improved energy density [88]. In general, flow batteries are a promising battery energy storage system solution, which have inherent advantages due to their chemistry, including 1) one of the longest cycle life among all battery types; 2) the ability to independently scale energy and power characteristics; 3) good energy density characteristics for stationary applications; and, 4) a broad operating temperature range. According to a report by the International Renewable Energy Agency (IRENA) [89], by 2030, the cost of flow batteries is expected to decrease to one third of its current cost, to a range about $300/kWh along with a cycle life of about 10,000 cycles.

The VVWRA system layout is shown in Figure 3-1. The VVWRA system consists of two onsite biogas CHP generators, two ZBFB packs, and an Energy Management System (EMS) controlling the flow battery.

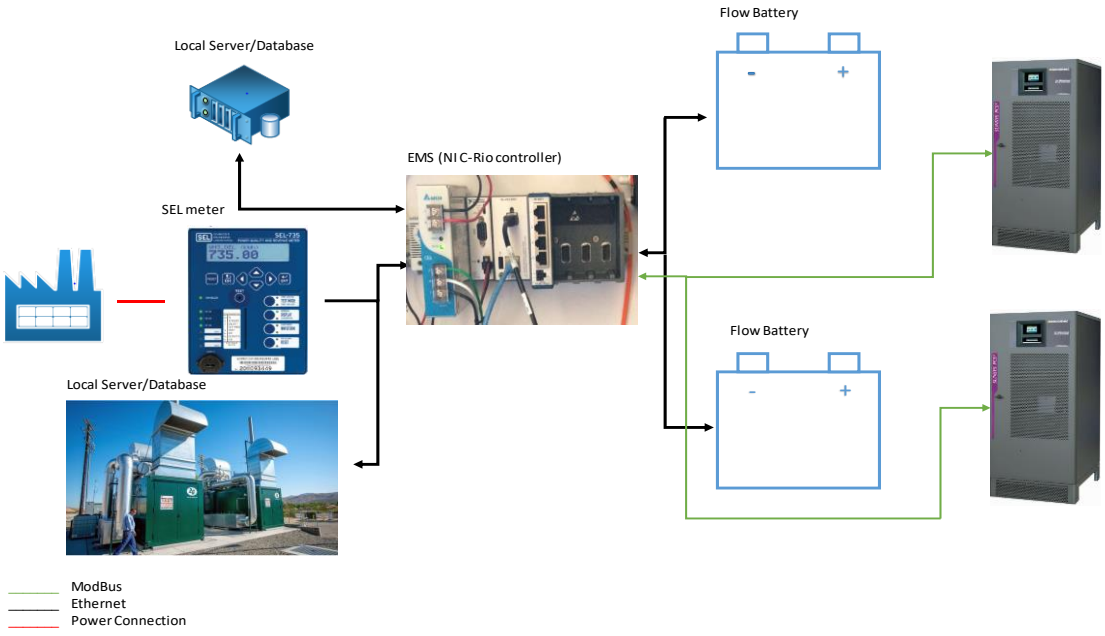

Figure 3-1. VVWRA System Layout

The EMS acquires and archives the flow battery system status data and SCE power import measurement data through TCP/IP. A Schweitzer Engineering Laboratories (SEL) meter SEL-735 provides SCE imported power measurements at 10 Hz. Each of the two flow battery packs, consists of four flow batteries and is rated at 100 kW/500 kWh. In order to efficiently integrate the flow battery and EMS with the onsite CHP generators, the CHP control algorithm is modified by changing SCE import power threshold values.

3.2 Problem statement

To avoid minimum import violations, the onsite CHP generators employ control logic through Programmable Logic Controllers (PLCs). The PLCs employ real-time SCE imported power measurements to adjust CHP generator output power in response to load fluctuation. However, due to the slow response rate of generator power output (1 kW/s), the PLC control strategy employs a buffer of 120 kW. The threshold value triggering a decrease in output power is 200 kW, while the import power value triggering the increase of the generator output is 250 kW. For example,

(i) If imported power < 200 kW, generator ramps down at 1 kW/s,

(ii) If imported power > 250 kW, generator ramps up at 1 kW/s,

(iii) If 200 kW ≤ imported power ≤ 250 kW, generator maintains its output.

The range from 80 kW to 200 kW for the imported power is used as a power buffer. While for the most part, this power buffer provides the ability to respond to rapid load fluctuations, at the same time, it also decreases the utilization of biogas generated power and leads to the underutilization of biogas. However, if the generator trigger set points are shifted from 200 kW and 250 kW, down to 150 kW and 200 kW (respectively), it would not only result in a power import reduction of 50 kW (up to 400

MWh per year), but also increase the renewable energy usage. Minimizing the power buffer could bring more benefits from economic and environmental perspectives.

Based on the previous discussion, the primary purpose of this study is to prevent the minimum power import violation. Although there are efforts in doing this via biogas generators implemented Programmable Logic Controllers, the ZBFB as energy storage system coupled with the two onsite biogas generators could be more beneficial. Through controlled battery system charging power $P_c(i)$ and discharging power $P_d(i)$ to prevent the minimum power import violation, the plant can increase renewable energy utilization by reducing power buffer and directly utilizing renewable energy.

3.3 Control algorithm

3.3.1 ZBFB constraint

In general, ZBFB has various advantages such as long cycle life, good energy density, a broad operating temperature range, and independently scalable energy and power characteristics. Nevertheless, some limitations for all flow battery chemistries exist, such as high self-discharge rate during dwell, the requirement for auxiliary systems for electrolyte circulation and temperature control, and relative low energy conversion efficiency [90]. Apart from the merits and disadvantages mentioned above, a specific set of operational constraints are used in this project, as listed below:

During charging period, the charging power P_c:

$$P_c = \begin{cases} bc, & 0\% \leq SOC \leq 75\% \\ 0, & otherwise \end{cases} \quad (3\text{-}1)$$

where *bc* denotes the value of charging power, which is one constant value, indicated by negative number $bc \in R^-$. During this period, the battery must be charged to 75% SOC before switching to another working mode.

During discharging period, the discharging power P_d:

$$P_d = \begin{cases} bd, & 25\% \leq SOC \leq 75\% \\ P_{max}, & SOC \leq 25\% \end{cases} \quad (3\text{-}2)$$

where *bd* denotes the value of discharging power, indicated by positive number $bd \in R$. *bd* can be any value, even negative value, which means ZBFB can be charged in a short time in discharging period.

After each full charge-discharge cycle, it is recommended that the flow battery completes a refresh cycle, which is intended to fully remove the residual Zn plating from the Ti electrodes. The refresh cycle is commanded by the Battery Management System (BMS). During the refresh cycle, the BMS takes control over the battery. At this stage, the flow battery neither receives nor responds to any external commands.

3.3.2 Mixed integer linear programming control algorithm

The primary purpose of this study is to prevent the minimum power import violation, while at the same time, to increase renewable energy utilization. The presented approach allows for the implementation at VVWRA site, by utilizing the onsite biogas CHP generators in combination with the energy storage capacity of the flow batteries. The control algorithm principle for VVWRA focuses on maintaining the SCE import power above 80 kW, while reducing the power buffer, as shown in Figure 3-2. The EMS, employing this control algorithm, commands the flow battery charging/discharging power based on the SCE import power measurement data [91].

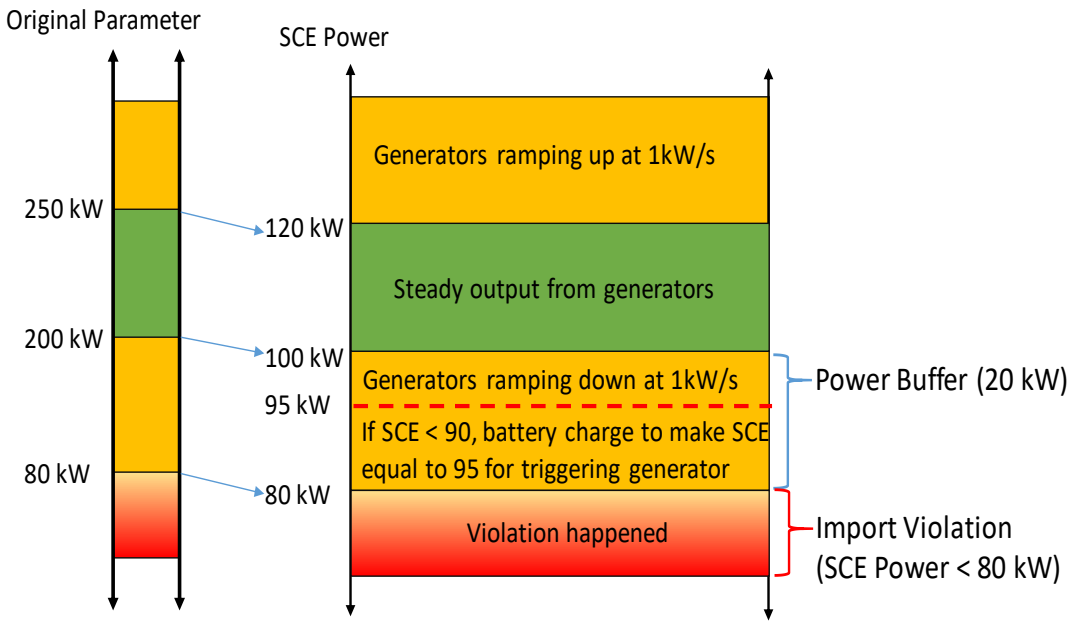

Figure 3-2. Proposed Control Algorithm targets

In order to prevent minimum import violation, battery pack is required to absorb a sudden drop in facility load, indicating the battery should be charged at the moment of import violation. However, the intermittent change of the facility load demand is unpredictable and irregular. A ZBFB with an operational requirement of keeping the charging rate constant and refresh mode could not support the continuously changing and fluttering power flow. The ZBFB offers more flexibility in discharging mode, where the battery could switch from discharging mode to charging mode briefly. While switching from discharging to charging mode, a larger drop in net load power could be addressed. With two or more systems, while one ZBFB is being charged or refreshed, the other is be discharged, the system limitation due to refresh cycle and constant charging period, respectively, can be effectively eliminated or reduced. Considering there are two ZBFB packs, while one is in the charging mode, the other one must stay in discharging mode. Due to the flexibility of the discharging battery, the whole system

can provide a more complexed solution and respond to a wider range of load variation. One drawback of this design is that it while one ZBFB stores the renewable energy, the other one releases it, which leads to decreased system energy efficiency due to losses.

To ensure that one battery pack is always available to absorb a sudden drop in facility load without triggering a minimum import violation, the algorithm operates two battery packs in opposing modes. This approach is used to balance the facility net load by adjusting the discharging rate to maintain the minimum power import requirement. The developed real-time battery control scheme consists of four battery operation stages described in detail below. They are 1) charging stage; 2) discharging stage; 3) pre-refresh stage; 4) refresh stage. One operational challenge is the requirement for the two ZBFB systems to interchange their working instantaneously. The proposed mothed posed a challenge on operating time:

$$t_d \geq t_c + t_{preR} + t_{ref} \quad (3\text{-}3)$$

where t_d denotes the time of discharging stage, t_c denotes the charging stage time, t_{preR} denotes the pre-discharging stage time, t_{ref} denotes the refresh stage time. In order to provide the power support for whole time period, the time of discharging stages should be stay online longer than the other three stages. And those time variables are related with the ZBFB parameters. Taking the charging stage time as example is shown in Eq. 3-4

$$t_c = \sum_{i=1}^{n} \frac{W}{P_c(i)} \quad (3\text{-}4)$$

where W denotes the ZBFB capacity, which is equal to 500 kWh in this study. $P_c(i)$ denotes the charging power rate, which is constant value in the range between -100 and 0. Based on the above function, Eq. 3-3 could be re-written in Eq. 3-5

$$\frac{0.5W}{P_d} \geq \frac{0.75W}{P_c} + \frac{0.25W}{P_{preR}} + 0.5 \quad (3\text{-}5)$$

where discharging stage operates in the SOC range between 25% and 75%, which only accounts for half of ZBFB's energy storage capacity. The charging stage operates in the SOC range between 0% and 75%, which only accounts for 75% of ZBFB's energy storage capacity. Additionally, the pre-refresh stage operates in the SOC range between 0% and 25%, which only account for 25% of ZBFB's energy storage capacity. Finally, the refresh mode needs half hour to complete this stage. After substitution and simplification, the relationship between P_c and P_d is derived in equation 3-6.

$$P_d \leq \frac{2}{3} P_c \quad (3\text{-}6)$$

Taking into account the ZBFB round trip efficiency of 70%, the charging power rate is set to -86 kW, and the discharging power is set up to 40 kW. The more details about this algorithm are provided in following sections.

3.3.2.1 Charging Stage

Following initialization, the EMS chooses the battery pack with the lower SOC as the discharging pack (see discharging stage below). The other pack acts as the charging battery pack in the charging stage. There are three scenarios for the battery pack working in the charging stage:

The charging power is maintained at -86 kW constant rate until the SOC reaches the upper limit 75% (a negative power value represents charging, while a positive value represents discharging).

$$P_c(i) = -86, \ (0\% \leq \mathrm{SOC}_i < 75\%) \quad (3\text{-}7)$$

The charging power progressively increases at 1 kW/s until it reaches 0 kW, allowing sufficient time for the CHP generators to decrease power output, after the SOC

reaches 75%. This averts a sudden drop in SCE import power that could be caused by the instantaneous increase in charging power from -86 kW to 0 kW.

$$P_c(i) = P_c(i-1) + 1, \ (\mathrm{SOC}_i < 75\% \text{ and } P_c(i-1) < 0) \quad (3\text{-}8)$$

When the charging pack SOC is beyond 75% and the charging power reaches 0 kW, the battery pack is kept in standby mode until the discharging battery pack is ready for the pre-refresh stage. At this point, the charging battery pack will transition to the discharging stage and assume the role of the discharging battery pack.

$$P_c(i) = 0, \ (\mathrm{SOC}_i < 75\% \text{ and } P_c(i-1) = 0) \quad (3\text{-}9)$$

3.3.2.2 Discharging Stage

As mentioned above, the discharging stage is the critical stage, which regulates the total output of the flow battery system to guarantee that the SCE import power is maintained above 80 kW. Considering the restricted power operation range and energy capacity, generators need to play an active role in the facility net load regulation process [92]. When a potential import violation is detected, the total flow battery system output is adjusted to trigger the onsite biogas CHP generators to ramp down their output. The discharging stage contains four phases shown in Figure 3-3.

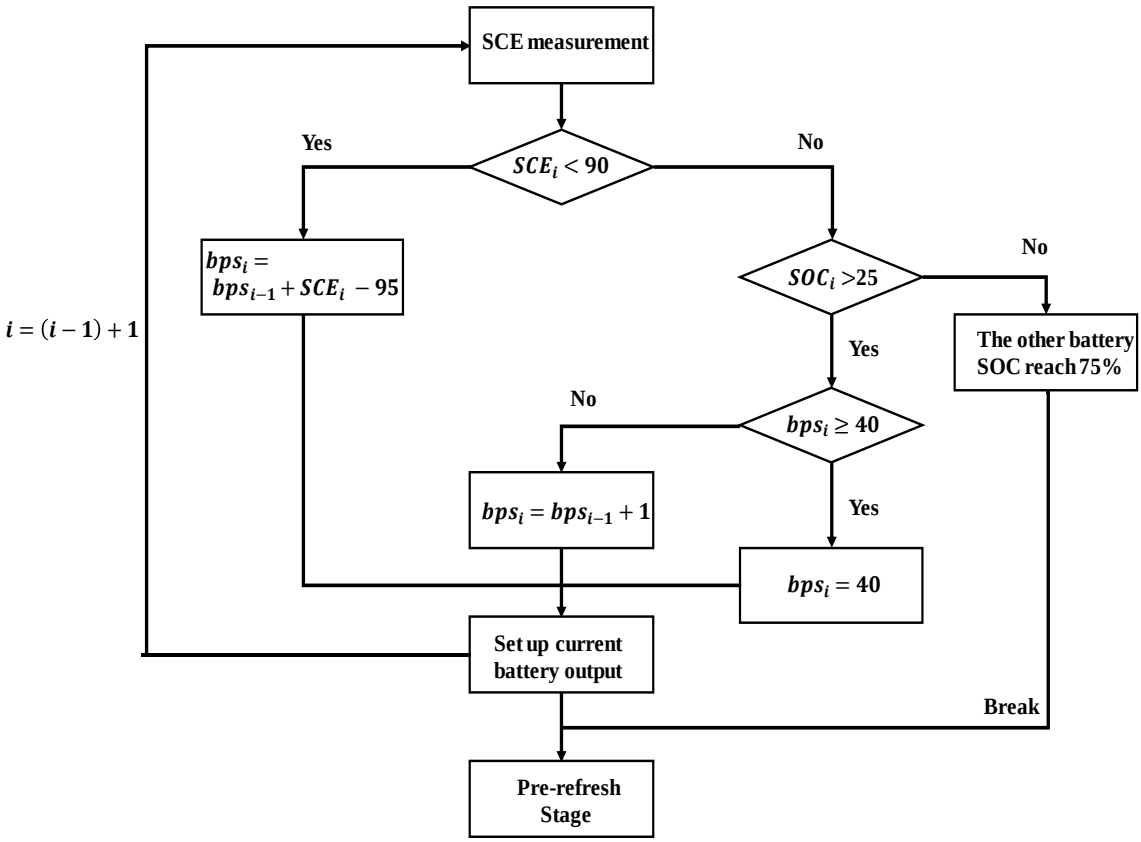

Figure 3-3. Discharging Stage Scheme

If the SCE import power is less than 90 kW (potential import violation threshold), the discharge power is adjusted to guarantee SCE import power reaches 95 kW. Meanwhile, the onsite biogas generators power production ramps down;

$$P_d(i) = P_d(i-1) + SCE(i) - 95,\ (SCE(i) < 90\ \text{kW}) \quad (3\text{-}10)$$

If SCE import power is more than 90 kW, the discharging battery maintains discharge power at 40 kW;

$$P_d(i) = 40,\ (SCE(i) > 90\ \text{kW} \cap \text{SOC}_i \geq 25\% \cap P_d(i-1) = 40) \quad (3\text{-}11)$$

If SCE import power and generator power output are within steady state range, while discharging power is less than 40 kW, the discharging power is programmed to increase at 1 kW/s rate

$$P_d(i) = P_d(i-1) + 1,$$

$$(SCE(i) > 90 \text{ kW} \cap \text{SOC}_i \geq 25\% \ \cap P_d(i-1) < 40) \quad (3\text{-}12)$$

When the discharging battery pack SOC reaches the discharging stage lower limit of 25%, the discharging battery pack will transition to pre-refresh stage, while the charging battery pack will switch to discharging stage.

3.3.2.3 Pre-refresh Stage

When the SOC of the discharging battery pack reaches 25%, while the SOC of the charging battery pack reaches the 75%, the discharging pack is ready to transition to pre-refresh stage and the charging pack switches to the discharging stage. The battery pack in pre-refresh stage will continue to discharge at a 100kW power rate. In this stage, the two battery packs exchange their working modes, where the original discharging pack gets into the pre-refresh stage, while the charging pack switches to the discharging stage. Therefore, there is always one battery working in the discharging stage, ensuring that the flow battery system output can compensate for fluctuations in the facility load and maintain SCE import power above 80 kW.

3.3.2.4 Refresh Stage

When the SOC of the battery in the pre-refresh stage reaches 1%, the battery BMS will send out the requirement “Refresh is needed”. If the system is in steady sate, i.e. SCE import power is more than 100 kW and onsite generators provide constant output power, the EMS will send a binary value 1 to the BMS. The BMS will take over control of this battery pack until completion of the refresh phase.

The control algorithm is presented in more detail and more intuitively in Figure 3-4. The graphs show two battery systems running in opposing charging/discharging cycles. As shown in Figure 3-4, battery 2 works in discharging mode initially. The discharging pack reduces discharging power to increase total net power demand, thus

preventing the minimum import violation. When a rapid load fluctuation happens, the discharging battery pack can shift into charging mode for further power demand increase. Meanwhile, battery 1 works in charging mode initially, and transfers into standby status until the discharging battery pack is ready to transition into the pre-refresh stage. The battery pack in the pre-refresh stage discharges at 100 kW, until fully discharged, while the charging battery pack switches to the discharging stage.

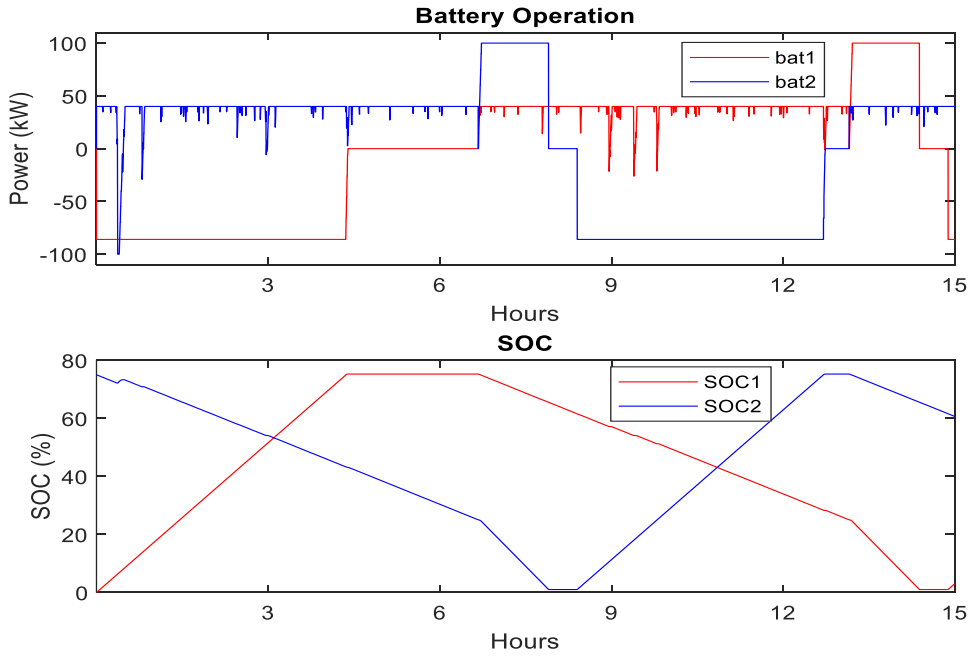

Figure 3-4. Flow Battery Simulation Output Profile

3.4 Simulation and result

This section presents numerical simulations to verify the effectiveness of the proposed control algorithm for preventing minimum import violations with different scenarios, which are based on the following three scenarios with different configurations and parameters of the system. These three scenarios stand for different methods for the primary purpose of this study.

Scenario 1: onsite biogas generators

With respect to scenario 1, the onsite biogas generators are utilized to prevent the minimum import violation. The biogas generated as byproduct of wastewater treatment has been full used to support the local electricity energy needs, while their operation logic is aimed to prevent the minimum import violation. The simulation results are shown in Figure 3-5. In Figure 3-5 (a), the profile of load and generation appear to be of similar magnitude. Figure 3-5 (b) shows the average import power keep in the range between 200 kW and 250 kW, but there are several times when import violations occurred, that is indicated by lower than 80 kW line.

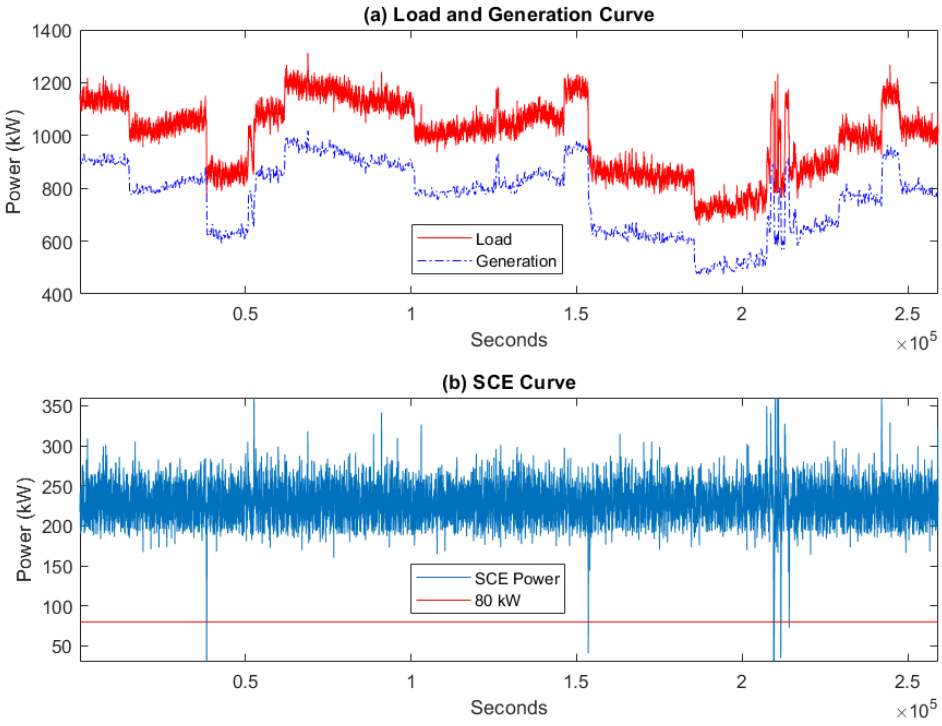

Figure 3-5. Simulation of control algorithm scenario 1.

The main limitation in utilizing only the onsite biogas generators for preventing import violation is obvious. The onsite biogas generators have large power capacity, but the rate of power change is too slow, and therefore they cannot respond quickly

enough to the sudden drop of local load. As seen by the first two import violations shown in Figure 3-5. More details are shown in Figure 3-6. Figure 3-6 (a), (b) indicated the first violation condition, Figure 3-6 (c), (d) indicated the second violation condition. SCE power value less than 200 kW triggered generators to ramp down the output, to increase the net load. However, the response rate is too slow and cannot match up the rate of change of the load.

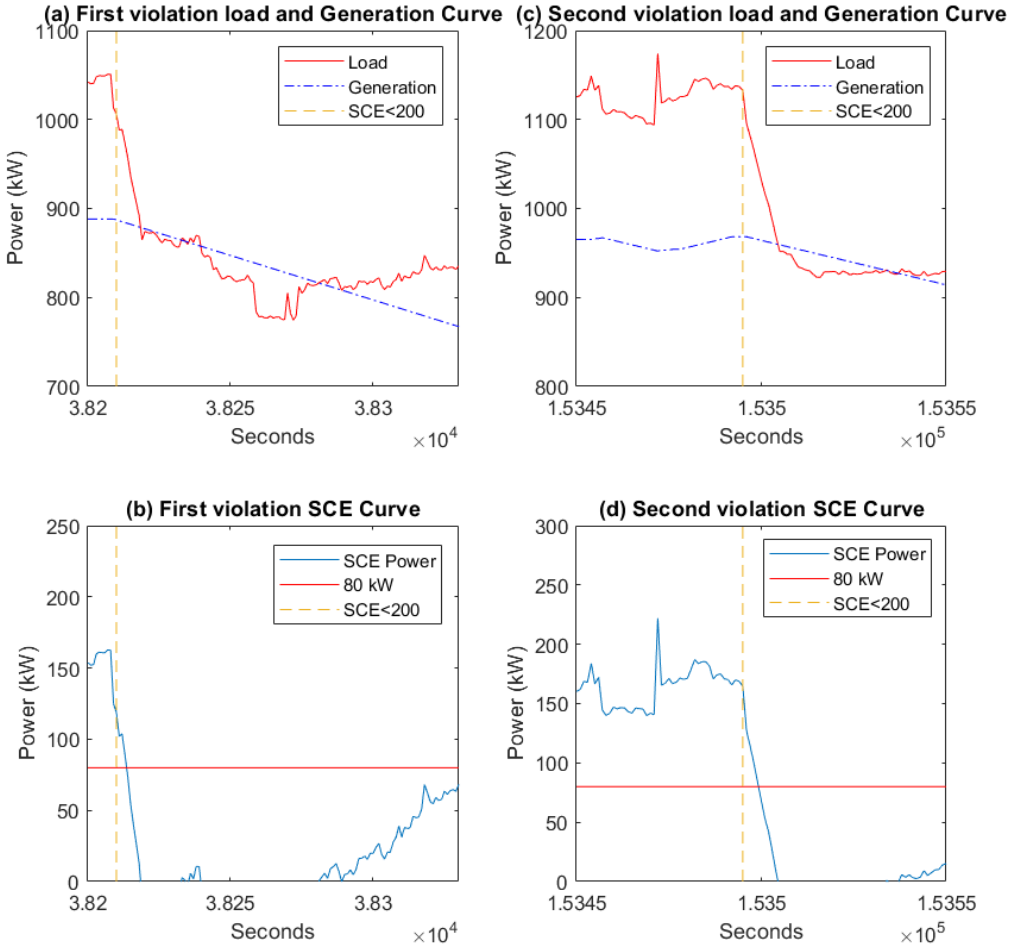

Figure 3-6. Conditions analysis of two violation examples (scenario 1)

Scenario 2: ZBFB assisted with biogas generators

With respect to scenario 2, one ZBFB is utilized to assist onsite biogas generators to prevent the minimum import violation. ZBFB stores biogas energy whenever SCE power drops below 120 kW. Due to the constant charging power constraint and in agreement with maximizing the absorbed power capacity, the maximum charging power of -86 kW is deployed when SCE power is triggered. During the discharging period, the battery can switch from charging to discharging mode quickly. This control scenario fully utilizes this characteristic to avoid the import violations.

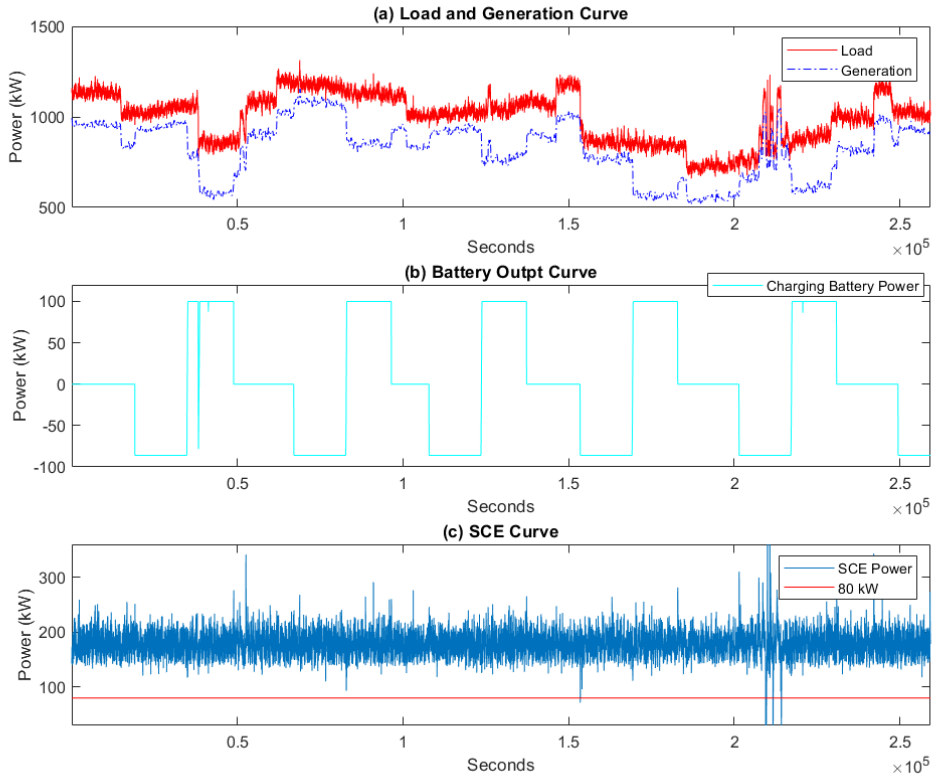

Figure 3-7. Simulation of control algorithm scenario 2

The simulation results of scenario 2 are shown in Figure 3-7, where Figure 3-7 (a) denotes the profile of load and generation, Figure 3-7 (b) shows the ZBFB power

profile. With the use of ZBFB in scenario 2, the generator trigger threshold has been modified to 150 kW and 200 kW. As the result, Figure 3-7 (c) shows import power is kept in the range between 150 kW and 200 kW. However there are still several times when import violation happened, that is indicated by lower than 80 kW line.

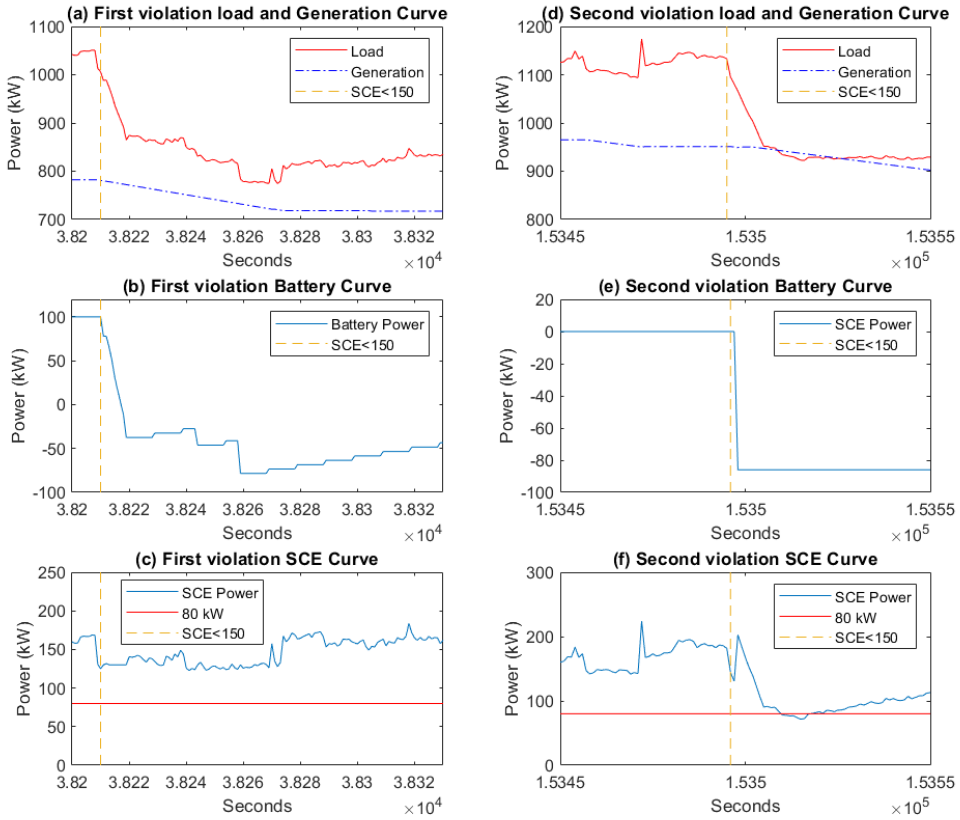

Figure 3-8. Conditions analysis of two violation examples (scenario 2)

The same time period data have been taken for analysis in Figure 3-8. Due to SCE power not dropping below 120 kW, the ZBFB stays in idle state. Figure 3-8 (a), (b), (c) show when SCE trigger is reached (38210 time index), ZBFB works in discharging mode to provide the negative power to prevent the import violation. Figure 3-8 (d), (e), (f) show, although the SCE trigger signal is sent to ZBFB, and ZBFB begins to absorb the renewable energy, the maximum constant charging power rate combined

with slow response of the biogas generator are no match for the sudden change in load power. However, in spite of violation occurrence, there are some improvements with scenario 2 compared to scenario 1.

Scenario 3: Proposed control algorithm with two ZBFBs and biogas generators

The proposed control algorithm with two ZBFBs combined with onsite biogas generators has been discussed in detail in previous sections. Here, Figure 3-9 details the control algorithm simulation results, and provides one use case to explain the two ZBFBs working patterns.

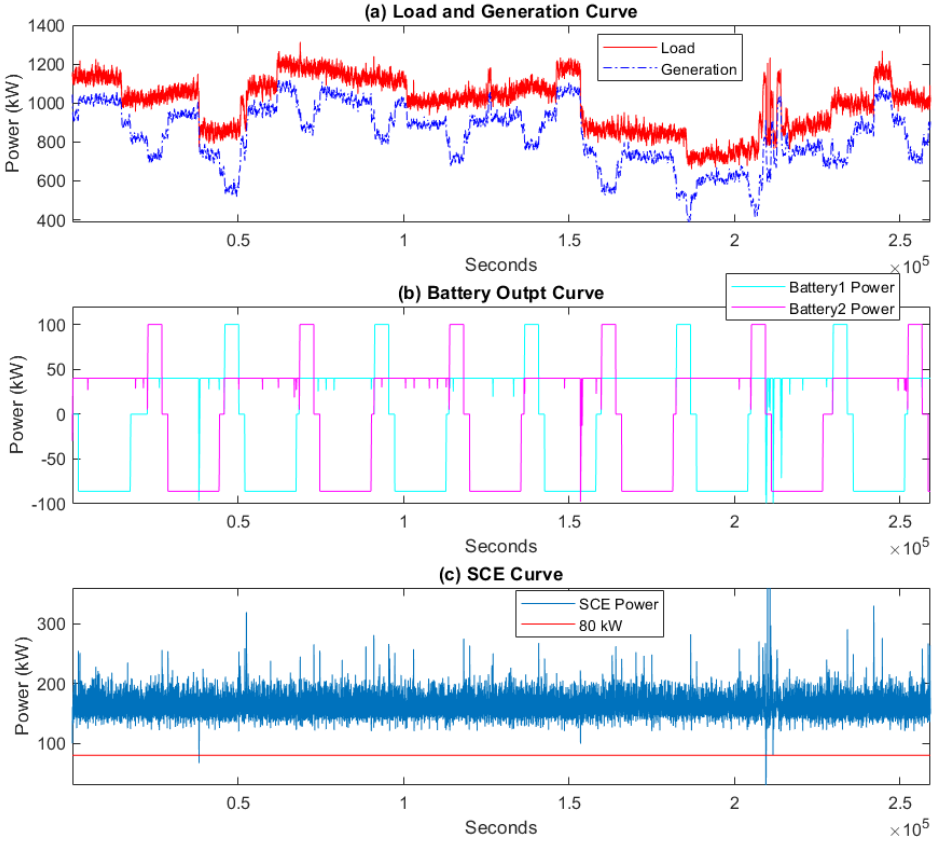

Figure 3-9. Simulation of control algorithm scenario 3.

The same time period data have been taken for analysis for the proposed control algorithm as in scenario 1 and 2, and are shown in Figure 3-10. In order to compare the simulated results between scenario 2 and proposed control algorithm in scenario 3, the same biogas generators trigger value has been adopted, which starts at 150 kW, while the battery response trigger has been set to 120 kW. Figure 3-10 (a), (b), (c) show when the SCE trigger is reached (38210 time index), the generator ramps down the output to increase net load in Figure 3-10 (a), ZBFB 2 works in charging mode, which provides the constant -86 charging power, while the ZBFB 1 remains in the discharging mode. However, not enough power is absorbed to compensate for the demand drop Figure 3-10 (b). As data show in Figure 3-10 (c), one violation ocurred.

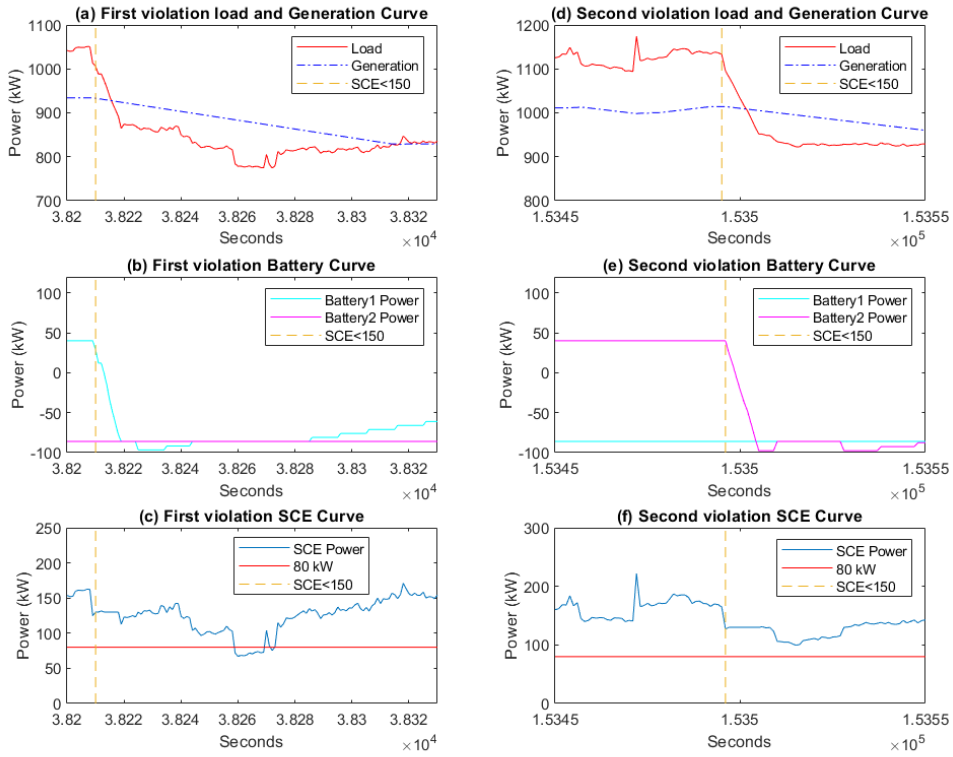

Figure 3-10. Conditions analysis of two violation examples (proposed control algorithm)

Figure 3-10 (d), (e), (f) show when the SCE trigger is reached (153458 time index), the generator ramps down the output to increase net load, as seen in Figure 3-10 (d). During this time, ZBFB 1 works in charging mode, while the ZBFB 2 is in discharging mode. Comparing scenario 3 results to results in Figure 3-6 and Figure 3-8, more renewable energy has been utilized with the proposed algorithm. One benefit is the load drop gap is smaller, since ZBFB 2 could provide enough power to offset the power deficit as seen from Figure 3-6 (e). Thus on violation has been eliminated in Figure 3-6 (f). In spite of violation occurring with scenario 3, there are some improvements compared to scenarios 1 and 2. Although this violation happened with the proposed control algorithm in scenario 3, it did not occur in scenario. This does not indicate that scenario 2 is better than scenario 3. However, the advantages of scenario 2 and 3 are hardly distinguishable in these two examples.

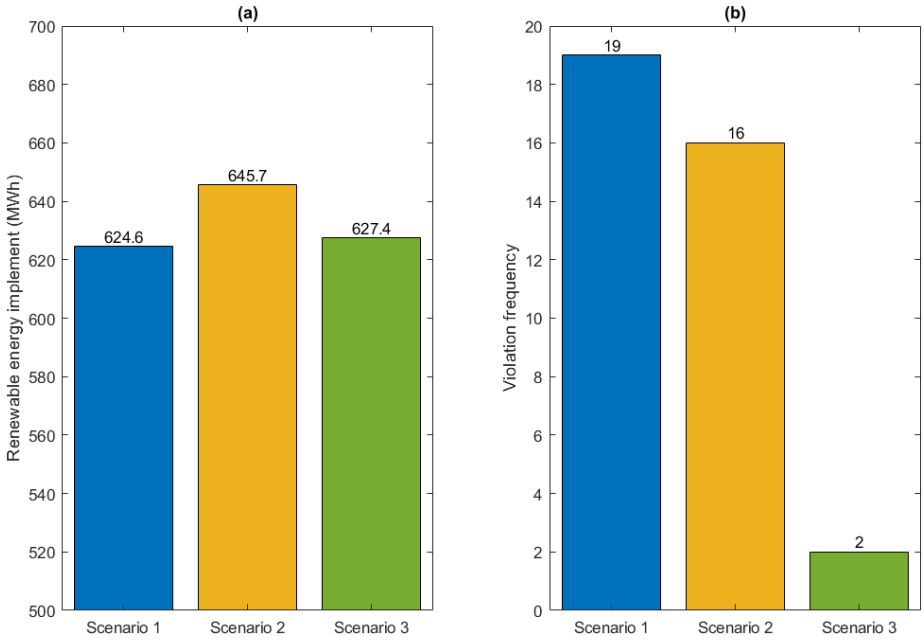

Figure 3-11. Simulation result comparison for 3 control scenarios

One month simulation is introduced to check the long term performance of various control scenarios, as shown in Figure 3-11. The minimum import violation is the primary target in this study. In terms of preventing import violation, the proposed control algorithm outperforms the other two scenarios.

However, the proposed control algorithm improved results a little compared to scenario 1. This can be attributed to the two ZBFBs always working in the charging stages alternately, which is equal to absorb the biogas generation. Although the onsite renewable generation and utilization is higher with the proposed control algorithm than the other two (indicated in Figure 3-6 (c), Figure 3-8 (d) and Figure 3-10 (d)), the increment of available renewable generation for proposed control algorithm with ZBFB consumption is limited.

3.5 Conclusion

The objective of this study is to design and deploy a real-time battery control algorithm utilizing a flow battery for the VVWRA facility to deal with minimum power import violations, while maximizing renewable energy utilization. The proposed control algorithm consists of four operational modes: charging, discharging, pre-refresh, and refresh. Through the combination of two flow battery packs working in opposing modes the system can: 1) absorb more power from the grid when there is the potential for a minimum import violation; 2) realize increased renewable energy generation by reducing the facility load power buffer; and, 3) leverage the inherent rapid power adjustment capability of the flow battery to compensate for the slow response of CHP generator output. This intuitive real-time control algorithm could not only significantly curtail the frequency of minimum power import violations, from the 19 times of original system to 2 times, but also provide some additional economic benefits by increasing

the onsite renewable generation. The proposed control algorithm could be widely applicable to other facilities that generate onsite renewable power, and face similar utility export restrictions.

4. TECHNO-ECONOMIC ANALYSIS OF A GRID CONNECTED PV-BATTERY SYSTEM WITH CONSTANT CHARGING POWER CONSTRAINS

4.1 Introduction and background

With the increasing concerns over the impact of fossil fuels on the environment, renewable energy has become an important aspect of the power generation sector. According to a report by the IRENA [93], the total renewable energy generation capacity reached 2,351 gigawatts (GW) at the end of 2018, accounting for one third of total installed electricity capacity.

Solar energy, spurred by technology innovation, reduction in costs and policy support, continues to be one of the most attractive sustainable energy resources [94]. However, due to their intermittent nature high penetration of renewable energy (i.e. PV and wind) into the power grid creates challenges in balancing supply and demand. Specific to solar, there is a mismatch between the time of peak solar generation and the time of peak demand.

ESSs can address intermittency by storing energy and making it available during times of high demand. In the last decade, ESSs have been recognized as a main component in power system distribution networks to provide grid stability support, energy system efficiency improvements, voltage-frequency regulation services, and reduce environmental impact through the deployment of renewable energy [95].

Several articles have investigated the techno-economic viability of microgrids using renewable energy combined with some form of energy storage as possible alternative

solutions to replacing or reducing the energy generated by conventional high-polluting generators.

A large-scale hybrid microgrid system consisting of solar, wind and battery was developed to provide energy for a remote off-grid island [96]. The results of this study showed that an off-grid power system with a small loss of power supply probability (LPSP) can meet optimal balance between energy reliability and economic cost. In another study, a diesel-solar hybrid system to provide electrical power to an isolated resident was investigated [97]. The Hybrid Optimization of Multiple Energy Resources (HOMER) simulation results indicated that this hybrid system could reduce cost of energy by 70%. The study in [98] presents the design of a backup PV-diesel microgrid, intended to supply electricity to a rural system with frequent blackouts. The author found the beneficial system is strongly dependent on the load level and durationof blackouts after examined economic viability of different scenarios. The study in [99] compared diverse technological options (wind, PV, and biomass) integrated with the grid, and analyzed their ability to improve the reliability of dispatch energy and the cost effectiveness of these hybrid systems for rural electrification. The study in [100] compared two performance scenarios of a large-scale wind farm with and without pumped hydro storage (PHS), by calculating the levelized cost of energy (LCOE). The results demonstrated that the scenario of the wind farm with added PHS generated additional economic benefits with slightly lower LCOE. All of the above mentioned articles aimed at assessing the viability of different energy storage systems for providing reliable power supply, while overlooking the value creation potential of combining applications such as power quality and frequency support. Capital

investment and economic benefits are the major factors in the decision making for implementing energy storage systems for single house or small-scale utilization.

Article [101] evaluated the feasibility of off-grid operation of a fully electric house with three operational energy source scenarios: PV plus battery, PV only, and PV plus generator. The study concluded that PV plus generator is financially the better choice. Another research study [102] examined the potential of lead-acid and lithium-ion battery systems each combined with solar PV generation for a single home under multiple energy tariffs in Switzerland. The study showed that constant retail tariffs throughout day is the best option for consumers deploying PV plus battery system. One study [103] addressed the economic viability of solar home systems in the UK, considering battery degradation. In this study, a comprehensive battery degradation model is developed based on long-term ageing test. Normally residential electricity tariffs only consider electricity energy component, while ignoring maximum power demand, which limits the battery maximum financial performance. The author in [104] proposed a method to pre-select the optimal group of applications for residential PV plus battery system, by employing the economic benefits and cost, and utilizing different strategies in power applications: PV self-consumption, load shifting, avoidance of PV curtailment and peak shaving.

There is a wide range of ESS technologies available on the market. A study prepared by the Energy Storage Systems Program for the U.S. DOE gives an overview of storage value propositions including several applications [104][105]. Many articles have been published in the last years on the technical and economic performance of battery systems. One study [106] performed the techno-economic analysis and compared the

performance of lithium-ion and lead-acid batteries in a microgrid consisting of solar PV, wind and diesel generation.

4.1.1 System configuration and basic parameters

The Chemehuevi Indian Tribe's Chemehuevi Community Center (CCC) is located in Havasu Lake, CA, which is a remote community with a single transmission line connected to the power grid. A deployed microgrid project at the CCC integrated advanced pre-commercial PV and the ZBFB system, providing economic benefits and reliable energy support to the community at the CCC building. In addition, the microgrid system was designed to meet demand response and energy management requests, while supplying energy to support critical load at the CCC, minimizing operational impacts to the Community Center.

Figure 4-1 shows the electricity use profile of CCC building for the summer and winter seasons.

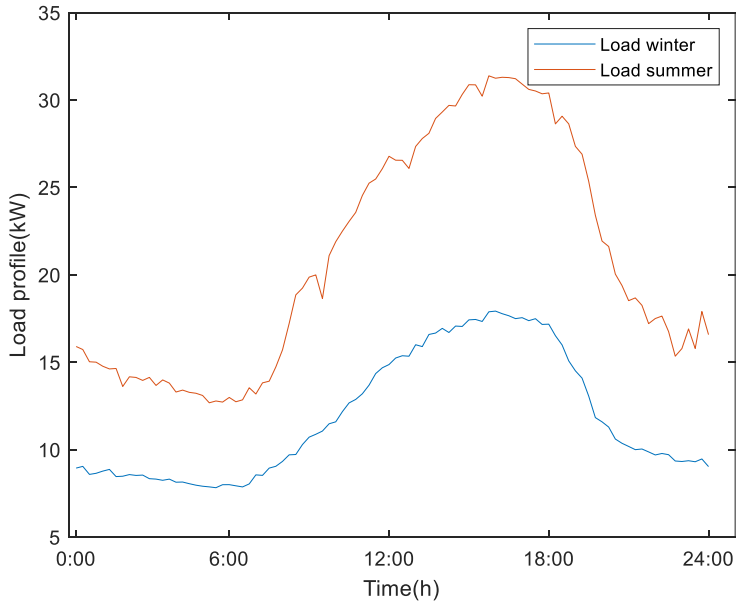

Figure 4-1. CCC building load for a summer and a winter day.

The method of solar generation prediction was introduced in section 2.1. Here, the main parameters and assumptions about the solar panel are introduced. Due to aging and an increasing internal resistance, PV systems cannot maintain the same output profile during their lifetime. Based on a published study [107], the individual modules or entire system have a mean degradation rate of 0.8%/year and a median value of 0.5%/year based on their analysis and literature review. In this study, 0.8%/year degradation rate is used. The main parameters of PV module are given in Table 4-1.

Parameter	**PV**
Solar panel cost	$2.29/ W [108]
Maintenance cost	1% of capital investment
Annual Capacity Degradation	0.8%
Calendar life	20 years

Table 4-1. PV parameters for economic analysis

As stated above, the ZBFB is a promising technology as an energy storage system, characterized by its ability to independently scale its energy and power characteristics, achieving 100% depth of discharging (DOD) without battery damage, having a broad operating temperature range, and long cycle life. But the specific operational constraints requiring the constant charging power, and respective lower energy efficiency of ZBFB raised the question that performance of ZBFB as energy storage system in energy cost reduction applications.

In order to maintain high battery storage capacity and prolong operating life, we adopt a slower charging rate near the end of the charging cycle. The threshold SOC value is set up as 95% and 85% for Li-ion battery and ZBFB, respectively. As for parameters used in the economic analysis, the lifespan and DOD of the battery systems are the main variables that determine the return on investment. Other battery parameters are also

selected for the techno-economic model. The cost values adopted in the present analysis are $350/kWh for battery energy capacity and $400/kW for inverter power capacity [104]. Since ZBFB is an emerging battery storage technology, there is limited cost information available. Based on the studies [5][109], the capital investment for ZBFB is $600/kWh for battery energy capacity and $650/kW for inverter power capacity. Additional information is presented in Table 4-2.

Parameter	**Li-ion**	**ZBFB**
Round trip efficiency (%)	90	75
Depth of discharge (DOD) (%)	80	100
Battery cost ($/kWh)	350	600
Inverter cost ($/kW)	400	650
Maintenance cost (% of capital investment)	1.5	1.5
Lifetime Energy Capacity Degradation (%)	30	5
Lifetime Power Capacity Degradation (%)	10	10
Annual Energy Capacity Degradation (%)	3.5	0.35
Annual Power Capacity Degradation (%)	1	1
Calendar life (years)	10	20

Table 4-2. The main parameters of Li-ion battery and ZBFB for analysis

4.2 Problem statement

It is a common application for energy storage system to minimize energy cost of local DRES by performing load shifting or peak demand. ZBFB as one promising battery energy storage system has a lot of advantages. However, the constant charging power operating constrains, respective lower energy efficiency raised new challenges when utilizing the ZBFB as energy storage system of local DRES. This chapter focuses on the testing and assessing the techno-economic aspects of ZBFB. In order to perform a comparative analysis, two different battery systems types are compared from a

technological and economical perspective under the same simulating conditions. By analyzing and comparing the performance between the ZBFB and the widely-spread Li-ion battery technology.

4.3 Control algorithm

The purpose of DRES is to support the building with an environmental friendly energy source, reduce building energy costs, and add extra distributed power flexibility. Despite its intermittent power output, the solar PV system has a longer lifespan with lower degradation rate compared to most battery chemistries. Alternatively, the battery system can dispatch power to meet demand. However, battery systems have a relative high capacity decline rates over long-time period. From economic performance, the capital investment and operating cost are mainly depended on the PV-battery system size and unit prices. However, the system revenue depends on the utilizing of the stored energy effectively, and therefore it could vary significantly. However, the peak demand charge requires that energy consumption, power demand and the operating period are considered. Through the optimal control of battery operation, the operating cost can be optimized. In this study, both Li-ion and ZBFB are utilized as energy storage system to do load shifting and demand response. Based on their different parameters and constrains to build model to simulate the technologic performance, while testing two system economic performance. Due to the addition of a microgrid system requires additional capital and maintenance costs, the PV-battery system is an attractive option to investors and customers only if the system provides economic benefits.

4.3.1 Economic assessment

In order to evaluate the system's economic performance, the long-term profitability of PV-battery system is quantified through some well-established methodologies for the

evaluation of investments. In this study, the economic assessment methodology LCOE has been chosen as the economic assessment parameter, which have to be considered both benefits and costs associated with the PV-battery system described above.

Typically, the LCOE is one commonly employed economic indicator. It is calculated as the long-term cost of energy (usually electricity) for a particular system, including all the costs over its lifetime, such as the initial capital investment, the cost of system operation and maintenance, and the energy fuel cost [104]. However, one drawback is that the original LCOE calculation for conventional power station, does not consider an energy storage system. One published study [110] proposed a method for a microgrid system employing energy storage system, in which LCOE calculation considering the energy storage system is demonstrated by Eq. (4-1):

$$\mathrm{LCOE_{sys}} = \mathrm{LCOE_{pv}} + \mathrm{LCOE_{ess}} \tag{4-1}$$

A battery system is considered a generation system which has no ability to generate electrical energy. As a consequence, the energy dispatch is based on how much energy is stored in the system.

Combining with [111] a simple formula to calculate LCOE is shown in Eq. (4-2):

$$\mathrm{LCOE} = \frac{\sum_{y=1}^{n}\left(\mathrm{CAP_{sys}} + \frac{\mathrm{OP_{sys}^{n}} + \mathrm{Elec\_cost_{sys}^{n}}}{(1+r)^{n}}\right)}{\sum_{y=1}^{n}\frac{\mathrm{Energy_{sys}^{n}}}{(1+r)^{n}}} \tag{4-2}$$

Where $\mathrm{CAP_{sys}}$ is the system capital investment, $\mathrm{OP_{sys}^{n}}$ is the annual operating expenditure, $\mathrm{Elec\_cost_{sys}^{n}}$ is the annual fuel expenditure (electricity cost to support the building load), $\mathrm{Energy_{sys}^{n}}$ is the generation of total microgrid system, in which $\mathrm{Energy_{sys}^{n}}$ equal to PV and battery dispatch energy, and r means the discount rate, which is defined as 5%.

The total system capital investment, which is based on the battery and the solar panel rated energy and power capacity is calculated using Eq. (4-3).

$$CAP_{sys} = C_{batE} \times P_{batE} + C_{batP} \times P_{invP} + C_{PV} \times P_{PV} \quad (4\text{-}3)$$

where, CAP_{sys} ($) contains the battery system and solar panel system capital investment cost, C_{batE} (kWh) indicates battery nominal capacity, C_{batP} (kW) denotes inverter power capacity of battery system, C_{PV} (kW) indicates solar system power capacity, P_{batE} ($/kWh) refers to the storage unit price, P_{invP} ($/kW) and P_{PV} ($/kW) corresponds to the battery inverter power capacity unit cost, and the unit price associated with the solar PV system generation rated capacity, respectively.

There are many published studies which address the maintenance and operation cost for the whole system. For example, one study makes the assumption that annual costs of maintenance are 1.25% of the system capital cost [112]. Another research study uses 1.5% as annual maintenance cost relative to initial investment [113]. The annual operational expenditure (OP_{sys}) used in this analysis is a constant value equal to 1.5% of capital investment. The maintenance cost is calculated using Eq. (4-4)

$$OP_{sys} = CAP_{sys} \times 1.5\% \quad (4\text{-}4)$$

In general, the fuel energy cost is calculated based on how much oil or gas is used to support the whole system running. However, for the case in which a microgrid consisting of PV-battery system is grid connected, only the cost of grid electricity consumption is considered. In the grid electricity cost calculation, the value of demand power and the energy consumption must be functions of time, since the unit price rates for power and energy are variable, dependent on the time of day, as indicated in the Time of Use (TOU) rate.

The yearly electricity cost is calculated by Eq. (4-5).

$$\mathrm{Elec\_cost_{sys}} = \sum_{m=1}^{12} (\mathrm{R_{de}^{p}} \times \mathrm{Max(Power_{m})} + \sum_{p=1}^{3} \mathrm{R_{en}^{p}} \times \mathrm{En_{consume}}) \quad (4\text{-}5)$$

Where in the above equation, $\mathrm{R_{de}^{p}}$ indicates the TOU demand rates (the superscript p indicate the different time period), $\mathrm{Power_{m}}$ is the monthly peak demand (m indicates the month index), $\mathrm{R_{en}^{p}}$ indicates the energy price rate, $\mathrm{En_{consume}}$ stands for the respective energy consumption during each specific time period.

4.3.2 Optimization model

The aim of this study is to derive an optimal microgrid design, which involves finding the optimal size of energy storage and PV. Meanwhile, the operating cost should be minimized to satisfy the objective of energy cost reduction. As the introduced in the LCOE method, the operating cost of the system is one essential part during the LCOE calculation. At the same time, the operating cost is dependent on the response of the ZBFB charging power and discharging power, $P_c(i)$ and $P_d(i)$, respectively. A bi-level optimal program is proposed for this microgrid design optimization problem. The battery operating algorithm that constrains the battery charging/discharging is the lower-level optimization problem, which provides optimal operating cost of each system respectively. The minimizing LCOE that limits the size of system components is the upper-level optimization problem. The objective function is:

$$Minimize\ \ LCOE\ (Ns, Nb)$$

However, the introduced LCOE method is non-linear and non-convex, evaluating the quality of candidate solutions is not straightforward. Therefore, a heuristic method is introduced to find the minimum LCOE value for each systems.

Algorithm 1: Heuristic LCOE Solution Algorithm

Input: current system size Ns and Nb, battery operating algorithm

Output: Minimum $LCOE(Ns, Nb)$

Define battery operating algorithm for Li-ion and ZBFB, respectively;
Ns^{max} ; // Ns is the solar panel size
Nb^{max} ; // Nb is the battery size
for $i = 1 : Ns^{max}$ **do**
  for $j = 1 : Nb^{max}$ **do**
    Calculate capital investment of system size (i, j) ;
    Run battery operating algorithm under system size (i, j) ;
    operating cost C(i, j) and distributed energy E(i, j) ;
    Calculate LOCE of system size (i, j);
    $j \leftarrow j + 1$;
  end
  $i \leftarrow i + 1$;
end
RETURN min LCOE for system size (i, j);

Figure 4-2. Pseudo-code of heuristic LCOE solution algorithm

The detail process for this algorithm is shown in Figure 4-2. Based on the proposed system size, the capital investment is calculated first. System size variables are used to drive the battery operating control algorithm to get optimal charging power $P_c(i)$ and discharging power $P_d(i)$, while the operating cost and system distributed energy calculations are collected. The LCOE (i, j) acts as a one candidate solution, calculated by the above collected values. In the end, the minimum LCOE (i, j) value is selected from the all candidate solutions.

The operating cost depends on the modelling of battery systems. Three battery model has been present in following parts. Minimizing Eq. 4-5 is the only objective function for all of battery models.

4.3.2.1 Li-ion battery model

Li-ion battery as energy storage system is deployed to meet practical applications, the response of battery are $P_c(i)$ and $P_d(i)$. However, there are some limiting constrains for the battery operational performance. In general, constrains for Li-ion battery are:

$$P_{min} \leq P_c(i) \leq P_{max} \quad (4\text{-}6)$$

$$P_{min} \leq P_d(i) \leq P_{max} \quad (4\text{-}7)$$

$$P_c(i) * P_d(i) = 0 \quad (4\text{-}8)$$

$$SOC_{min} \leq SOC(i) \leq SOC_{max} \quad (4\text{-}9)$$

$$SOC(i) = SOC(i-1) + {(P_c(i) \times eff - P_d(i)/eff) \times \Delta t}/{Bat_{cap}} \quad (4\text{-}10)$$

where $SOC(i)$, eff and Bat_{cap} denote the state of charge at time index of i, charging/discharging efficiency and battery capacity, respectively. P_{min} and P_{max} denotes the minimum and maximum battery power, P_{min} = 0, and P_{max} = 100.

SOC_{min} and SOC_{max} denotes the minimum and maximum value of SOC. The Li-ion battery has been designed with 80% DOD, SOC_{min} = 20%, and SOC_{max} = 100%. A Eq. 4-8 imposes a restriction on $P_c(i)$ and $P_d(i)$, preventing the battery from charging and discharging at the same time.

4.3.2.2 Scheduled ZBFB control model for constant charging power

Due to the specific constant charging requirement, the scheduled control algorithm needed to be adjusted. The general scheduled control algorithm is designed to charge battery when the renewable energy is more than the local load, and released the stored energy to support the local demand at a later time. The only constrain on the charging power and discharging power is the maximum allowable power range. Considering the

constant charging power, the new scheduled control algorithm is designed to constrain the charging power with constant value. The designed method is shown in Figure 4-3.

Algorithm 2: Control Algorithm for ZBFB constant charging

Input: building load data l, renewable generation s, current time index i, initial battery state SOC_{init}, efficiency eff, *and* batery capacity Bat_{cap}

Output: Decision of $P_c(i)$ *and* $P_d(i)$

```
for i = 1 : 24 do
    P^grid(i) + P_d(i) + s(i) = l(i) + P_c(i) ;
    SOC(i) = SOC(i − 1) + (P_c(i) ∗ eff − P_d(i)/eff) ∗ Δt/Bat_cap ;
    if s(i) ≥ l(i) then
        find the Maximum charging energy in this period with (P_c, t);
        if MCE ≥ bat_cap then P_c = bat_cap/t;
        else P_c = MSE/t;
    end
    i ← i + 1;
end
```

Figure 4-3. Pseudo-code of rule-based ZBFB constant charging power constrain

Based on the demand and renewable generation, each timeslot potential charging energy is calculated and recorded. Then, the maximum potential charging energy is chosen to compare with battery capacity. If the maximum potential charging energy is larger than battery capacity, then the constant charging power is set to equal the battery capacity divided by the processing time. Otherwise, the constant charging power is the maximum potential charging power divided by the processing time.

4.3.2.3 MILP ZBFB model for constant charging power

The Mixed Integer Linear Programming (MILP) ZBFB model is subject to the following constrains:

$$0 \leq P_{grid}(i) \leq P_{unmet}(i) \tag{4-11}$$

if $P_{load}(i) \geq P_{solar}(i)$,

$$P_{unmet}(i) = P_{load}(i) - P_{solar}(i) \quad (4\text{-}12)$$

else

$$P_{unmet}(i) = 0$$

$$0 \leq P_c(i) \leq P_{solar\_e}(i) \quad (4\text{-}13)$$

if $P_{solar}(i) \geq P_{load}(i)$,

$$P_{solar\_e}(i) = P_{solar}(i) - P_{grid}(i) \quad (4\text{-}14)$$

else

$$P_{solar\_e}(i) = 0$$

where $P_{unmet}(i)$ denotes the unmet demand that renewable energy cannot support in instances like during the morning (sunrise) and the evening (sunset). $P_{solar\_e}(i)$ denotes surplus renewable energy when generation is larger than demand (e.g. noon period). Eq. 4-11 and Eq. 4-12 indicate that grid power supports the unmet power. Eq. 4-13 and Eq. 4-14 indicate that renewable energy is the primary energy source to charge the battery. For ZBFB operation, Eq. 4-6 to Eq. 4-10 should also be satisfied.

$$P_c(i) \leq M(1 - u(i)) \quad (4\text{-}15)$$

$$P_{grid}(i) \leq Mu(i) \quad (4\text{-}16)$$

$$u(i) \in \{0,1\}$$

Eq. 4-15 and Eq. 4-16 are constrained grid power to charge battery system [114].

$$P_{grid}(i) + P_{solar}(i) - P_c(i) + P_d(i) = P_{load}(i) \quad (4\text{-}17)$$

$$P_{grid}(i) + P_d(i) = P_{unmet}(i) \quad (4\text{-}18)$$

$$P_c(i) = p \times c(i) \quad (4\text{-}19)$$

$$c(i) \in \{0,1\}, \qquad p \in R$$

Eq. 4-19 introduced one way to describe $P_c(i)$ is constant charging power with p and $c(i)$. p is one value variable, and $c(i)$ is one binary variable. However, this equation is not linear programming, which cannot directly apply to MILP ZBFB optimal model. Here, the McCormick relaxation has been utilized to transfer the Eq. 4-19 into Eq. 4-20 to Eq. 4-23.

$$P_c(i) \geq 0 \tag{4-20}$$

$$P_c(i) \geq p + 100 \times c(i) - 100 \tag{4-21}$$

$$P_c(i) \leq 100 \times c(i) \tag{4-22}$$

$$P_c(i) \leq p \tag{4-23}$$

$$c(i-1) \geq 1 - 0.001 - M \times (1 - y1(i)) \tag{4-24}$$

$$c(i-1) \leq 1 + M \times \ y1(i) \tag{4-25}$$

$$c(i) \geq 1 - 0.001 - M \times \big(1 - y2(i)\big) \tag{4-26}$$

$$c(i) \leq 1 + M \times y2(i) \tag{4-27}$$

$$y2(i) \geq y(i) \tag{4-28}$$

$$y2(i) \geq y(i) \tag{4-29}$$

$$y(i) + 1 \geq y1(i) + y2(i) \tag{4-30}$$

$$sequ(i) = sequ(i-1) + y(i) \tag{4-31}$$

$$c, y1, y2 \ and \ y \in \{0, 1\}, sequ \ \in \ R^+$$

Eq. 4-24 to Eq. 4-31 make sure that the charging power in a series timeline.

The optimization problem is solved in the MATLAB® environment [129] by using the MOSEK solver [130].

4.4 Simulation and results

In this study, the primary purpose is to find the optimal size for different system configurations using two different battery systems by minimizing the LCOE value. The

operating cost plays a significant influence in the LCOE calculation, while operating cost is dependent on battery charging power P_c and discharging power P_d , which are constrained by the battery model. In this section, the operating cost of battery model under the various system size has been simulated. Before introducing the simulation results, there are several scenarios that need to be established. For Li-ion battery systems, there is only one Li-ion battery model. The scheduled control algorithm of ZBFB is defined as scenario 1, and the MILP ZBFB model with constant charging power is scenario 2.

4.4.1 Optimal system size with various system configurations

Due to the operating constrains, retail rates and control method are different, optimal size for these systems is diverse. The optimal system size for different system are shown in Table 4-3.

Main Variables	Li	Scenario 1	Scenario 2
Solar size(kW)	100	104	100
Battery size (kWh)	200	108	90
LCOE	0.346	0.516	0.485

Table 4-3. Simulation result for different system configurations

From the above table, the li-ion battery system has the greater energy capacity while achieving the lowest LCOE. There are several reasons that make the Li-ion battery system as the best option in this simulation. The first one is the lower capital cost of battery system. Another point that cannot be ignored is the flexibility of Li-ion battery operation. In contrast with ZBFB, the only drawback is the narrower DOD when the li-ion battery is utilized to reduce energy cost. However, this constraint has been offset by

increasing the battery system size, while taking advantage of the economies of scale to keep capital investment under control.

The LCOE result of MILP ZBFB model is better than the schedule control method. Although the MILP ZBFB model has a smaller scale battery capacity, this system could get better operating cost due to a comparable discharging power that reduces the potential peak demand. Additional the smaller scale battery system has less capital investment of MILP ZBFB system, comparing with the scheduled one. Although scenario 1 in above table indicated the minimum LCOE value, the performance of scheduled control algorithm for ZBFB with constant charging power constraint is not as good as the others. This is due to an inherent lower energy efficiency compared to Li-ion and higher capital cost compared to the MILP approach.

In order to indicate the influence of system components in the optimal system, the main results of the simulation are presented in Table 4-4.

Main Variables		Li-ion	Scenario 1	Scenario 2
Solar PV	Energy(kWh)	76260.5	79832.7	79350.7
	Capital (%)	63.5%	74.8%	77.4%
Battery	Energy(kWh)	66023.7	32107.7	26345.2
	Capital (%)	36.5%	25.2%	22.6%
PV-battery	Operating ($)	13381.8	15339.1	15682.1

Table 4-4. Results comparison.

4.4.2 Comparative analysis of ZBFB models

The two models develop for ZBFB: scheduled control algorithm and MILP modelling method, both charged the ZBFB with constant charging power. The battery

curve are shown in Table 4-4. In Table 4-4 (a), (c) denote the ZBFB with scheduled control algorithm with 108 kWh battery capacity, while (b), (d) denote the ZBFB with MILP optimal control algorithm with 90 kWh battery capacity. Both scenarios are working under the optimal system size. When the renewable energy is larger than system load, the scheduled control algorithm gets the maximum charging energy from all candidate solutions. For the MILP ZBFB model, due to a smaller scale battery size, the constant charging power is only 15.6 kW. During the discharging period, the drawback of the schedule method is observable, because this control method discharges energy to support the system load without concern economic performance. In contrast, the MILP ZBFB model discharges energy to reduce the whole system energy cost, decreasing the LCOE value for the whole system.

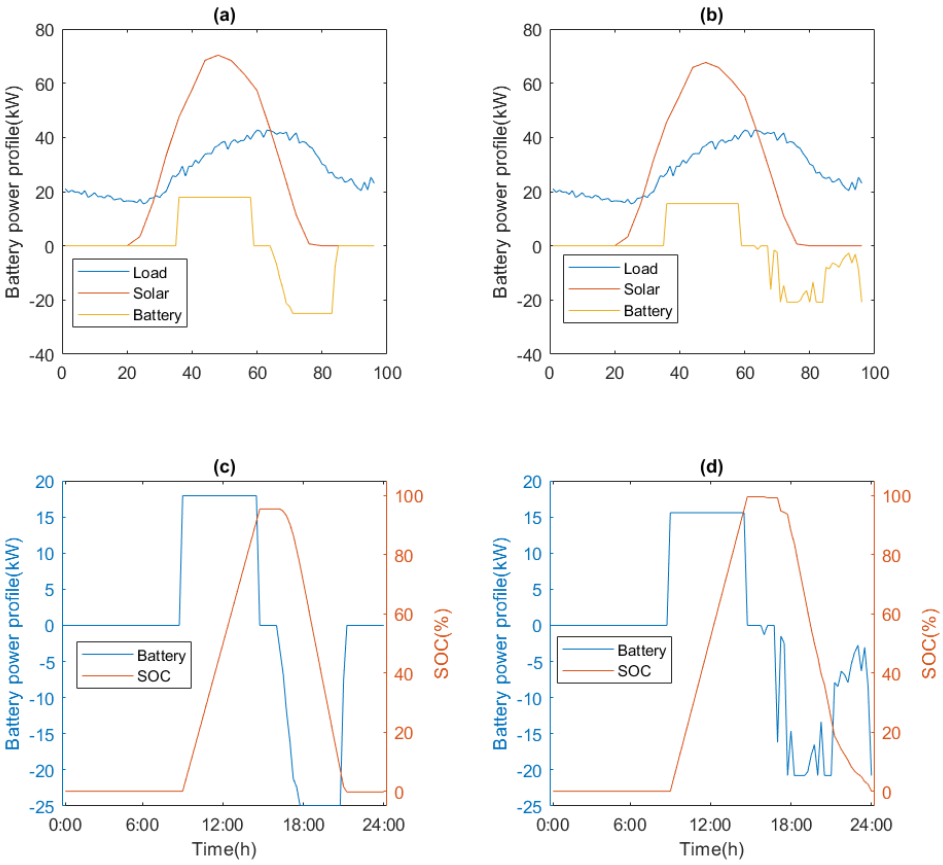

Figure 4-4. ZBFB operating curve for optimal system size (scenario 1 and scenario 2)

4.5 Conclusion

The techno-economic analysis of PV-battery DRES with two different battery technologies reveals that the economic benefits of DRES are encouraging, both in terms of reduced on-grid energy consumption, and in terms of support of increasing deployment of renewable energy. The comparative analysis of different optimal size configurations of PV-battery system with the two types of batteries, indicated that lithium-ion batteries are characterized by excellent investment performance from both technological and economic perspective, under the current market price and application purpose. For both two ZBFB control algorithm considering the constant charging power

constraint, the MILP optimal control algorithm provide the better result. The ZBFB shows lower economic performance, explained by its higher projected capital investment. Under this simulation, ZBFB could compete with Li-ion battery in economic assessment at least with 60% capital investment decreasing.

5. PROFITABLE EMISSION CONTROL STRATEGY FOR PV-ZBFB HYBRID MICROGRID WITH MODELLING OF REFRESH MODE

5.1 Introduction the Background

The proliferation of DRES is strengthened by global awareness that urges all of its participants to reduce their GHG emissions. Besides, environmental concerns and relative positive financial returns are identified as major motives for adopting DRES. California has declared an ambitious plan to reduce its emission by 26–28% below the 2005 levels by 2030 [115]. In California, a significant amount of renewable energy is generated from small scale solar PV systems which add 19.6% of total renewable energy generation. There is no doubt that renewable energy generation holds the key in reducing the environmental impact of fossil fuels, and decreasing reliance on traditional energy sources [66]. While at the same time, energy storage systems have been touted as a promising solution for the intermittent nature of renewable resources, and therefore a valuable contribution towards broader utilization of renewable energy and distributed energy resource systems. For a hybrid system, the typical end-user is not only focused on economic benefits of the system, but also its de-carbonization potential. Many studies have proposed renewable portfolio standards, requirement of GHG emission reduction. For example, SGIP provides incentive for GHG emission reduction, which requires qualifying prospective projects to achieve 5 kg CO_2/kWh without significantly impacting energy bill saving [67].

Significant efforts have been made around the world to address these GHG emission reduction issues. Many propose that the hybrid system with deployed renewable energy can reduce the whole system GHG emission. However, based on the discussion and literature review in previous chapter, the hybrid system may not reduce emission, but

instead exacerbate environmental impacts. The main reason for that is the control algorithms and specific strategies used to manage energy storage systems.

There are two main operation mechanisms of energy storage that can cause increased emissions for grid-connected hybrid system [68]. The first is caused by the market electricity retail price incentives, which encourage end-users to charge the energy storage system during off-peak hours and discharge during peak afternoon or evening periods. In general, the marginal electricity generation during off-peak times is often produced by a coal-fired plants and the marginal generation during peak periods is produced by natural gas plants, which means that storage is effectively displacing cleaner natural gas-generated electricity with coal-fired generated electricity. So, when assessing the impacts of energy storage system with utilizing an average GHG emission factor value, would ignore the difference of GHG emission rates associated with the grid energy used for charging and discharging at different times. As the result, the average GHG emissions factors or signals are discarded in this study.

Second, all storage technologies experience energy losses due to their internal resistance or self-discharge, defined by their round-trip efficiency. This inefficiency means that the storage system would effectively lose some of the energy when system operates. Additionally, due to the energy storage system use the whole hybrid system is required to use extra electrical energy in a passive way, and consequently generate more GHG emission related to these losses. These two characteristics of energy storage operation remain true, whether the storage system is operated with a revenue-maximizing goal in mind or operated with load-shifting or demand response goal in mind. However, researchers have not come to an agreement as to which one of these two mechanisms plays the primary role in emission effect [69] [70].

Unfortunately, while renewable energy generation combined with storage system is effective in meeting electricity power demand and energy, it remains unclear how effective a hybrid system can be in reducing GHG emissions, under current energy market structure and the mentioned battery operating mechanisms.

5.2 Problem statement

Under the primary motivation of reducing energy consumption and pollutant emissions, researchers have been investigating reducing energy consumption and pollutant emissions of hybrid systems. One study [116] proposed a dynamic control algorithm to solve optimization problem with target of reducing the economic cost and CO_2 equivalent emissions. The author of a published report [117] utilized bi-level optimization and Pareto analysis and found that renewable generation from microgrids can significantly reduce the negative impacts of the policies. Another research study [118] proposed an advanced demand-side management and control strategy for an efficient energy management system in smart grid and indicated this method effectively reduced the energy cost, emission cost, and peak-to-average ratio of the smart grid. Although those research studies have indicated the target of emission reduction can be realized with proper control method, the unique characteristics of ZBFB may raise new challenges. The refresh mode is the one critical constraint for control algorithm and optimization.

Although ZBFB is a promising battery technology with appealing advantages, its drawbacks should not be ignored. As mentioned previously, the battery round-trip efficiency is one factor, which plays a significant role in the GHG emission effects. However, the ZBFB has the respective lower efficiency, which means extra energy (more emissions) would be produced. Another concern is the refresh mode, which raises

a new challenge for the hybrid system control algorithm, which in turn takes minimizing economic cost as primary objective.

There are some papers proposed simulating models or methods to implement the refresh mode in practical applications and simulations. First and easily implement is do refresh cycle after every daily usage. The papers [33] [61] require that the batteries be completely discharged to prevent dendrite growth and maintain the health of the batteries. This requires that the batteries be periodically stripped to properly clean and maintain them. However, this requires that Energy storage system periodically stay offline. The author [62] mentioned the stripping cycle is repetitively forced every 5 workdays. If above mentioned methods have been deployed, there are some subtle features would be neglected. For example, the report [30] found the first cycle efficiency would be slightly lower after refresh cycle, due to the base coat of zinc is being re-plated. If one refresh cycle per day schedule has been used, the performance of ZBFB would be negative effect comparing with the normal utilized way. There are some researches indicated another way to implement the refresh mode in simulation model or real applications. The report [49] indicated the battery efficiency would decline after a number of cycles. Within a set of no-strip cycles, this efficiency loss is exhibited as decreasing capacity. As a report [63] indicated stripping procedure should be taken once in every four or five full charging and discharging cycles. The author [30] prefer ZBFB should do one strip cycle after five operating cycles. However based on the limited knowledge, the ZBFB model with refresh mode based on operating cycle has not been introduced.

In this section, the control algorithm of PV-ZBFB hybrid system based on a novel battery model with refresh mode has been proposed, which aims to maximize revenue,

while reducing emission of whole system. The refresh mode is executed dependent on the number of operating cycles.

5.3 ZBFB model

Modelling of ZBFB is highly relevant to provide necessary tools for research, simulation and practical application to improve their performances. Different types of models for ZBFB have been proposed with different end goals. Several battery models have been developed for improving battery design, parameter identification and performance. One study [119] reported a model aimed to optimize system parameters to reduce losses. Several studies 0[120][121] reported improved models focusing on electrochemical reaction kinetics and charge transfer losses in the electrolyte. Most of these models have focused on the modelling of electrochemical reactions or species transport, there are requirements of battery model, which can simulate battery performance and operating constraints in actual applications. Some efforts have been made by researchers to address this type of battery model. Published research accounts [33] reported battery model used to simulate refresh mode after daily usage. The author of a study [62] has demonstrated one model in MATLAB Simulink environment, which runs refresh mode once every 5 days. These models focus on simulating refresh mode on time interval, but the model created to closer mimic actual operation requires more accurate control and operation, based on smaller time intervals, like, hours, minutes even in seconds. In this part, modelling of ZBFB for simulating refresh mode in real application has been proposed. This strategy of ZBFB model is built based on the number of battery operating cycle.

5.3.1 Basic strategy and implement method of refresh mode

Before introducing the details about the modelling of ZBFB with refresh mode, the assumptions and design method should be investigated first. The reason for

implementing a forced stripping cycle after every five charge/discharge cycles is the sharp decrease of energy efficiency [30]. According to a research report [64], the author indicated that the refresh time could be a constant value, if the power conversion component of ZBFB is well designed. Based on practical operating experience and mentioned research reports, the stripping cycle can be done after each charge/discharge cycle or after several cycles. However, after five cycles the stripping cycle would be enforced, which requires one hour per stripping cycle to complete.

ZBFB as energy storage system is deployed to meet practical application needs, the response of ZBFB are charging power and discharging power, $P_c(i)$ and $P_d(i)$, respectively. However, there are some limit constraints of the battery operational performance. In general, the basic constraints are:

$$P_{min} \leq P_c(i) \leq P_{max} \tag{5-1}$$

$$P_{min} \leq P_d(i) \leq P_{max} \tag{5-2}$$

$$P_c(i) * P_d(i) = 0 \tag{5-3}$$

$$SOC_{min} \leq SOC(i) \leq SOC_{max} \tag{5-4}$$

$$SOC(i) = SOC(i-1) + {(P_c(i) \times eff - P_d(i)/eff) \times \Delta t}\Big/{Bat_{cap}} \tag{5-5}$$

where $SOC(i)$, eff and Bat_{cap} denote the state of charge at time index of i, charging/discharging efficiency and battery capacity, respectively. P_{min} and P_{max} denote the minimum and maximum of battery power, P_{min} = 0, and P_{max} = 100, here. SOC_{min} and SOC_{max} denote the minimum and maximum value of SOC. Due to ZBFB's ability of 100% DOD, SOC_{min} = 0%, and SOC_{max} = 100%, are used here. Eq. 5-3 imposes restriction of $P_c(i)$ and $P_d(i)$, which requires battery not be charged and discharged synchronously.

Additionally, the refresh mode has specific constraints. Based on previously described reasons, refresh is carried out if SOC reaches 0%, while the number of battery operational cycles equals 5. The battery cycle counting algorithm will be presented in details next.

5.3.1.1 Battery cycle counting algorithm

Cycle-counting is a major topic in battery degradation field. Equivalent full cycle counting and Rainflow cycle counting are two main methods. According to the literature, Rainflow cycle counting is the most widely adopted algorithm for material fatigue analysis [122], lifetime assessment of power switches [123] as well as for battery degradation analysis [124][125]. Although the Rainflow method is suitable for so many applications, it's not a good method in this application. For example, the Rainflow approach was expressed the information of peak points and valley points, which ignored the real time power characteristics [126]. However, the power value at each time interval is import for the simulation the operating of ZBFB. Therefore, a cycle estimation method that could processes real time data is needed.

A battery cycle counting method is proposed for approximate evaluation of charge/discharge operating cycle of grid-tied BESS, which is created based on equivalent battery full charge-discharge cycles method. The proposed operating cycle counting method, as shown in Figure 5-1, is used to count the number of full cycles a battery has endured by real time battery operating data.

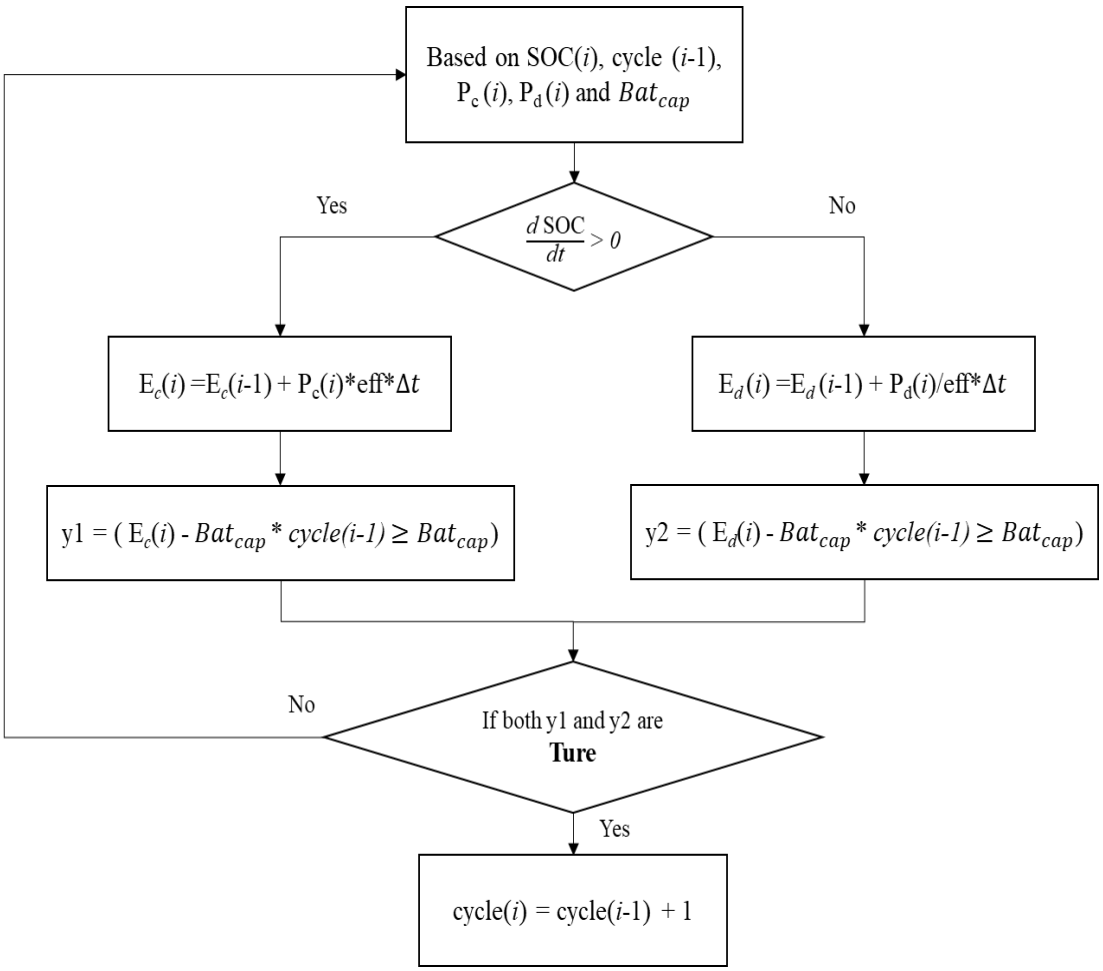

Figure 5-1. Flowchart of the cycle counting algorithm

The method is described as following: estimating the battery charging or discharging operation based on the change of SOC between the adjacent time nodes. When the SOC value increases, battery is being charged. Based on this classification, calculating the charging energy and discharging energy of battery by using the power at time *i* separately, as shown in Eq. 5-6, 5-7:

$$E_c(i) = E_c(i-1) + P_c(i) * eff * \Delta t \quad (5\text{-}6)$$

$$E_d(i) = E_d(i-1) + P_d(i)/eff * \Delta t \quad (5\text{-}7)$$

When both battery charging energy and discharging energy equal battery storage capacity, one fully charging/discharging cycle is completed. Once a full cycle is counted, the cycle value is incremented by 1.

Thus, $E_c(i)$ and $E_d(i)$, the charging energy and discharging energy, need to be evaluated to determine when they equal the battery capacity at every time node, as indicated by Eq. 5-8, 5-9, respectively.

$$\mathrm{y1}(i) = E_c(i) - Bat_{cap} * cycle(i-1) \geq Bat_{cap} \quad (5\text{-}8)$$

$$\mathrm{y2}(i) = E_d(i) - Bat_{cap} * cycle(i-1) \geq Bat_{cap} \quad (5\text{-}9)$$

$$\mathrm{y1}(i), \mathrm{y2}(i) \in \{0,1\}, E_c(i), E_d(i) \in R^+$$

where $\mathrm{y1}(i)$ and $\mathrm{y2}(i)$ are the binary variable, which indicate the increment of charging energy or discharging energy are more than the battery capacity, if more than battery capacity, the $\mathrm{y1}(i)$, $\mathrm{y2}(i)$ are set to 1, others are 0. Only if both $\mathrm{y1}(i)$ and $\mathrm{y2}(i)$ equal to 1, then $cycle^C(i)$ are updated as Eq. 5-10 shows,

$$cycle^C(i) = cycle^C(i-1) + 1 \quad (5\text{-}10)$$

$$cycle^C(i) \in Z^+$$

where $cycle^C(i)$ denotes the cumulative cycle value, which will continuously increase, beyond the original design. As above equations show, there are three types of variables, $\mathrm{y1}(i), \mathrm{y2}(i)$ are the binary variables, $cycle^C(i)$ is an integer variables, and the $P_c(i)$, $P_d(i)$, $E_c(i)$, $E_d(i)$ belong to the positive real number group (R^+). As stated above, it is impossible that charging and discharging occurs at the same time. As a result, at any time index, there is only one equation used between Eq. 5-6, 5-8 and Eq. 5-7, 5-9.

5.3.1.2 Refresh mode implement method

There are two prerequisites of refresh mode implementation. The first one is that operating cycle is reached at the recommend maximum operating cycle, another one is

SOC of battery system is closer (less than 0.1%) or equal to 0%. Based on the designed strategy of refresh mode, extra steps are required to complete implementation of refresh mode. The primary target is verifying the fourth operating cycle ($cycle^A(i) = 4$) is complete, which is used in the original value of cycle ($cycle^A(i) = 0$). The transfer function is shown by Eq. 5-11.

$$cycle^C(i) = 5 * num^C(i) + cycle^A(i) \quad (5\text{-}11)$$

$$cycle^A(i) \in \{0,1,2,3,4\}$$

Eq. 5-11 is used to transfer this cumulative cycle value to the desired one, $cycle^A(i)$. The modulo method is adopted here. $cycle^A(i)$ is an integer variable with range between 0 and 4. Besides this transfer function, one indicator $r1(i)$ that indicates the ZBFB already met the requirement of maximum operating cycle is requisite.

$$r1(i) = 1 \leftarrow cycle^A(i) = 0'$$

$$r1(i) = 0, \quad others \quad (5\text{-}12)$$

where $cycle^A(i) = 0'$ means the operating cycle transfer from 4 to 0, which indicated maximum operating cycle is reached. $0'$ is used to show the difference between the transfer function and the operating cycle value at the beginning.

During the same time, another signal $r2(i)$ denoted the SOC is closer to 0% is designed as following Eq.5-13

$$r2(i) = 1 \leftarrow SOC(i) \leq 0.1\%$$

$$r2(i) = 0, \quad others \quad (5\text{-}13)$$

Only if both indicators $r1(i)$ and $r2(i)$ are equal to 1, which is signified as *true*, the refresh mode is initiated. During refresh mode process, ZBFB has no ability to respond to any power commands from the end-user of designated controller. In order to simulate

this process of refresh mode, the charging power $P_c(i)$ and discharging power $P_d(i)$ are set to 0.

Algorithm 1: Modelling of ZBFB with refreh mode

Input: current time index i, initial battery state SOC_{init}, efficiency eff, *and* batery capacity Bat_{cap}

Output: Decision of $P_c(i)$ *and* $P_d(i)$

for $i = 1 : 24$ **do**
- $SOC(i) = SOC(i-1) + (P_c(i) * eff - P_d(i)/eff) * \Delta t / Bat_{cap}$;
- $E_c(i) = E_c(i-1) + P_c(i) * eff * \Delta t$;
- $E_d(i) = E_d(i-1) + P_d(i)/eff * \Delta t$;
- **if** $E_c(i) \geq Bat_{cap}$ *and* $E_d(i) \geq Bat_{cap}$ **then**
  - $cycle_C(i) = cycle_C(i-1) + 1$;
- **end**
- $cycle_C(i) = 5 * num(i) + cycle_A(i)$;
- **if** $cycle_A(i)$ $(4 \rightarrow 0)$ *and* $SOC(i) \leq 0.1\%$ **then**
  - $P_c(i) = 0$;
  - $P_d(i) = 0$;
- **end**
- $i \leftarrow i + 1$;

end

Figure 5-2. Pseudo-code of ZBFB model with refresh mode

The main procedures of refresh mode has been discussed in above subsection and equations. However, those part is based on the idea, the equations are nor suitable directly applied in optimal questions.

5.3.2 Battery model

The focus of this chapter is on the problem of determining simultaneously the behavior and operation of ZBZB with refresh mode to meet energy operation needs. Which is formulated here as an optimization due to the complexity of the problem and the need to select from among the many possible solutions one that meets a particular objective, minimizing energy cost and GHG emissions.

Based on the designed strategy of refresh mode, there are two type of variables of choice: discrete (binary and integer) and continuous. The discrete variables denote whether the requirement is met and the cycle counting value; whereas the continuous variables typically represent the energy capacity, power response and SOC. This optimization problem is clearly not original convex for the discrete variables and the logic operations. However, the Mixed Integer Programming (MIP) is one method to describe and solve this type of optimization problems. Actually, MIP can further be classified into Mixed MILP and Mixed Integer non-Linear Programming (MINLP). In this dissertation, MILP is utilized to describe and solve the optimization problem of ZBFB control with refresh mode. Due to all constraints and the objective function being linear function, the main advantages of MILP are normally quicker solution and the linear constraints resulting in a convex feasible region, which means that one is in principle guaranteed to obtain a global optimum [127]. Furthermore, the integer variables are typically determined using a branch-and-bound algorithm [128]. Although several mathematical formulations in the model are not linear functions, some tools and technical methods are utilized to transfer the non-linear into linear functions.

The modelling of ZBFB is designed to simulate battery behavior in the condition utilizing battery to meet practical applications. Due to the complexity of the model and practical application recorded data, the pre-conditions should be declared before getting into the ZBFB model. In this model, the time interval is 1 hour ($\Delta t = 1$), the index i denotes hours ($i \in \{1 \dots 24\}$), and every simulation time period is 1 day, the information is stored and turned over to the next daily simulation. The ZBFB model is created in MATLAB environment [129] and in MOSEK optimization solver [130].

The detail formulations of ZBFB model are expressed as follows:

$$ec + \sum_{i=1}^{n} P_c(i) * eff * \Delta t - Bat_{cap} * cycle^C(i-1) \geq$$

$$Bat_{cap} + 0.001 - M * (1 - y1(i)) \quad (5\text{-}14)$$

$$ec + \sum_{i=1}^{n} P_c(i) * eff * \Delta t - Bat_{cap} * cycle^C(i-1) \leq Bat_{cap} + M * y1(i) \quad (5\text{-}15)$$

$$ed + \sum_{i=1}^{n} P_d(i)/eff * \Delta t - Bat_{cap} * cycle^C(i-1) \geq$$

$$Bat_{cap} + 0.001 - M * (1 - y2(i)) \quad (5\text{-}16)$$

$$ed + \sum_{i=1}^{n} P_d(i)/eff * \Delta t - Bat_{cap} * cycle^C(i-1) \geq Bat_{cap} + M * y2(i) \quad (5\text{-}17)$$

where ec and ed denote the prior charging energy and discharging energy before the current simulation period, respectively, because ec or ed may not exceed Bat_{cap} in one-day simulation. However, this prior energy information is significant for the posterior decision. This important information is transmitted in the daily simulation. The Eq. 5-14 to Eq.5-17 show how to detect the increment of ec and ed. The increment of ec means higher battery capacity by comparing with prior cycle value that means $y1(i) = 1$, otherwise, $y1(i)$=0 as Eq. 5-14 and 5-15 present.

Only if both $y1(i)$ and $y2(i)$ equal to 1, then ZBFB accomplishes one full charging/discharging cycle ($y(i) = 1$). Here a logic operation *and* is demanded.

$$y1(i) \geq y(i) \quad (5\text{-}18)$$

$$y2(i) \geq y(i) \quad (5\text{-}19)$$

$$y(i) + 1 \geq y1(i) + y2(i) \quad (5\text{-}20)$$

$$y(i), y1(i), y2(i) \in \{0,1\}$$

Eq. 5-18, 5-19 and 5-20 are the implement method using the logic *and* operation [131]. The default values of these binary variables are 0. Additional details are shown in Table 5-1.

$y(i)$	$y1(i)$	$y2(i)$
0	0	0
0	0	1
0	1	0
1	1	1

Table 5-1. Correlation table of $y(i)$ and $y1(i), y2(i)$

$y(i)$, $y1(i)$ and $y2(i)$ are momentary variables, which turn into the default value 0. As a result, there is an updated version of Eq. 5-10 as shown in Eq. 5-21. When $y(i)$ default value is 0, there is no difference between $cycle^C(i-1)$ and $cycle^C(i)$. $cycle^C(i)$ only updated value when $y(i) = 1$.

$$cycle^C(i) = cycle^C(i-1) + y(i) \tag{5-21}$$

$$cycle^C(i) = 5 * num^C(i) + cycle^A(i) \tag{5-22}$$

where $cycle^A(i)$ is calculated by Eq. 5-22. After this transfer, the $cycle^A(i)$ equals an integer value in the range of 0 to 4, after $cycle^A(i) = 4$, this value would automatically change to 0, which indicates the system restart count the equivalent operating cycle.

$$cycle^A(i) \geq cycle^A(i-1) - 0.001 - M * r1(i) \tag{5-23}$$

$$cycle^A(i) \leq cycle^A(i-1) - 0.001 + M * (1 - r1(i)) \tag{5-24}$$

In order to find the time period where the designed conditions are met, the time slot should be identified when battery remains in the required conditions [132]. Eq. 5-23 and 5-24 are used to detect the maximum value of operating cycle is met by comparing the current $cycle^A(i)$ and previous timeslot $cycle^A(i-1)$. When $cycle^A(i) > cycle^A(i-1)$, which means the $cycle^A(i)$ follows designed order to count the operating cycle, and $r1(i) = 0$. If $cycle^A(i) < cycle^A(i-1)$, that indicated the

battery resets operating cycle count to 0, tantamount to completing the maximum cycle value 4. At the same time the trigger $r1(i)$ is set to 1. The function of the cycle value is listed in Table 5-2. Correlation table of $r1(i)$ and $cycle^A(i-1), cycle^A(i)$.

$r1(i)$	$cycle^A(i-1)$	$cycle^A(i)$
0	0	1
0	1	2
0	2	3
0	3	4
1	4	0

Table 5-2. Correlation table of $r1(i)$ and $cycle^A(i-1), cycle^A(i)$

Eq. 5-25 and 5-26 are used to detect whether the ZBFB SOC value is less than 0.1% or not. When $SOC(i) < 0.1\%$, then the trigger $r2(i)$ is set equal to 1, otherwise, $r2(i) = 0$.

$$SOC(i) \geq 0.1 - M * r2(i) \tag{5-25}$$

$$SOC(i) \leq 0.1 + 0.001 + M * (1 - r2(i)) \tag{5-26}$$

Eq. 5-27, 5-28 and 5-29 perfrom the logic *and* operation as the Eq. 5-18, 5-19 and 5-20 did. After those steps, all timeslots which meet the above requirements are marked out with the trigger variable $r(i) = 1$.

$$r1(i) \geq r(i) \tag{5-27}$$

$$r2(i) \geq r(i) \tag{5-28}$$

$$r(i) + 1 \geq r1(i) + r2(i) \tag{5-29}$$

After the all timeslots have met the requirements marked out, the refresh mode should be deployed as soon as possible. After refresh mode completes, the battery system could

resume normal operation. Based on this strategy, the first timeslot among the all met required timeslot needs to be identified. That is what the Eq. 5-30 and 5-31 are used for. These functions detect the value changing from 0 to 1. If $r(i)$ from $0 \rightarrow 1$, then $z(i) = 1$, otherwise, $z(i) = 0$.

$$r(i) \geq r(i-1) + 0.001 - M * (1 - z(i)) \quad (5\text{-}30)$$

$$r(i) \leq r(i-1) + 0.001 + M * z(i) \quad (5\text{-}31)$$

Finally, $P_c(i)$ and $P_d(i)$ equal to zero dependent on the design. However, the Eq. 4-3 is not linear function that cannot be implemented in MILP model. Extra transfer of those non-linear function into linear one, the Eq. 5-1, 5-2 and 5-3 are replaced by Eq. 5-32, 5-33 and 5-34. And $P_c(i)$ and $P_d(i)$ are set to zero by Eq. 5-35.

$$0 \leq P_c(i) \leq P_{max} * c(i) \quad (5\text{-}32)$$

$$0 \leq P_d(i) \leq P_{max} * d(i) \quad (5\text{-}33)$$

$$0 \leq c(i) + d(i) \leq 1 \quad (5\text{-}34)$$

$$0 \leq c(i) + d(i) \leq 1 * (1 - z(i)) \quad (5\text{-}35)$$

The ZBFB model with refresh mode dependent on operating cycle counting has been established and outlined by Eq. 5-14 to Eq.5-35.

5.3.3 Simulation and result

The novel ZBFB model with specific refresh mode has been presented in previous sections of this chapter. In this section, this model is tested and verified by simulation based on real practical applications.

Many efforts have been made in utilizing renewable energy and battery hybrid systems in residential [133] and commercial [134] applications with minimizing the electricity energy cost. The simulation based on the ZBFB model is applied towards the general target of microgrid.

The objective function is shown in Eq. 5-36

$$\text{Minimize: } \sum_{i=1}^{n} \left(R_p^{grid} \times \text{Max}\left(P^{grid}\right) + R_e^{grid} \times P^{grid} \times \Delta t \right) \quad (5\text{-}36)$$

where R_p^{grid} and R_e^{grid} denote the electricity demand rates and electricity energy rates, respectively. P^{grid} denotes the electricity energy coming from grid, which depends on the original building load, renewable energy generation and the battery charging/discharging power based on the ZBFB model.

The constraints contain the modelling of ZBFB with refresh mode (Eq. 5-14 to Eq. 5-35) and PV-battery system power balance (Eq. 5-37).

$$load(i) = renew(i) + P_d(i) + P^{grid}(i) - P_c(i) \quad (5\text{-}37)$$

where $load(i)$ represents the building load, $renew(i)$ denotes the renewable energy generation, $P^{grid}(i)$ indicates the electricity energy from utility, and $P_c(i)$ and $P_d(i)$ denote ZBFB charging power and discharging power, respectively. This equation sets a constraint on energy balance during the simulation period.

The simulation is tested with the one year historic load data of a commercial building. The main parameters of the battery are shown in Table 5-3.

Parameter name	value
ZBFB capacity	400 kWh
ZBFB maximum power	100 kW

Table 5-3. ZBFB main parameters in simulation

Here, the main objective is to verify the modelling of ZBFB with refresh mode function. Many efforts have been made by other researchers that focused on the prediction of renewable generation and load. In this part, all system recorded values are directly utilized in simulations. Thus, the verification is tested by observing whether ZBFB

behaviors can follow the designed strategy. In one month simulation for July, there are 4 times total when refresh mode ocurred.

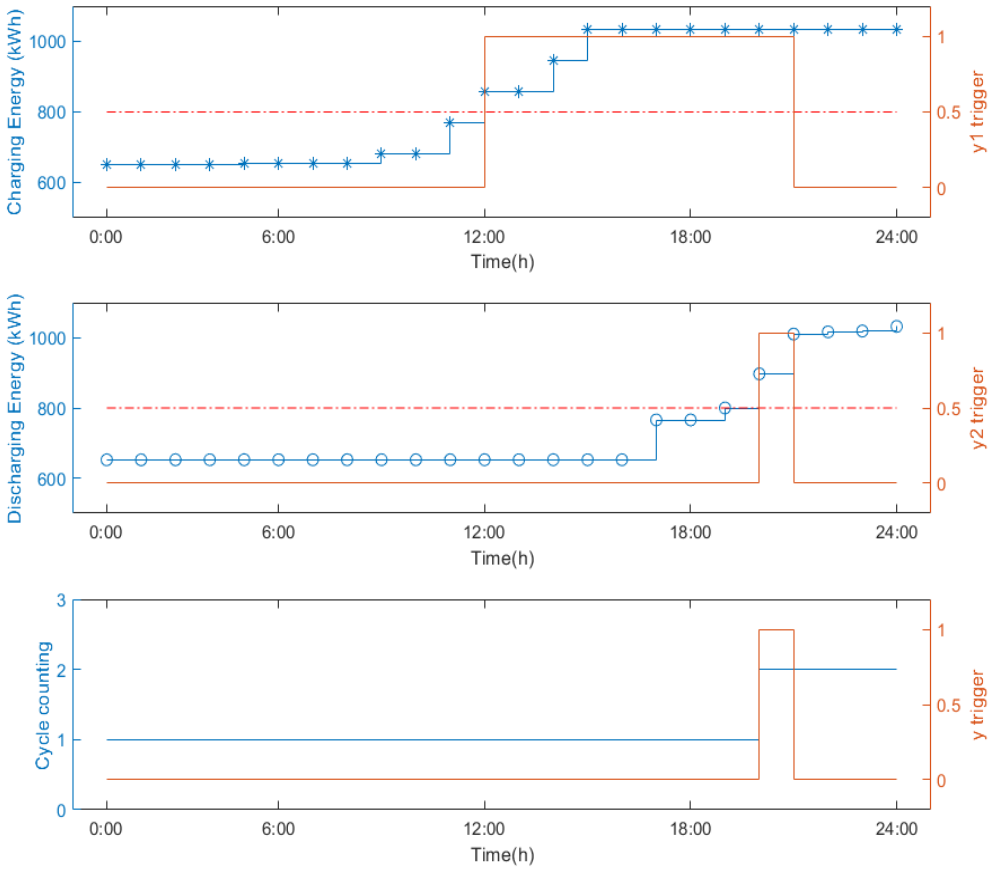

Figure 5-3. Cycle counting function result of ZBFB model

Figure 5-3 indicates the cycle counting function of the model. Because the battery capacity is 400 kWh, from Figure 5-3 (a) (b), which shows the charging energy/ discharging energy has already exceeded 600, it can be concluded that the current cycle value of ZBFB current is 1. With the battery operating, the charging energy in Figure 5-3 (a) is more than 800 kWh, while the y1(i=12) trigger step is 1.

However, due to battery discharging energy not being large enough for changing the y2 trigger, the value of variable y didn’t change Figure 5-3 (c). With the ZBFB releasing

energy to grid during 5 pm to 8 pm, the discharging energy meets the threshold value 800 kWh, which triggeres the y2(*i*=20) value to 1, as seen in Figure 5-3 (b). At the same time, the y value changes to 1. That means the cycle value is 2 after 9 pm. As defined by the Eq. 5-14 to Eq.5-17, y(*i*=20) value automatically returns to 0 after changing to 1 in Figure 5-3 (c).

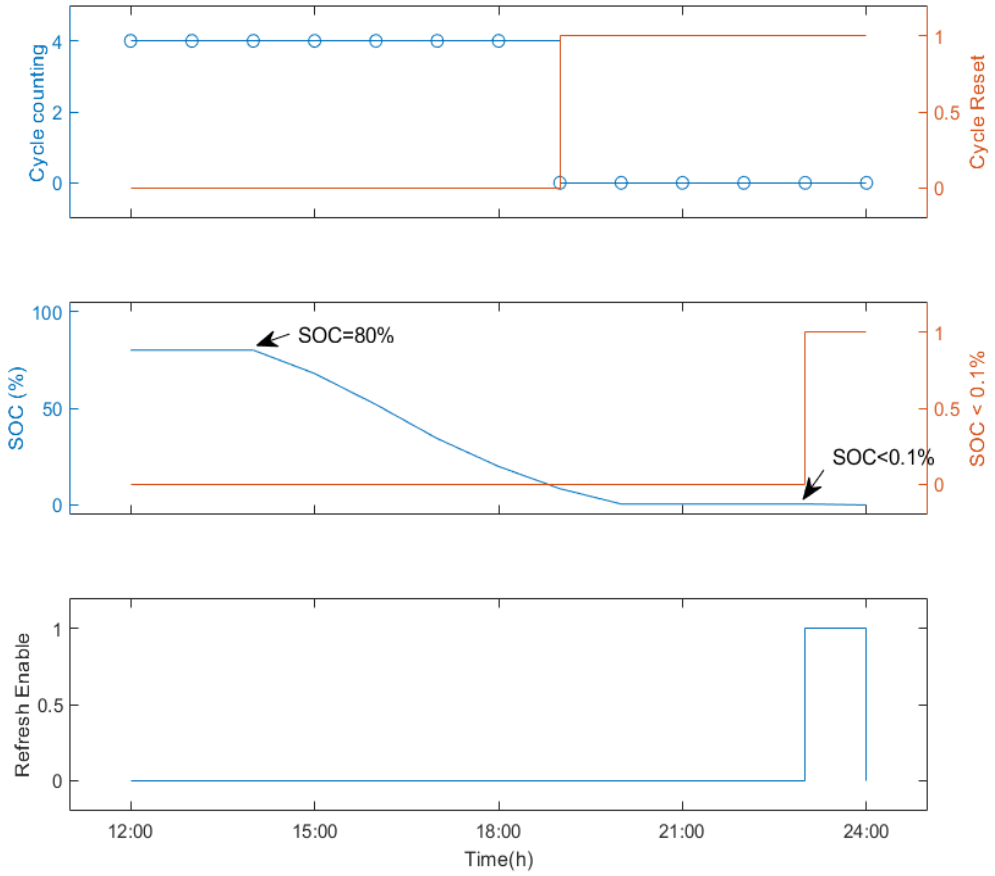

Figure 5-4. Refresh mode implementation function of ZBFB model

As Figure 5-4 (a) shows, the cycle value equals 4 until 7 pm, after that the cycle reset trigger r1(*i*=19) is set to 1, while the cycle value transfers to the initial cycle 0. Figure 5-4 (b) demonstrates SOC value changing from 80% at 12 pm to less than 0.1% at 11pm. At 11 pm, the SOC value meets the requirement of Eq. 5-25, 5-26. The r2(*i*=23) trigger

is set to 1. Meanwhile, the refresh enable value r(*i*=23) is set to 1. During the refresh enable time period, the BMS automatically runs ZBFB in refresh mode to strip all zinc deposited on electrodes.

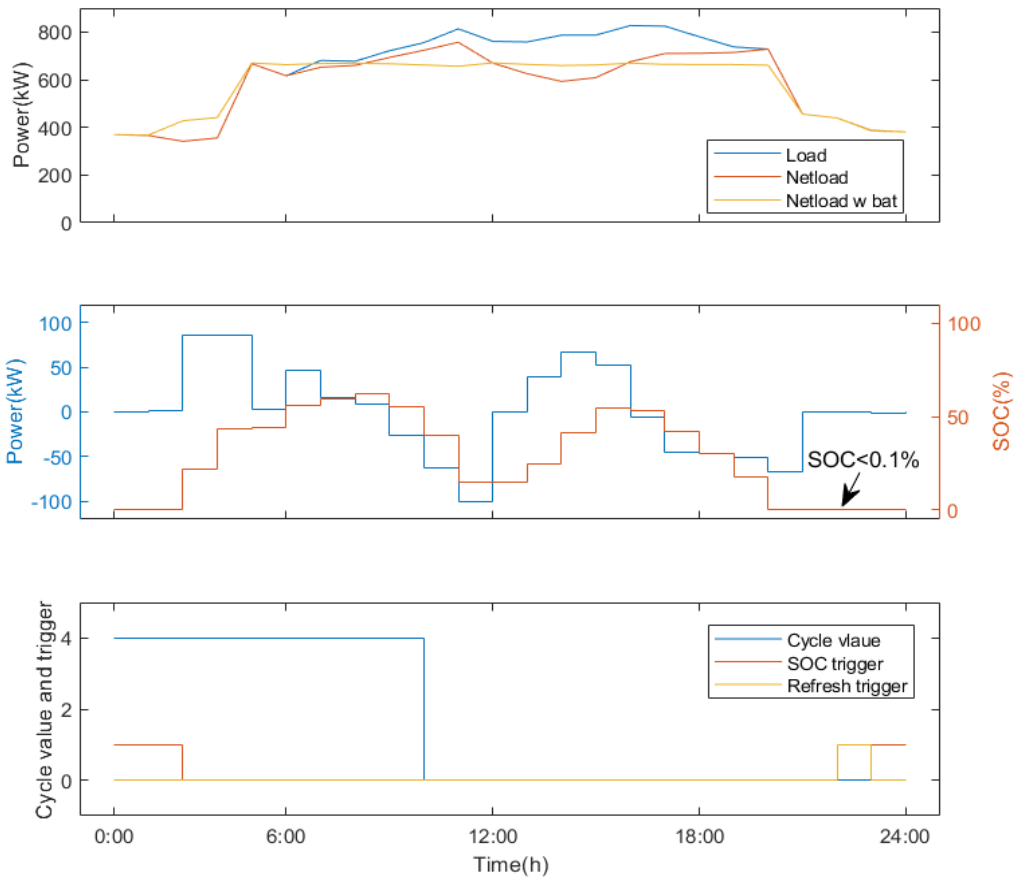

Figure 5-5. A simulation result for July 17th from ZBFB model

Figure 5-5 demonstrates the battery function of reducing energy cost. The ZBFB releases energy to support a little peak due to the decrease in renewable generation (Figure 5-5 (b)), and store energy again afternoon. The reason is higher rates during the period of 4 pm to 9 pm. At the beginning of this simulated day, SOC of ZBFB is less than 0.1%, as a result, r2(*i*=0,1) equals 1. However, current cycle value is 4, which cannot trigger r1 variable. So, the refresh enable trigger stays in idle state (Figure 5-5

(c)). Only when both r1(i=22) and r2(i=22) equal 1, the refresh enable trigger is set to 1.

5.4 Emission reduction control algorithm

Based on the International Energy Agency report [135], the total global energy consumption in 2019 was about 120 million tons of oil equivalent (Mtoe), which accounts for around 33.2 gigatons (Gt) carbon dioxide (CO_2) emissions. Furthermore, according to the U.S. Energy Information Administration [136], total electricity energy consumption in the U.S. in 2019 was about 4.12 trillion kilowatt-hours (kWh), which equals to about 1.82 Gt CO_2 emissions. The global climate change, energy shortage and exponentially growing greenhouse gas emissions have raised awareness and put emphasis on utilizing sustainable and environmental friendly energy sources. One significant motivation of widely deployed DRES is to reduce GHG emission [137]. There is no doubt that the renewable energy could reduce the GHG emission compared to traditional energy. However, battery system charging adds more complexity. That is due to the battery inherent efficiency loss and the emission amount difference between the charging energy and discharging energy due to the emission rate and operating time [68]. Many studies focused on the positive influence of renewable energy on the environment, have neglected the negative effects of battery systems in the grid-connected hybrid system [138]. In this dissertation, a control algorithm for grid-connected hybrid system has been created, which makes maximizing revenue and minimizing emissions its main targets, by quantify battery influence with modelling of ZBFB with refresh mode.

5.4.1 Introduction and background

This simulation utilizes a large official building located in Southern California with solar PV generating system, as the project and demonstration site. The building is under Southern California Edison large commercial Time of Use rate schedule. Electricity cost contains two components: energy (kWh) and peak demand (kW).

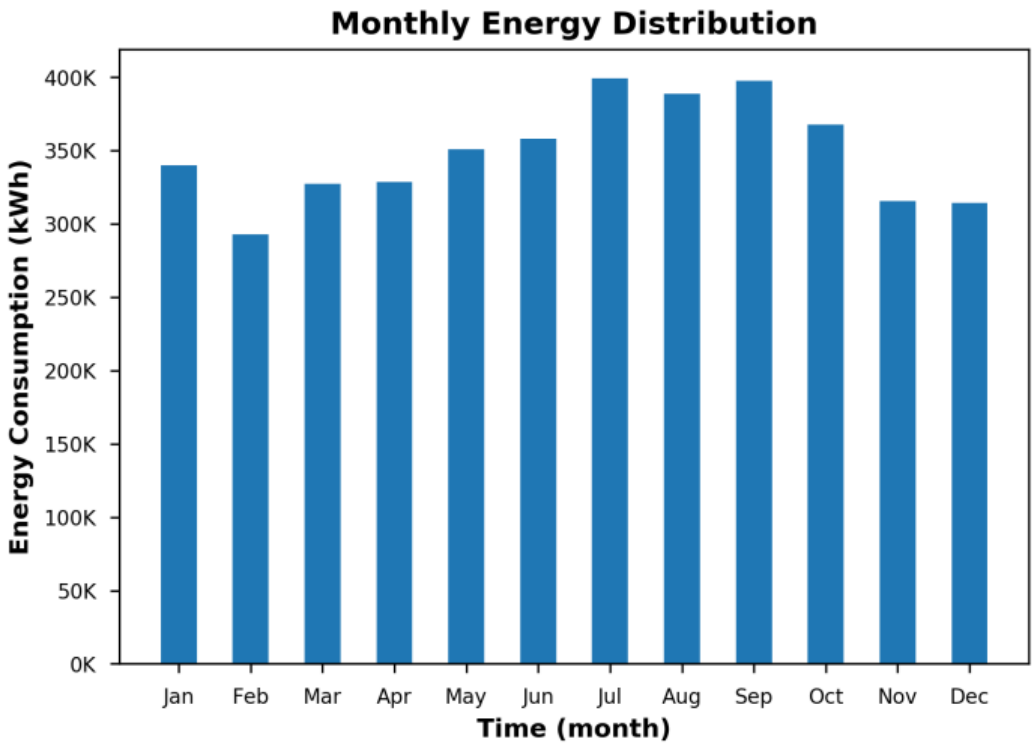

Figure 5-6. The Building Monthly Energy Distribution

According to TOU provisions, the energy cost is dependent on how much energy is consumed during specific periods in terms of time of day, day of the week, and time of year. While the peak demand cost is determined by the maximum power demand during those respective periods. Figure 5-6 shows the building consumes as much as 400,000 kWh in July, and the monthly average consumption is around 350,000 kWh, and is relatively constant throughout the year.

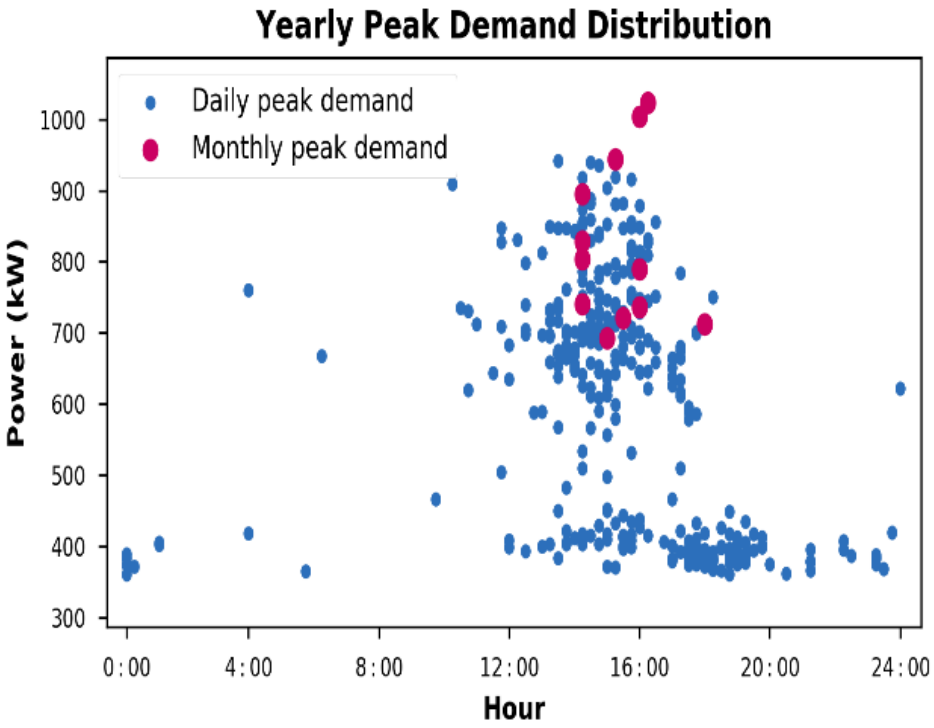

Figure 5-7. The Building Peak Demand Distribution

Another significant data is the maximum value of demand, which is relevant with the demand cost portion. More details are shown in Figure 5-7. From this figure, the majority of demand peaks (96.3%) occurred between 10 AM to 9 PM in one-year recorded data. Some demand peaks occurred within the on-peak demand period of the TOU rate schedule, defined from 4 PM to 9 PM. There are two examples, one peak occurred on a working day, around the 700 kW, another one on the weekend, around 400 kW. Due to TOU tariff rates, the peak demand cost could equal or even exceed energy cost in the summer. Taking the August bill as an example, the peak demand cost was $34,577, almost equal to the energy cost of $34,918. During the winter season, the demand cost could be more than 30% of total electricity bill. According to above information, it is unrealistic to only utilized local renewable energy to support the energy requirement of this commercial building. As a result, grid-connected DRES is

an optional choice, which can bring in cleaner energy, while reducing the high electricity bill.

5.4.2 Emission factor

Much of research works have begun to focus on reducing GHG emissions. Among those works, there is one essential and unavoidable problem which needs more attention; that is how to quantify the GHG emissions. The measurement of GHG emissions require professional equipment and tests in various application scenarios. Most research reports utilized the equivalent conversion method, which derives emissions value by calculating the consumption of fuel or electricity energy [139][140][141]. There are two parameters which can be used to convert the electricity energy into GHG emission value. They are average emission factor (AEF) and marginal emission factor (MEF). The AEF is defined as the total direct CO_2 emissions of the electricity generation sector, divided by the total electricity generation around a given region over a certain period [142]. In this evaluation method, the emission value is evenly distributed over all generation facilities, which overlooks the difference between the fuel resources, such as coal- and natural gas-fired power plants. However, this is not in line with the functioning of electricity markets, since in practice a decrease in requested supply results in decreased electricity generation of facilities operating at the margins. Usually, AEF is used to estimate the emissions of the replaced electricity generation [143].

For reducing GHG emissions of the whole system, Marginal Emission Factor (MEF) has been employed to assess system emission performance [144]. MEF could embody the emissions rate from the marginal generator used to meet demand [145]. MEF is regarded as the incremental change in GHG emissions as a result of a change in demand [146][147]. The marginal GHG emission factor (MEF) used in this work has

been derived from the SGIP, which aims at providing incentives to support clean distributed energy systems [148]. The MEF is updated or recorded at 5-minute intervals, which can approximately reflect the real time emissions rate of power demand. According to the data of SGIP marginal GHG emission signal, emission rates for a winter and a summer day, respectively, are shown in Figure 5-8.

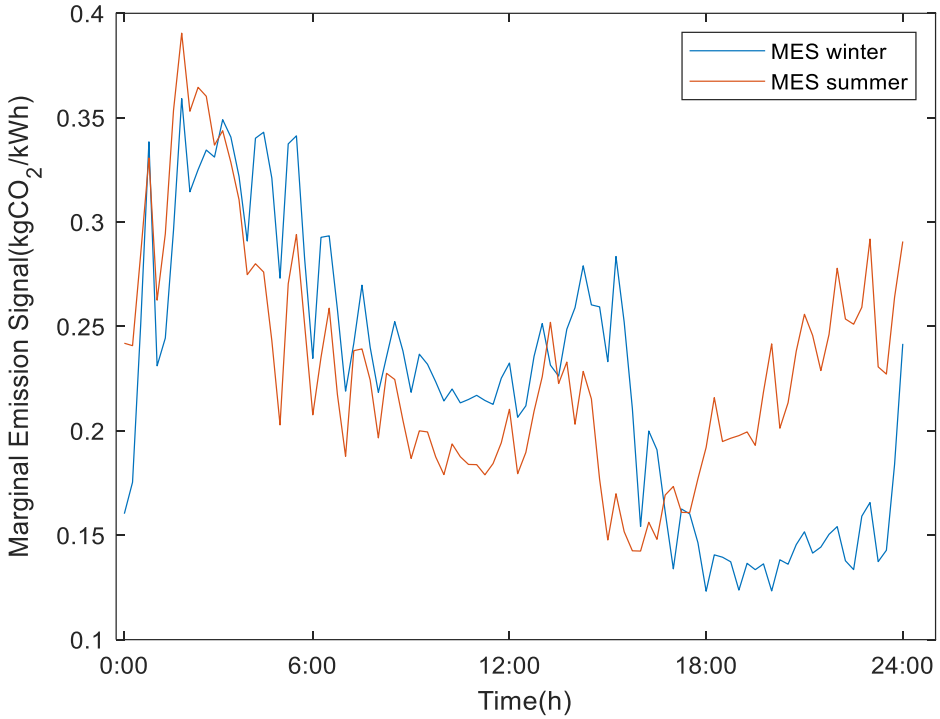

Figure 5-8. Marginal Emission Signal cases of a summer and a winter day

Figure 5-8 shows the difference between the two seasons is indiscernible. However, the MEF reflects the emission rates based on the entire electricity market system demand at that moment. As the result, the MEF value is rapidly changing.

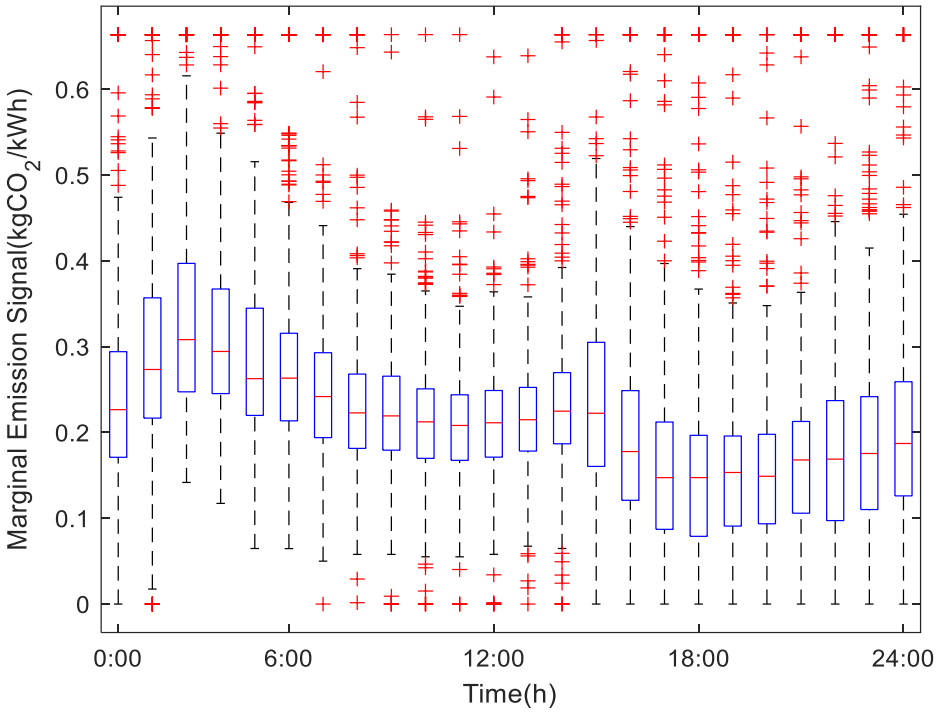

Figure 5-9. Marginal Emission Signal hourly distribution

Based on the MEF value in 2019, the hourly distribution has been shown in Figure 5-9. In this figure, the MEF value during peak period (4 pm-9 pm) is generally lower than other periods based on MEF historical data. The main reason is that with huge increments of energy requirement during that period, generators fueled by natural gas will be utilized in this situation. As previously stated, the emission performance of natural gas is better than other fossil fuels. This means charging battery during night and releasing the stored energy during peak time period has probability to increase GHG emission. This is one reason grid-connected PV-battery hybrid system could result in increased net GHG emissions.

Considering local DRES energy requirement is quite small compared with the total energy consumption of the entire market, the assumption has been made that demand of this local DRES cannot cause fluctuation of whole electricity market. The

dynamic MEF has been chosen to represent the GHG emissions based on power demand of the microgrid.

5.4.3 Control algorithm

In this control algorithm, there are two targets for the optimization problem that are minimizing microgrid system operating cost and reducing GHG emissions. One study [140] found GHG emissions reduction is one benefit of minimizing the system annual energy cost. Another research study [141] presented a multi-objective optimization model for cost-emission performance of PV/battery/fuel cell hybrid energy system, but neglected the positive influence of battery system. A study [149] conducted optimization for the LCOE and CO_2 emission using the multi-objectives GA approach to optimize the size of a hybrid system. Another report [150] optimized a PV/WT/Diesel/Battery unit for minimizing the energy cost and CO_2 emissions using a multi-objective optimization. The multi-objective optimization is widely utilized by researchers with two or more targets, due to its simplicity and efficiency without transferring the objectives of different field into one unit or the same field. To account for the GHG emissions cost component, the Social Cost of Carbon (SCC) has been introduced. Based on published reports [151][152], the SCC value [153] is equal to \$123/Mt CO_2.

Therefore, the objective function is defined as one objective function with two parts: $\text{Minimize (Operating cost} + \text{ Emission cost)}$

where operating cost is the cost of grid energy usage:

$$\sum_{d=1}^{n} \left(R_p^{grid} \times \text{Max}\left(P^{grid}\right) + R_e^{grid} \times P^{grid} \times \Delta t \right) \quad (5\text{-}38)$$

The emission cost is:

$$0.123 \times \sum_{i=1}^{n} \left[R_p^{emis} \times (P^{grid} + (P_c \times (1 - \text{eff}) + P_d \times \left({}^{1}/_{eff} - 1 \right))) \times \Delta t \right] \quad (5\text{-}39)$$

Where R_p^{grid} is the TOU price rate of grid power, R_e^{grid} is the TOU price rate of grid energy, P^{grid} is the grid electricity power, P_c is the battery charging power, P_d indicates the battery discharging power, eff represents ZBFB charging/discharging efficiency, which equals the square root of the round-trip efficiency, and R_p^{emis} denotes the MEF value with unit CO_2 kg/kWh. The local DRES operating constraints and ZBFB model have been discussed in Eq.5-1 to Eq. 5-35.

Algorithm 2: Control Algorithm for reducing cost and emission

Input: building load data l, renewable generation s, current time index i, initial battery state SOC_{init}, efficiency eff, *and* batery capacity Bat_{cap}

Output: Decision of $P_c(i)$ *and* $P_d(i)$

for $i = 1 : 24$ **do**
- $P^{grid}(i) + P_d(i) + s(i) = l(i) + P_c(i)$;
- $SOC(i) = SOC(i-1) + (P_c(i) * eff - P_d(i)/eff) * \Delta t / Bat_{cap}$;
- **if** $E_c(i) \geq Bat_{cap}$ *and* $E_d(i) \geq Bat_{cap}$ **then**
  - $cycle_C(i) = cycle_C(i-1) + 1$;
- **end**
- $cycle_C(i) = 5 * num(i) + cycle_A(i)$;
- **if** $cycle_A(i)$ $(4 \rightarrow 0)$ *and* $SOC(i) \leq 0.1\%$ **then**
  - $P_c(i) = 0$;
  - $P_d(i) = 0$;
- **end**
- $i \leftarrow i + 1$;

end

Figure 5-10. Pseudo-code of Cost and Emission reduction with ZBFB model with refresh mode

In this study, the simulation method is presented to determine the optimal control battery charging/discharging power P_c and P_d in this PV-battery hybrid system

with consideration of the specific ZBFB operational constraints, as shown in Figure 5-10. Pseudo-code of Cost and Emission reduction with ZBFB model with refresh mode, which represents pseudo-code of cost and emission reduction with ZBFB model with refresh mode. All simulations are based on real data. The presence of integer decision variables with constraints in the optimization problem leads to a mixed-integer nonlinear programming problem. MOSEK solver is used to solve this optimization problem under the MATLAB environment.

5.5 Simulation and result

In this section, numerical simulations to verify the effectiveness of various control scenarios and different refresh strategies for primary emission reduction purpose are presented. For modelling of battery with refresh mode, the simulation results between refresh mode after daily usage strategy and the refresh mode employed based on cycle usage, are compared and analyzed. For emission reduction, the widely utilized maximizing system revenue approach is employed as the baseline control scenario. Then, the control algorithm including ZBFB refresh mode is introduced, which is based on the refresh mode with different settings and parameters of the system.

5.5.1 Refresh mode of ZBFB model control simulation

In this section, one simulation is introduced based on the two main refresh mode strategies, 1) refresh mode after daily usage 2) refresh mode after specific equivalent cycle usage.

For the refresh mode after daily usage, the prerequisite for refresh cycle is same as previously described, which requires the SOC value reach 0%. In this refresh mode strategy, the ZBFB performs refresh cycle after one day operation and the SOC value matches the requirement.

The refresh mode after specific equivalent cycle usage strategy is more complex because the refresh mode can be done by specific equivalent cycle. In a previous section, the simulation for ZBFB model was set to drive refresh mode after 4 equivalent cycles, was created to test whether it could meet the expectations of modelling. However, the equivalent cycle value could in reality vary from 1 to 4. For example, the ZBFB can perform refresh mode after one equivalent cycle instead of the four equivalent cycles. The performance for ZBFB model with different specific cycle values is verified in this section. Furthermore, the cycle value has an impact on the ZBFB energy efficiency. One study [30] reported the first new cycle efficiency being slightly lower, due to the base coat of zinc being re-plated. The specific cycle energy efficiency of ZBFB is presented in Table 5-4, which is constructed based on the aforementioned report.

Parameter name	cycle 0	cycle 1	cycle 2	cycle 3	cycle 4
ZBFB efficiency	0.72	0.78	0.76	0.74	0.72

Table 5-4. Specific cycle energy efficiency of ZBFB [30]

Using these efficiency values and the created ZBFB model, one month simulation results for minimizing energy cost and GHG emission (Eq. 5-39 and Eq. 5-39) with those two main strategies are obtained and presented in Table 5-5.

Simulation result	Refresh times	Energy cost ($)	Emission (kg)	Total cost ($)
Cycle = 1	6	46333.17	87680.72	56854.86
Cycle = 2	5	46349.05	87660.15	56868.26
Cycle = 3	5	46349.00	87681.53	56870.78
Cycle = 4	4	46361.37	87705.23	56886.00
Daily refresh	-	46389.59	87754.22	56920.10

Table 5-5. Simulation result with two refresh mode strategies

Based on the results shown in the Table 5-5, performing refresh mode after the first equivalent cycle is completed, results in the minimum cost for both energy cost and emission cost. The refresh process duration varied depending on the cycle value setting. When specific cycle value is 1, there are 6 refresh occurrences over the span of one month simulation. There is a negative correlation between the cycle value and the refresh frequency. The higher the specific cycle value is, the less frequently refresh mode happens. From the above data, it appears there is only limited difference for each case. Cycle value equal to 1 outperforms other cases with a little advantage for a month long simulation. However, the simulation results of each day varied based on the cycle value setting. Even when using the same load data as input, the results would be different due to the different cycle value setting and the current cycle status. Considering the emission rates of 0.123 $/kg, the emission component plays a limited role in determining operation. From the data in Table 5-5, it is not obvious that the simulated results difference is entirely due to the specific cycle value. Given that the

refresh mode with one equivalent cycle has the best long term cost performance, this specific cycle value has been chosen as the default setting in in following simulation.

5.5.2 Emission control simulation

Scenario 1: using original building load data

The original building load data has been chosen as the baseline for simulation and analysis in this section.

Scenario 2: Maximizing the system revenue as only objective function

With respect to scenario 1, the Eq. 5-38

$$\sum_{\mathrm{d=1}}^{\mathrm{n}} \left(\mathrm{R}_{\mathrm{p}}^{\mathrm{grid}} \times \mathrm{Max}\left(P^{grid}\right) + \mathrm{R}_{\mathrm{e}}^{\mathrm{grid}} \times P^{grid} \times \Delta \mathrm{t} \right) \tag{5-38}$$

as the only objective function to minimize the whole system energy cost using the two main refresh mode strategies, which consist of the daily refresh and the refresh mode with one equivalent cycle usage. In this scenario, the ZBFB paired with solar PV has been utilized to reduce energy cost as the only objective function.

Scenario 3: Minimizing the energy cost and Emission cost as objective function

With respect to scenario 3, the Eq. 5-38 and Eq. 5-39 as objective functions to

$$0.123 \times \sum_{\mathrm{i=1}}^{\mathrm{n}} \left[\mathrm{R}_{p}^{\mathrm{emis}} \times (P^{grid} + (P_c \times (1 - \mathrm{eff}) + P_d \times \left({}^{1}/_{eff} - 1 \right))) \times \Delta \mathrm{t} \right] \tag{5-39}$$

minimize the whole system energy cost and emission cost, using the two main refresh mode strategies.

In the following section, the emission results with three mentioned scenarios are presented and discussed.

5.5.2.1 Comparative analysis of three scenarios

Compared to the original building system (baseline), the control algorithm scenario 2 and scenario 3 for PV-ZBFB with refresh mode could reduce the whole system energy cost and GHG emission. In order to compare those cases, the energy and emission data are converted to cost in USD, which are shown in Figure 5-11.

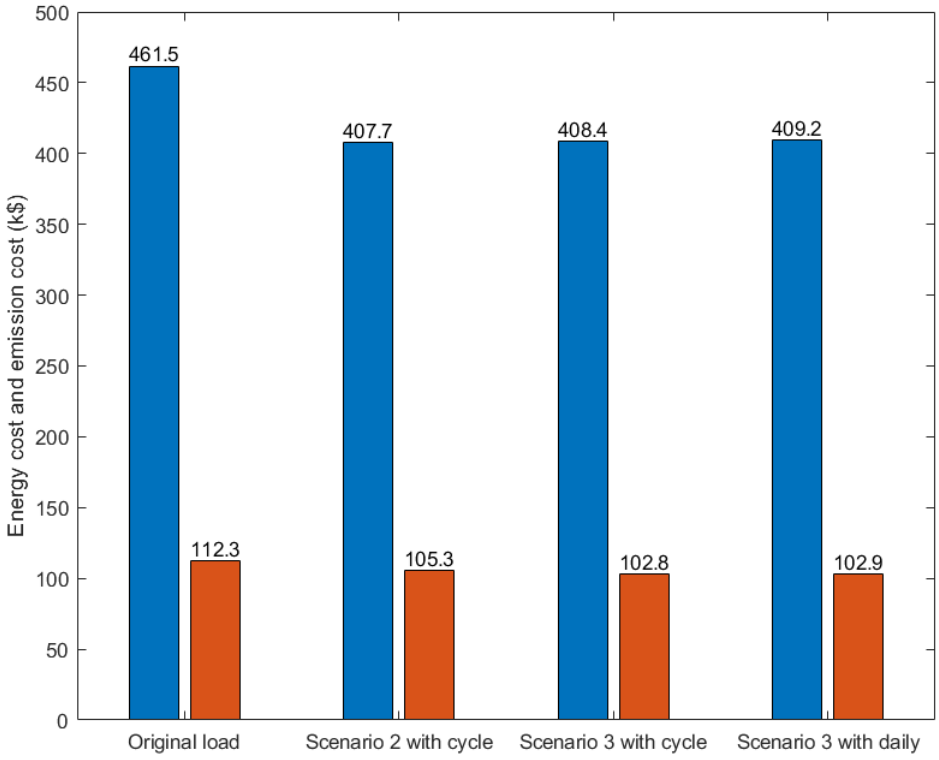

Figure 5-11. Simulation result of scenarios with two refresh mode strategies

As shown in above figure, for one-year simulation, there is only limited difference in economic performance between the refresh mode with one equivalent cycle and daily refresh mode strategy. They provide similar results in this type of optimization problem.

5.5.2.2 Simulation results of scenarios 2 and scenario 3 with refresh mode after one equivalent cycle

For scenario 2, one primary target is minimizing the energy cost which is only utilized in Eq. 4-38 as objective function. Scenario 3 pursues minimizing the energy cost, while also aiming at minimizing the emission cost for the whole system. In scenario 3, there are two unavoidable contradictory conditions, which arise from the negative effects of battery operation on emission cost. In the first one, for example, higher charging/discharging battery operation leads to more energy losses due to the inherent battery's less than perfect efficiency. The second reason is the mismatch in the electricity rates and the marginal emission factor. In this section, the same refresh mode with one equivalent cycle has been utilized in scenario 2 and scenario 3. By comparing the simulation results, the essential role of emission component can be further understood and explained.

All objective functions have been transformed into the economic cost, from energy (kWh) and GHG emission (kg). The economic performance with these two scenarios is first examined and discussed. The corresponding results are presented in Table 5-6.

	Energy cost ($)	Emission cost ($)	Objective value
Minimize Energy & Emission	408412.6	102823	511235.6
Minimize Energy only	407697.8	105295.1	407697.8

Table 5-6. Objective energy and emission cost of scenario 3 and scenario 2

Due to these two scenarios' objective functions being different, comparison between the results of these objective functions less rigorous in objectivity. From Table

5-6, it is evident that if comparing the objective function results, scenario 2 is better in terms of economic performance. However, the emission value should not be neglected, by minimizing the energy cost without considering the influence of emission. The calculated emission cost based on optimal battery operational power, under scenario 2 objective function is present in Table 5-6. From the perspective of energy cost, scenario 2 has slightly better performance. From the point of emission cost, scenario 3 has a small advantage. After combining these values, total economic performance in scenario 3 is better. Despite the fact that scenario 2 has better performance in energy cost, scenario 3 performs better overall for total cost, considering emission cost.

For this chapter, the major topic is reducing the emission, while minimizing the energy cost. The local renewable energy has positive impact on reducing emission compared to the original system. However, energy storage system, as the main factor in decreasing the energy cost, has negative effect on GHG emission. Based on above mentioned, there are two ways a battery can increase the local microgrid GHG emission. In order to build a numerical and intuitionistic comparison and analysis, Eq. 5-40 and Eq. 5-42 have been created to quantify the emission influence with different control algorithm scenarios.

$$\sum_{\mathrm{i}=1}^{\mathrm{n}}\left[\mathrm{R}_{p}^{\mathrm{emis}} \times (P_c - P_d) \times \Delta t\right] \tag{5-40}$$

$$\sum_{\mathrm{i}=1}^{\mathrm{n}}\left[\mathrm{R}_{p}^{\mathrm{emis}} \times (P_c \times (1 - \mathrm{eff}) + P_d \times \left({}^{1}/_{eff} - 1\right)) \times \Delta \mathrm{t}\right] \tag{5-41}$$

Where $\mathrm{R}_{p}^{\mathrm{emis}}$ is the MEF with unit of kg/kWh, P_c denotes the charging power from grid (kW), P_d denotes the discharging power from grid (kW). eff denotes the battery efficiency.

Eq. 5-40 indicates emission variation due to battery charging/discharging operation. When ZBFB stores energy from grid, the GHG emission increases with higher power consumption. During ZBFB release of energy to decrease the local demand, GHG emission is reduced by indirectly decreased grid power demand. The MEF and battery charging/discharging operations are determinants of the annual emission. Eq. 5-41 indicates emission increasing due to battery efficiency. From this equation, two elements, efficiency and battery charging/discharging operations, play a significant role in determining the final emission result. Both scenarios utilize the refresh mode with one equivalent cycle strategy, which extremely attenuates the function of efficiency.

Figure 5-12 represents emission results of battery emission under scenario 3 and scenario 2. The left column stands for scenario 3, and the right column stands for scenario 2. From this figure, it is evident that the scenario 3 has better ZBFB emission performance, when compared with scenario 2. There is roughly 20.6 metric ton equivalent CO_2 reduction for the entire local microgrid.

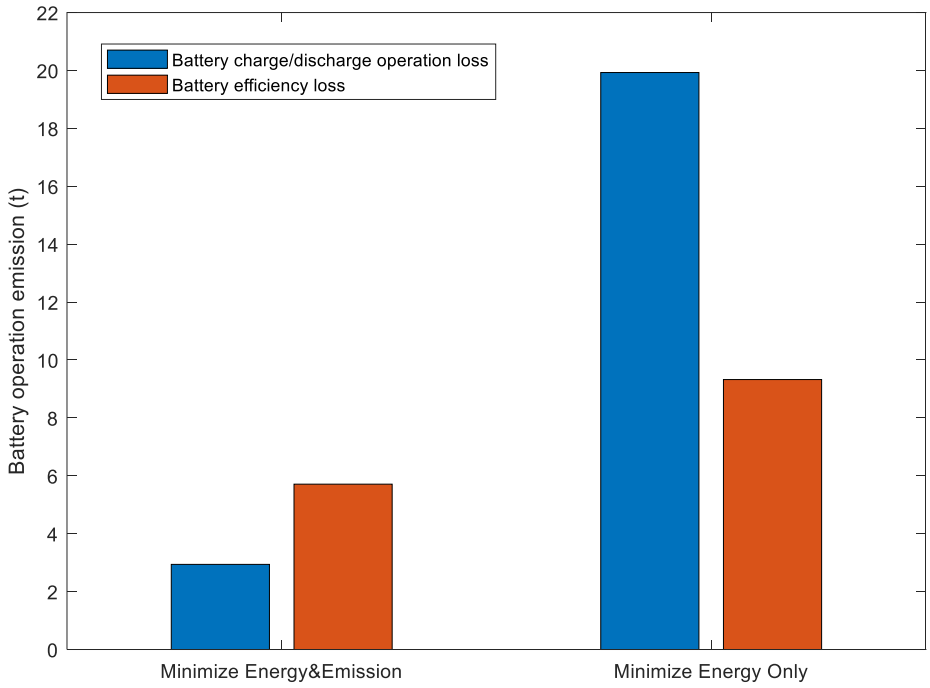

Figure 5-12. Comparison of battery emission with scenario 3 and scenario 2

Emission associated with ZBFB operation is based on Eq. 5-40. More details are shown in Figure 5-13 and Figure 5-14. The blue line indicates the daily numerical emission from ZBFB charging/discharging operation. The red curve denotes the accumulated value of the daily emission. Due to lack of any emission constraints on ZBFB operation, the ZBFB operation result in enormous increasing of annual emission curve under scenario 2. The simulation used the same recorded data with scenario 3, the daily emission by ZBFB operations is less than the one under scenario 2.

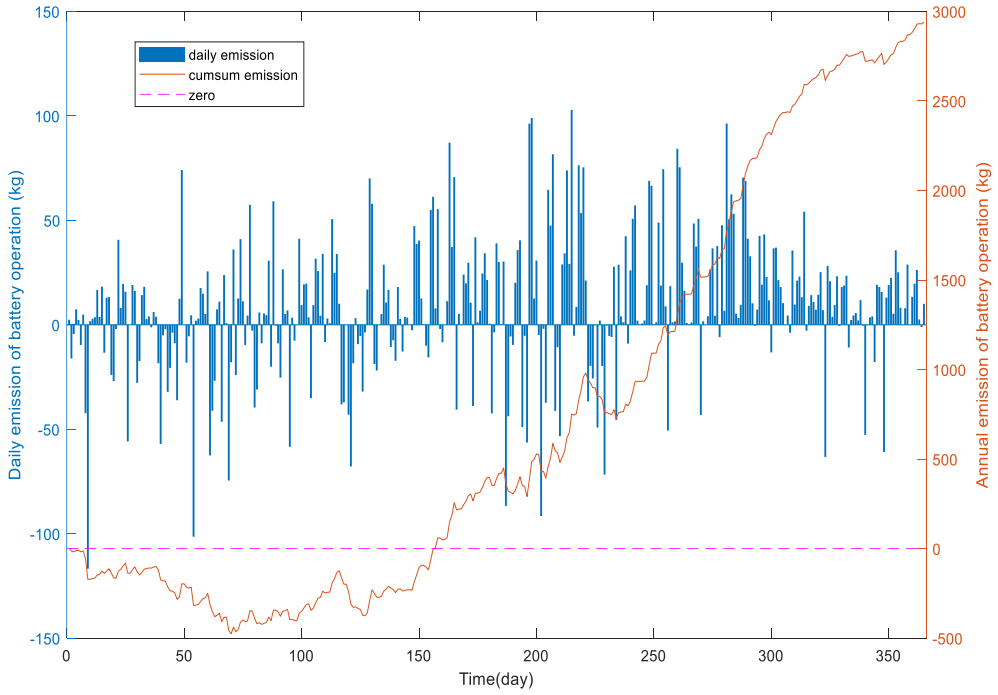

Figure 5-13. Annual emission for battery operation under scenario 3

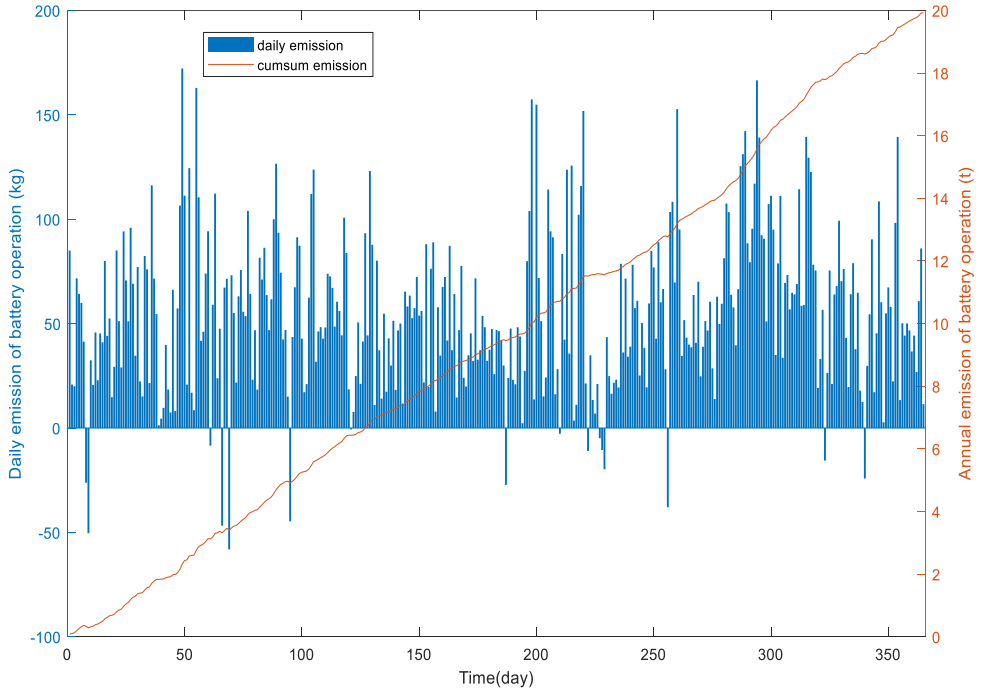

Figure 5-14. Annual emission for battery operation under scenario 2

Figure 5-13shows that accumulated emission value is initially less than 0. A counterintuitive condition occurred where ZBFB discharging operation caused emission increase. The statistic distribution of MEF indicated lower numerical emission factor during peak time in Figure 5-9. However, it does not mean all MEF shared this pattern. The first 3 most minimum negative values were collected on specific dates (9th, 54th and 202nd). To elaborate these result, the data is shown in Figure 5-15. In this figure, discharging power combined with the higher MEF value resulted in ZBFB having positive effects on emission reduction.

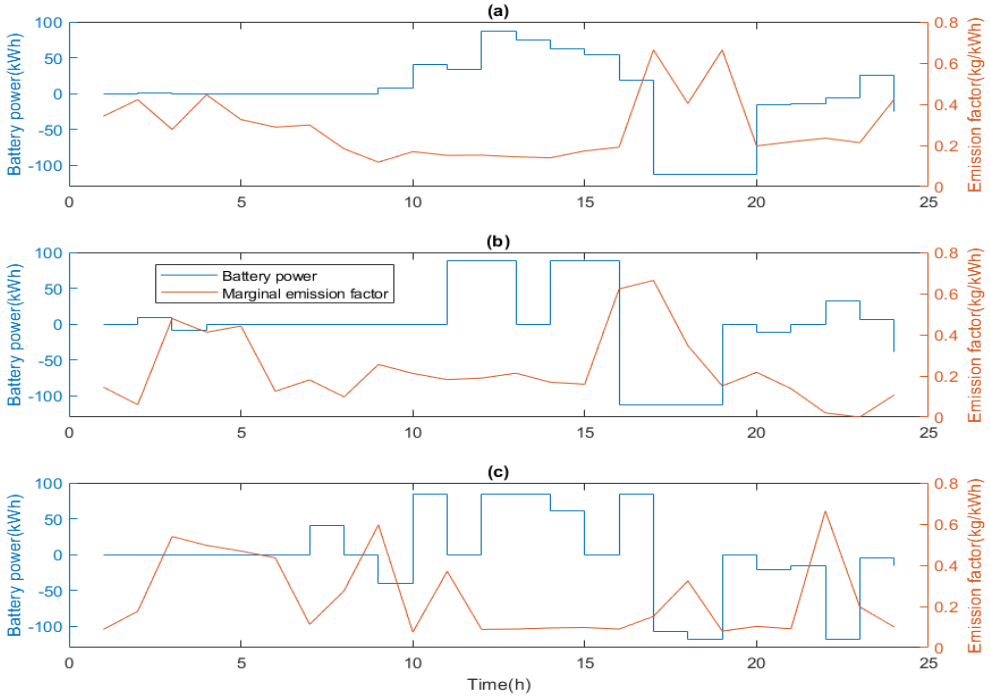

Figure 5-15. Negative daily emission analysis for specific dates (a). 9th date in one-year simulation, (b) 54th date in one-year simulation and (c) 202nd date in one-year simulation

As for emission increase due to ZBFB efficiency, under both scenarios utilizing the refresh mode with one equivalent cycle strategy, its influence between these two scenarios is limited. The main reason for a large variation of emission is the annual

energy volume of battery operation. Table 5-7 shows the ratio of annual emission performance under the two scenarios is close to the ratio of annual energy by battery operations.

	Annual Emission value by efficiency loss (t)	Annual ZBFB charging/ discharging Energy (MWh)
Minimize Energy & Emission	5.711	189.58
Minimize Energy only	9.324	296.46
Ratio	0.612	0.639

Table 5-7. Annual emission performance and battery operation under scenario 3 and scenario 2

5.6 Conclusion

In this chapter, one novel MILP model of ZBFB systems based on equivalent cycle counting method has been presented. This modelling method differs from the method using refresh mode after daily usage. By utilizing the ZBFB model into minimizing the conflicting objectives, local DRES energy cost and emission, several control scenarios have been created and simulated. Based on simulation results, ZBFB performance can be improved, when emission reduction is an objective function used to constrain the battery operation.

6 CONCLUSION

In this dissertation, two limiting constrains in Zinc Bromine Flow Batteries, namely the requirement for a “refresh mode” and “constant charging power” have been investigated and resolved by developing an optimization method to control the operation of ZBFBs in practical use cases. These operational constrains are necessary to manage and reduce the risk of dendrite formation during ZBFB operation, which is a potentially harmful process leading to critical failure. To mitigate risks and optimize operational performance, while accounting for the above constrains, different ZBFB models and control algorithms, have been proposed and evaluated through simulations, analysis and field demonstration. Specifically, this dissertation outlines the following achievements:

The modeling of ZBFB considering the operational constrains is developed by using a Mixed Integer Linear Programming method. First, the modeling of the ZBFB “refresh mode” uses an equivalent charging/discharging cycle counting algorithm. Second, utilizing this model to simulate and evaluate the ZBFB performance in terms of reducing energy cost and GHG emission is performed by considering the influence of the control algorithms and battery constrains.

Unique to ZBFBs, the modelling of the constraint for constant charging power is developed by using a relaxation method. The model is demonstrated and utilized in two real use case applications: minimum import violations and load shifting. The simulation results demonstrate that operational efficiency and performance is improved, while the function of design is satisfied.

Reference:

[1]. IEA (2020), Key World Energy Statistics 2020, IEA, Paris https://www.iea.org/reports/key-world-energy-statistics-2020

[2]. Tomás Tapia, Álvaro Lorca, Daniel Olivares, Matías Negrete-Pincetic, Alberto J. Lamadrid L, "A robust decision-support method based on optimization and simulation for wildfire resilience in highly renewable power systems", European Journal of Operational Research, 2021.

[3]. Folkers, A., Kornberger, M., Bowker, G.C., Elyachar, J., Mennicken, A., Miller, P., Nucho, J.R. and Pollock, N., "Smart Grids and Smart Markets: the Promises and Politics of Intelligent Infrastructures", Research in the Sociology of Organizations, Emerald Publishing Limited, Bingley, pp. 255-272, 2019.

[4]. M. Y. Ali Khan et al., "Environmental Impacts on Energy Utilization of Smart Grid Consumers," 2019 2nd International Conference on Computing, Mathematics and Engineering Technologies (iCoMET), pp. 1-6, 2019.

[5]. P. Ralon, M. Taylor, A. Ilas, H. Bone and K. P. Kairies, , Electricity Storage and Renewables: Costs and Markets to 2030, International Renewable Energy Agency (IRENA), Abu Dhabi, 2017.

[6]. Thomas Ackermann, Göran Andersson, Lennart Söder, "Distributed power generation in a deregulated market environment", Electric Power Systems Research, Volume 57, Issue 3, Pages 195-204, 2001.

[7]. A. Nourai, R. Sastry and T. Walker, "A vision & strategy for deployment of energy storage in electric utilities", IEEE Power and Energy Society General Meeting, pp. 1-4, 2010.

[8]. W. Zhang, D. Dong, I. Cvetkovic, F. C. Lee and D. Boroyevich, "Lithium-based energy storage management for DC distributed renewable energy system," 2011 IEEE Energy Conversion Congress and Exposition, pp. 3270-3277, 2011.

[9]. Fu, Ran, Feldman, David J., and Margolis, Robert M. "U.S. Solar Photovoltaic System Cost Benchmark: Q1 2018", United States: N. p., 2018. Web.

[10]. J. Ren, S. Gao, S. Tan, L. Dong, "Hydrogen economy in China: strengths–weaknesses–opportunities–threats analysis and strategies prioritization", Renewable and Sustainable Energy Reviews, vol 41, pp. 1230-1243, 2015.

[11]. A. Abbas, S. Suardi, Z. Gholamreza, B. Alireza, "A Review on the Drawbacks of Renewable Energy as a Promising Energy Source of the Future". Arab J Sci Eng, vol 38, pp. 317–328, 2013.

[12]. Z. Feng, W. Niu, C. Cheng, “China’s large-scale hydropower system: operation characteristics, modeling challenge and dimensionality reduction possibilities”, Renewable Energy, vol 136, pp. 805-818, 2019.

[13]. J. Lu, J. Shen, C. Su, Q. Shen, “Trans-regional transmission of large-scale hydropower: problems and solutions in receiving power grid”, Global Energy Interconnection, volume 2, no. 4, pp. 342-350, 2019.

[14]. V. Yaramasu, B. Wu, P. C. Sen, S. Kouro and M. Narimani, "High-power wind energy conversion systems: State-of-the-art and emerging technologies," Proceedings of the IEEE, vol. 103, no. 5, pp. 740-788, May 2015.

[15]. J. E. Lovich, J. R. Ennen, “Assessing the state of knowledge of utility-scale wind energy development and operation on non-volant terrestrial and marine wildlife”, Applied Energy, vol 103, pp. 52-60, 2013.

[16]. I. Kumar, W. E. Tyner, K. C. Sinha, “Input–output life cycle environmental assessment of greenhouse gas emissions from utility scale wind energy in the United States”, Energy Policy, vol 89, pp. 294-301, 2016.

[17]. L. Y. Pao and K. E. Johnson, "Control of Wind Turbines," in IEEE Control Systems Magazine, vol. 31, no. 2, pp. 44-62, April 2011.

[18]. A. N. Celik, “Energy output estimation for small-scale wind power generators using Weibull-representative wind data”, Journal of Wind Engineering and Industrial Aerodynamics, vol 91, no. 5, pp. 693-707, 2003.

[19]. M. Adaramola, *Solar Energy: Application, Economics, and Public Perception*, CRC Press, 2014.

[20]. S. Izquierdo, C. Montañés, C. Dopazo, N. Fueyo, “Analysis of CSP plants for the definition of energy policies: The influence on electricity cost of solar multiples, capacity factors and energy storage”, Energy Policy, Volume 38, no. 10, pp. 6215-6221, 2010.

[21]. A. B. Acharya, M. Ricco, D. Sera, R. Teoderscu and L. E. Norum, "Performance Analysis of Medium-Voltage Grid Integration of PV Plant Using Modular Multilevel Converter," in IEEE Transactions on Energy Conversion, vol. 34, no. 4, pp. 1731-1740, Dec. 2019.

[22]. Koebrich, Samuel, Bowen, Thomas, & Sharpe, Austen. “2018 Renewable Energy Data Book”, U.S. Department of Energy (DOE), Office of Energy Efficiency & Renewable Energy (EERE), 2019.

[23]. G. Angenendt, S. Zurmühlen, H. Axelsen, D. U. Sauer, “Comparison of different operation strategies for PV battery home storage systems including forecast-based operation strategies”, Applied Energy, vol. 229, pp. 884-899, 2018.

[24]. IRENA (2020), Renewable Power Generation Costs in 2019, International Renewable Energy Agency, Abu Dhabi.

[25]. S. Dhundhara, Y. P. Verma, A. Williams, “Techno-economic analysis of the lithium-ion and lead-acid battery in microgrid systems”, Energy Conversion and Management, vol. 177, pp. 122-142, 2018.

[26]. A. Lorestani, G.B. Gharehpetian, M. H. Nazari, “Optimal sizing and techno-economic analysis of energy- and cost-efficient standalone multi-carrier microgrid”, Energy, vol. 178, pp. 751-764, 2019.

[27]. A. Mahesh, K. S. Sandhu, “A genetic algorithm based improved optimal sizing strategy for solar-wind-battery hybrid system using energy filter algorithm”. Energy vol. 14, pp. 139–151, 2020.

[28]. National Solar Radiation Database (NSRDB) online: https://nsrdb.nrel.gov/

[29]. Blair, Nate, Nicholas DiOrio, Janine Freeman, Paul Gilman, Steven Janzou, Ty Neises, and Michael Wagner. 2018. System Advisor Model (SAM) General Description (Version 2017.9.5). Golden, CO: National Renewable Energy Laboratory. NREL/ TP-6A20-70414.

[30]. P. C. Butler, P. A. Eidler, P. G. Grimes, S. E. Klassen, and R. C. Miles, CHAPTER 37 ZINC/BROMINE BATTERIES, 2001, sandia.

[31]. G. P. Rajarathnam and A. M. Vassallo “The Zinc/Bromine Flow Battery: Materials Challenges and Practical Solutions for Technology Advancement”, chapter 2, Springer Briefs in Energy, 2016.

[32]. M.C. Wu, T.S. Zhao, H.R. Jiang, Y.K. Zeng, Y.X. Ren, “High-performance zinc bromine flow battery via improved design of electrolyte and electrode”, Journal of Power Sources, Volume 355, Pages 62-68, 2017.

[33]. R. Faries, M. Wasco, T. Stepien, B. Riel and B. Butt, “Zinc Bromide Flow Battery Installation for Islanding and Backup Power”, Environmental Security Technology Certification Program (ESTCP), 2016.

[34]. R. A. Putt, “Assessment of technical and economic feasibility of zinc/bromine batteries for utility load leveling”, Final Report Gould, Inc. Rolling Meadows, IL, 1979.

[35]. M.C. Wu, T.S. Zhao, H.R. Jiang, Y.K. Zeng, Y.X. Ren, "High-performance zinc bromine flow battery via improved design of electrolyte and electrode," Journal of Power Sources, vol. 355, pp. 62-68, 2017.

[36]. D. Darcy and P. Gibson, "Zinc-Flow® batteries for extended duration energy storage at cell towers," INTELEC 2008 - 2008 IEEE 30th International Telecommunications Energy Conference, San Diego, CA, USA, pp. 1-4, 2008.

[37]. K. L. Wang , P. C. Pei , Z. Ma , H. C. Chen , H. C. Xu , D. f. Chen and X. Z. Wang, "Dendrite growth in the recharging process of zinc–air batteries", ournal of Materials Chemistry, vol.3, pp. 22648-22655, 2015.

[38]. M.C. Wu, T.S. Zhao, L. Wei, H.R. Jiang, R.H. Zhang, "Improved electrolyte for zinc-bromine flow batteries", Journal of Power Sources, vol. 384, pp. 232-239, 2018.

[39]. H.S. Yang, J.H. Park, H.W. Ra, C.S. Jin, J.H. Yang, "Critical rate of electrolyte circulation for preventing zinc dendrite formation in a zinc-bromine redox flow battery", J. Power Sources, vol. 325, pp. 446-452, 2016.

[40]. S. J. Banik and R. Akolkar, "Suppressing Dendrite Growth during Zinc Electrodeposition by PEG-200 Additive", Journal of the Electrochemical Society, vol. 160, 2013.

[41]. F. Han, A. S. Westover, J. Yue, X. Fan, F. Wang, M. Chi, D. N. Leonard, N. J. Dudney, H. Wang and C. Wang, "High electronic conductivity as the origin of lithium dendrite formation within solid electrolytes." Nature Energy vol. 4, pp. 187–196, 2019.

[42]. F. Han, J. Yue, X. Zhu and C. Wang, "Suppressing Li Dendrite Formation in Li2S-P2S5 Solid Electrolyte by LiI Incorporation", Advanced Energy Materials, vol. 8, 2018.

[43]. J. Kasemchainan, S. Zekoll, D. Spencer Jolly, Z. Ning, G. O. Hartley, J. Marrow and P. G. Bruce, "Critical stripping current leads to dendrite formation on plating in lithium anode solid electrolyte cells", Nature Materials. Vol. 18, pp. 1105–1111, 2019.

[44]. R. Raj and J. Wolfenstine, "Current limit diagrams for dendrite formation in solid-state electrolytes for Li-ion batteries", Journal of Power Sources, vol. 343, pp. 119-126, 2017.

[45]. Z. C. Xu, Q. Fan, Y. Li, J. Wang and P. D. Lund, "Review of zinc dendrite formation in zinc bromine redox flow battery", Renewable and Sustainable Energy Reviews, vol. 127, 2020.

[46]. F.C. Walsh, M.E. Herron, "Electrocrystallization and electrochemical control of crystal growth: fundamental considerations and electrodeposition of metals", Applied Physics, vol. 24, pp. 217-225, 2000.

[47]. R.V. Moshtev, P. Zlatilova, "Kinetics of growth of zinc dendrite precursors in zincate solutions", Journal of Applied Electrochemistry, vol. 8, pp. 213-222, 1978.

[48]. A. R. Despic, J. Diggle, J. O. Bockris, “Mechanism of the formation of zinc dendrites”, Journal of Electrochemical Society, vol. 115, 1968.

[49]. P. Eidler, "Development of Zinc/Bromine Batteries for Load-leveling Applications: Phase 1 Final Report,” Sandia National Laboratories report, 1999.

[50]. J. Jeon, H. S. Yang, J. Shim, H. S. Kim et al, “Dual function of quaternary ammonium in Zn/Br redox flow battery: Capturing the bromine and lowering the charge transfer resistance”, Electrochimica Acta, vol. 127, pp. 397-402, 2014.

[51]. J. Lee, E. Do, Y. Kim, J. Yu and K. J. Kim, “Development of titanium 3D mesh interlayer for enhancing the electrochemical performance of zinc–bromine flow battery”, Scientific reports, vol. 11, 2021.

[52]. H. Lin, L. Bai , X. Han , Y. Zhang and J. Shi, “Pyrolytic carbon felt electrode Inhibits Formation of Zinc Dendrites in Zinc Bromine Flow Batteries”, International Journal of Electrochemical Science, vol. 13, 2018.

[53]. S. Suresh, M. Ulaganathan, N. Venkatesan, P. Periasamy, P. Ragupathy, “High performance zinc-bromine redox flow batteries: Role of various carbon felts and cell configurations”, Journal of Energy Storage, vol. 20, pp. 134-139, 2018.

[54]. S. Maurya, P. T. Nguyen, Y. S. Kim, Q. Kang and R. Mukundan, “Effect of flow field geometry on operating current density, capacity and performance of vanadium redox flow battery”, Journal of Power Sources, vol. 404, pp. 20-27, 2018.

[55]. Redflow Limited, “Redflow Installation and Operation Manual – ZBM2,” Version: 4.0, 2019.

[56]. N. Clark, P. Eidler and P. Lex, "Development of Zinc/Bromine Batteries for Load-leveling Applications: Phase 2 Final Report,” Sandia National Laboratories report, 1999.

[57]. M. Jarnut, S. Wermiński and B. Waśkowicz, “Comparative analysis of selected energy storage technologies for prosumer-owned microgrids”, Renewable and Sustainable Energy Reviews, vol. 74, pp. 925-937, Jan. 2017.

[58]. B. P. Williams1, G. L. Shebert1 and Y. L. Joo, “Metal Oxide Coatings on Carbon Electrodes with Large Mesopores for Deeply Charged Zinc Bromine Redox Flow Batteries”, Journal of The Electrochemical Society, vol. 166, 2019.

[59]. P. J. Lex and J. F. Mathews, “Recent Developments in Zinc/Bromine Battery Technology at Johnson controls”, IEEE, 1992.

[60]. M. Nakatsuji-Mather and T. K. Saha, "Zinc-bromine flow batteries in residential electricity supply: Two case studies," 2012 IEEE Power and Energy Society General Meeting, pp. 1-8, 2012.

[61]. Y. Xue, M. Penchev, H. Xin and A. Martinez-Morales, "Flow Battery Control Strategy Implementation and Cost Benefit Analysis for Microgrid under Updated Time-of-Use Periods," 2020 IEEE Power & Energy Society Innovative Smart Grid Technologies Conference (ISGT), Washington, DC, USA, pp. 1-5, 2020.

[62]. M. Jarnut, S. Wermiński and B. Waśkowicz, "Comparative analysis of selected energy storage technologies for prosumer-owned microgrids," Renewable and Sustainable Energy Reviews, vol. 74, pp. 925-937, Jan. 2017.

[63]. D. M. Rose and S. R. Ferreira, "Initial test results from the redflow 5kW, 10kWh zinc-bromide module, phase 1," Sandia National Laboratories report, 2012.

[64]. J. Lim, S. Lee, K. Kang, Y. Cho and G. Choe, "A modular power conversion system for zinc-bromine flow battery based energy storage system," 2015 IEEE 2nd International Future Energy Electronics Conference (IFEEC), pp. 1-5, 2015.

[65]. G. P. Rajarathnam and A. M. Vassallo, "The Zinc/Bromine Flow Battery Materials Challenges and Practical Solutions for Technology Advancement," MA: Springer, 2016.

[66]. K. S. Evans, L. Azevedo, M. G. Morgan and J. Apt, " Regional variations in the health, environmental, and climate benefits of wind and solar generation", Proceedings of the National Academy of Sciences, vol. 110, no. 29, pp. 11768-11773, 2013.

[67]. DECISION APPROVING GREENHOUSE GAS EMISSION REDUCTION REQUIREMENTS FOR THE SELF GENERATION INCENTIVE PROGRAM STORAGE BUDGET. 2019.

[68]. E. S. Hittinger and M. L. Azevedo, " Bulk Energy Storage Increases United States Electricity System Emissions," Environmental Science & Technology, vol. 49, no. 5, pp. 3203-3210, 2015.

[69]. D. J. Olsen and D. S. Kirschen, "Profitable Emissions-Reducing Energy Storage," IEEE Transactions on Power Systems, vol. 35, no. 2, pp. 1509-1519, 2020.

[70]. M. J. Fisher and J. Apt, "Emissions and Economics of Behind-the-Meter Electricity Storage," Environmental Science & Technology, vol. 51, no. 3, pp. 1094-1101, 2017.

[71]. B. C. Ummels, E. Pelgrum and W. L. King, "Integration of large-scale wind power and use of energy storage in the Netherlands' electricity supply", IET Renewable Power Generation, vol. 2, no. 1, pp. 34-46, 2010.

[72]. R. T. Carson and K. Novan, "The private and social economics of bulk electricity storage", Journal of Environmental Economics and Management, vol. 66, no. 3, pp. 404-423, 2013.

[73]. S. Ramteen, “Emissions Impacts of Wind and Energy Storage in a Market Environment”, Environmental Science & Technology, vol. 45, no. 24, pp. 10728-10735, 2011.

[74]. O. Babacan, A. Abdulla, R. Hanna, J. Kleissl and D. G. Victor, “Unintended Effects of Residential Energy Storage on Emissions from the Electric Power System”, Environmental Science & Technology, vol. 52, no. 22, pp. 13600-13608, 2018.

[75]. C. G. Hoehne and M. V. Chester, “Optimizing plug-in electric vehicle and vehicle-to-grid charge scheduling to minimize carbon emissions”, Energy, vol. 115, no. 1, pp. 646-657, 2016.

[76]. L. M. Arciniegas and E. Hittinger, “Tradeoffs between revenue and emissions in energy storage operation”, Energy, vol. 143, pp. 1-11, 2018.

[77]. Y. Lin, J. X. Johnson and J. L. Mathieu, “Emissions impacts of using energy storage for power system reserves”, Applied Energy, vol. 168, pp. 444-456, 2016.

[78]. M. Zheng, X. Wang, C. J. Meinrenken and Yi Ding, “Economic and environmental benefits of coordinating dispatch among distributed electricity storage”, Applied Energy, vol. 210, pp. 842-855, 2018.

[79]. J. Liu and J. Li, "A Bi-Level Energy-Saving Dispatch in Smart Grid Considering Interaction Between Generation and Load," IEEE Transactions on Smart Grid, vol. 6, no. 3, pp. 1443-1452, May 2015.

[80]. S. Wong and J. Pinard, "Opportunities for Smart Electric Thermal Storage on Electric Grids with Renewable Energy," IEEE Transactions on Smart Grid, vol. 8, no. 2, pp. 1014-1022, 2017.

[81]. Rule 21 application, Southern California Edison 2016. [Online] Available:- https://www1.sce.com/NR/sc3/tm2/pdf/Rule21_1.pdf.

[82]. K. J. Cathro, “Zinc-bromine batteries for energy storage applications”, Department of Resources and Energy, 1986.

[83]. M.C. Wu, T.S. Zhao, H.R. Jiang, Y.K. Zeng, Y.X. Ren, “High-performance zinc bromine flow battery via improved design of electrolyte and electrode”, Journal of Power Sources, vol. 355, pp. 62-68, 2017.

[84]. C. Wang, X. Li, X. Xi, P.C. Xu, Q.Z. Lai, H.M. Zhang, “Relationship between activity and structure of carbon materials for Br2/Br− in zinc bromine flow batteries”, RSC Advances, vol. = 6, pp. 40169-40174, 2016.

[85]. K. Bradbury, L. Pratson, D. P. Echeverri, “Economic viability of energy storage systems based on price arbitrage potential in real-time U.S. electricity markets”, Applied Energy, vol. 114, pp. 512-519, 2014.

[86]. T. L. Montoya, P. G. Meacham, D. A. Perry, R. S. Broyles, S. Hickey and J. Hernández, "Flow Battery System Design for Manufacturability", Sandia National Laboratories, Albuquerque, New Mexico, U.S., 2014.

[87]. Document of Victor Valley Wastewater Reclamation Authority project, U.S. Department of Energy. [Online] Available: https://betterbuildingsinitiative.energy.gov-/partners/victor-valley-wastewater-reclamation-authority.

[88]. R. Faries. (2016, Sep.). Zinc Bromide Flow Battery Installation for Islanding and Backup Power. [Online].

[89]. A Z Amin, P. Ralon, M. Taylor and A. Ilas (2017, Oct.). "Electricity Storage and Renewables: Costs and Markets to 2030". Abu Dhabi. International Renewable Energy Agency. [Online]. Available: https://www.irena.org/media/Files/IRENA-/Agency/Publication/2017/Oct/IRENA_Electricit_Storage_Costs_2017.pdf .

[90]. P. Singh and B. Jonshagen, "Zinc bromine battery for energy storage, Journal of Power Sources", vol. 35, pp. 405-410, 1991.

[91]. A. Lucas, S.s Chondrogiannis, "Smart grid energy storage controller for frequency regulation and peak shaving, using a vanadium redox flow battery", International Journal of Electrical Power & Energy Systems, vol. 80, pp. 26-36, 2016.

[92]. E. O. Ogunniyi and H. Pienaar, "Overview of battery energy storage system advancement for renewable (photovoltaic) energy applications", 2017 International Conference on the Domestic Use of Energy (DUE), Cape Town, pp. 233-239, 2017.

[93]. IRENA (2019), Renewable capacity statistics 2019, International Renewable Energy Agency (IRENA), Abu Dhabi.

[94]. IRENA (2017), Electricity Storage and Renewables: Costs and Markets to 2030, International Renewable Energy Agency, Abu Dhabi.

[95]. A. Abdon, X. Zhang, D. Parra, M. K. Patel, C. Bauer, J. Worlitschek, "Techno-economic and environmental assessment of stationary electricity storage technologies for different time scales", Energy, vol. 139, pp. 1173-1187, 2017.

[96]. M. S. Javed, A. Song, Tao Ma, "Techno-economic assessment of a stand-alone hybrid solar-wind-battery system for a remote island using genetic algorithm", Energy, vol. 176, pp. 704-717,2019.

[97]. L. Lozano, E. M. Querikiol, M. L. S. Abundo, L. M. Bellotindos, "Techno-economic analysis of a cost-effective power generation system for off-grid island communities: A case study of Gilutongan Island, Cordova, Cebu, Philippines", Renewable Energy, vol. 140, pp. 905-911, 2019.

[98]. C. Bastholm, F. Fiedler, “Techno-economic study of the impact of blackouts on the viability of connecting an off-grid PV-diesel hybrid system in Tanzania to the national power grid”, Energy Conversion and Management, vol. 171, pp. 647-658, 2018.

[99]. J. Ahmad, M. Imran, A. Khalid, W. Iqbal, S. R. Ashraf, M. Adnan, S. F. Ali, K. S. Khokhar, “Techno economic analysis of a wind-photovoltaic-biomass hybrid renewable energy system for rural electrification: A case study of Kallar Kahar”, Energy, vol. 148, pp. 208-234, 2018.

[100]. M. Kapsali, J.S. Anagnostopoulos, “Investigating the role of local pumped-hydro energy storage in interconnected island grids with high wind power generation”, Renewable Energy, vol. 114, pp. 614-628, 2017.

[101]. Z. Ren, P. Paevere, D. Chen, “Feasibility of off-grid housing under current and future climates”, Applied Energy, vol. 241, pp. 196-211, 2019.

[102]. D. Parra, M. K. Patel, “Effect of tariffs on the performance and economic benefits of PV-coupled battery systems”, Applied Energy, vol. 164, pp. 175-187, 2016.

[103]. K. Uddin, R. Gough, J. Radcliffe, J. Marco, P. Jennings, “Techno-economic analysis of the viability of residential photovoltaic systems using lithium-ion batteries for energy storage in the United Kingdom”, Applied Energy, vol. 206, pp. 12-21, 2017.

[104]. D. Parra, M. K. Patel, “The nature of combining energy storage applications for residential battery technology”, Applied Energy, vol. 239, pp. 1343-1355, 2019.

[105]. J. Eyer, G. Corey, “Energy Storage for the Electricity Grid: Benefits and Market Potential Assessment Guide”, Sandia National Laboratories, 2010.

[106]. S. Dhundhara, Y. P. Verma, A. Williams, “Techno-economic analysis of the lithium-ion and lead-acid battery in microgrid systems”, Energy Conversion and Management, vol. 177, pp. 122-142, 2018.

[107]. D. C. Jordan, S. R. Kurtz, “Photovoltaic Degradation Rates — An Analytical Review”, National Renewable Energy Laboratory (NREL), 2012

[108]. A. Kaabeche, R. Ibtiouen, “Techno-economic optimization of hybrid photovoltaic/wind/diesel/battery generation in a stand-alone power system”, Solar Energy, vol. 103, pp. 171-182, 2014.

[109]. T. Aquino, C. Zuelch, C. Koss, “Energy Storage Technology Assessment”, Public Service Company of New Mexico, 2017.

[110]. C. S. Lai and M. D. McCulloch, “Levelized Cost of Energy for PV and Grid Scale Energy Storage Systems”, Pre-print submitted to Elsevier Applied, 2016.

[111]. Calculation of LCOE, online: https://atb.nrel.gov/electricity/2017/equations - variables.html

[112]. J. M. Santos, P. S. Moura, A. T. de Almeida, “Technical and economic impact of residential electricity storage at local and grid level for Portugal”, Applied Energy, vol. 128, pp. 254-264, 2014.

[113]. G. Angenendt, S. Zurmühlen, H. Axelsen, D. U. Sauer, “Comparison of different operation strategies for PV battery home storage systems including forecast-based operation strategies”, Applied Energy, vol. 229, pp. 884-899, 2018.

[114]. A. S. Hassan, L. Cipcigan, N. Jenkins, “Optimal battery storage operation for PV systems with tariff incentives”, Applied Energy, vol. 203, pp. 422-441, 2017.

[115]. D. Marvin, D. R. Cameron, M. C. Passero, and J. M. Remucal, “Ecosystem Management and Land Conservation Can Substantially Contribute to California's Climate Mitigation Goals”, vol. 2017, 2017.

[116]. H. Kanchev, F. Colas, V. Lazarov and B. Francois, "Emission Reduction and Economical Optimization of an Urban Microgrid Operation Including Dispatched PV-Based Active Generators," IEEE Transactions on Sustainable Energy, vol. 5, no. 4, pp. 1397-1405, 2014.

[117]. F. Feijoo, T. K. Das, “Emissions control via carbon policies and microgrid generation: A bilevel model and Pareto analysis”, Energy, vol. 90, pp. 1545-1555, 2015.

[118]. B. E. Sedhom, M. M. El-Saadawi, M.S. El Moursi, M..A. Hassan, A. A. Eladl, “IoT-based optimal demand side management and control scheme for smart microgrid”, International Journal of Electrical Power & Energy Systems, vol. 127, 2021.

[119]. J. Van Zee, “An analysis of a back fed porous electrode for the Br2/Br− redox reaction”, Journal of Electrochemic Society., vol. 130, 2006.

T.I. Evans, “A mathematical model of a zinc/bromine flow cell”, Journal of Electrochemic Society, vol. 134, 2006.

[120]. M.J. Mader, “A mathematical model of a Zn/Br2 cell on charge”, Journal of Electrochemic Society, vol. 133, 1986.

[121]. Z. Xu, J. Wang, S.C. Yan, Q. Fan, P. D. Lund, “Modeling of Zinc Bromine redox flow battery with application to channel design”, Journal of Power Sources, vol. 450, 2020.

[122]. C. Amzallag, J. Gerey, J. Robert, and J. Bahuaud, “Standardization of the rainflow counting method for fatigue analysis,” International journal of fatigue, vol. 16,

no. 4, pp. 287–293, 1994.

[123]. L. Reddy et al., "Rainflow Algorithm-Based Lifetime Estimation of Power Semiconductors in Utility Applications," IEEE Trans. Ind. Appl., vol. 51, pp. 3368-3375, 2015.

[124]. Y. Shi, B. Xu, Y. Tan, D. Kirschen and B. Zhang, "Optimal Battery Control Under Cycle Aging Mechanisms in Pay for Performance Settings," in IEEE Transactions on Automatic Control, vol. 64, no. 6, pp. 2324-2339, June 2019.

[125]. K. Abdulla, J. De Hoog, V. Muenzel, F. Suits, K. Steer, A. Wirth, and S. Halgamuge, "Optimal operation of energy storage systems considering forecasts and battery degradation," 2017 IEEE Power & Energy Society General Meeting, Chicago, IL, USA, 2017.

[126]. B. Gundogdu and D. T. Gladwin, "A Fast Battery Cycle Counting Method for Grid-Tied Battery Energy Storage System Subjected to Microcycles," 2018 International Electrical Engineering Congress (iEECON), Krabi, Thailand, 2018.

[127]. Sheila Samsatli, Nouri J. Samsatli, “A general mixed integer linear programming model for the design and operation of integrated urban energy systems”, Journal of Cleaner Production, vol. 191, pp. 458-479, 2018.

[128]. Floudas, Christodoulos A. 1995. Nonlinear and mixed-integer optimization: fundamentals and applications. New York: Oxford University Press.

[129]. Matlab. https://www.mathworks.com/products/matlab.html

[130]. MOSEK. https://www.mosek.com/products/mosek/

[131]. MOSEK Modeling Cookbook. https://docs.mosek.com/modeling-cookbook/-index.html

[132]. Logic and operation. https://faculty.math.illinois.edu/~mlavrov/docs/482-spring-2020/lecture32.pdf

[133]. K. Say, M. John, R. Dargaville, “Power to the people: Evolutionary market pressures from residential PV battery investments in Australia”, Energy Policy, vol. 134, 2019.

[134]. Ghada Merei, Janina Moshövel, Dirk Magnor, Dirk Uwe Sauer, “Optimization of self-consumption and techno-economic analysis of PV-battery systems in commercial applications”, Applied Energy, vol. 168, 2016.

[135]. IEA (2020), Global Energy Review 2019, IEA, Paris https://www.iea.org/reports/global-energy-review-2019

[136]. Energy Information Administration (EIA), Monthly Energy Review 2020 https://www.eia.gov/totalenergy/data/monthly/pdf/sec7.pdf

[137]. Hamid Karimi, Shahram Jadid, "Optimal energy management for multi-microgrid considering demand response programs: A stochastic multi-objective framework", Energy, vol. 195, 2020.

[138]. M.A. Hannan, M. Faisal, Pin Jern Ker, R.A. Begum, Z.Y. Dong, C. Zhang, "Review of optimal methods and algorithms for sizing energy storage systems to achieve decarbonization in microgrid applications", Renewable and Sustainable Energy Reviews, vol. 131, 2020.

[139]. R. Tu, Y. Gai, B. Farooq, D. Posen, M. Hatzopoulou, "Electric vehicle charging optimization to minimize marginal greenhouse gas emissions from power generation", Applied Energy, vol. 277, 2020.

[140]. U.G.K. Mulleriyawage, W.X. Shen, "Optimally sizing of battery energy storage capacity by operational optimization of residential PV-Battery systems: An Australian household case study", Renewable Energy, vol. 160, 2020.

[141]. S. Nojavan, M. Majidi, A. Najafi-Ghalelou, M. Ghahramani, K. Zare, "A cost-emission model for fuel cell/PV/battery hybrid energy system in the presence of demand response program: ε-constraint method and fuzzy satisfying approach", Energy Conversion and Management, vol. 138, 2017.

[142]. P. Mancarella, G. Chicco, "Global and local emission impact assessment of distributed cogeneration systems with partial-load models", Applied Energy, vol. 86, pp. 2096-2106, 2009.

[143]. S. Wouter, L. Ioannis, A. Tarek, V. Wilfried, "On the use of average versus marginal emission factors", SMARTGREENS 2019 - Proceedings of the 8th International Conference on Smart Cities and Green ICT Systems, pp. 187 – 193, 2019.

[144]. K. Siler-Evans, I. L. Azevedo, and M. Granger Morgan, "Marginal Emissions Factors for the U.S. Electricity System", Environmental Science & Technology, vol. 46, pp. 4742-4748, 2012.

[145]. K. Siler-Evans, I. L. Azevedo, and M. G. Morgan, "Marginal Emissions Factors for the U.S. Electricity System", Environmental Science & Technology, vol. 46, pp. 4742-4748, 2012.

[146]. W. Wang, Q. Luo, B. Li, X. Wei, L. Li, Z. Yang, "Recent progress in redox flow battery research and development", Advanced Functional Materials, vol. 23, pp. 970-986, 2013.

[147]. A. D. Hawkes, "Long-run marginal CO2 emissions factors in national electricity systems", Applied Energy, vol. 125, pp. 197-205, 2015.

[148]. California Self-Generation Incentive Program Greenhouse Gas Signal. Online: https://sgipsignal.com/download-data

[149]. “The Use of the Social Cost of Carbon in the Federal Proposal “Safer Affordable Fuel-Efficient (SAFE) Vehicles Rule for Model Years 2021–2026 Passenger Cars and Light Trucks.”, M. Auffhammer, George Pardee Jr. Family Professor in International Sustainable Development and Associate Dean of Social Sciences, University of California Berkeley, 2018.

[150]. “SOCIAL COST OF CARBON Identifying a Federal Entity to Address the National Academies’ Recommendations Could Strengthen Regulatory Analysis”, United States Government Accountability Office, 2020

[151]. California PUC Uses SCC to Help Determine Value of DERs, online: https://costofcarbon.org/states/entry/california-puc-uses-scc-to-help-determine-value-of-ders

[152]. Z. Zheng, F. Han, F. Li and J. Zhu, "Assessment of marginal emissions factor in power systems under ramp-rate constraints," CSEE Journal of Power and Energy Systems, vol. 1, no. 4, pp. 37-49, 2015.

[153]. California PUC Uses SCC to Help Determine Value of DERs. https://costofcarbon.org/states/entry/california-puc-uses-scc-to-help-determine-value-of-ders